

Dissertation
submitted to the
Combined Faculties for the Natural Sciences and for Mathematics
of the Ruperto-Carola University of Heidelberg, Germany
for the degree of
Doctor of Natural Sciences

**The Role of Hepatic Transforming Growth
Factor-Beta1 Stimulated Clone-22 D4 (TSC22D4)
in Acute Metabolic Dyslipidemia**

Presented by
Allan Jones (dipl. biol.)
Born in Ascot, United Kingdom

Heidelberg 2011

The Role of Hepatic Transforming Growth Factor-Beta1 Stimulated Clone-22 D4 (TSC22D4) in Acute Metabolic Dyslipidemia

Referees: Prof. Dr. Rainer Zawatzky
 Prof. Dr. Stephan Herzig

Date of oral examination:

ACKNOWLEDGEMENTS

I would like to express my gratitude to all those who supported me during my thesis. First and foremost I thank Dr. Stephan Herzig for welcoming me into his lab and giving me his inspiration and support throughout my project. Special thanks also go to Manfred Kögl, Mauricio Berriel Diaz, Adam Rose and Alexandros Vogiopoulos for sharing their in-depth knowledge and experience with me. Their advice and our scientific discussions were invaluable. I am incredibly grateful to our technicians Daniela Strzoda, Anja Reimann, Annika Zota and Tjeerd Sijmonsma for all the work they put into my project, but an extra special thank you goes to Oksana Seibert for the tremendous help she gave me during the last few months of my PhD. Without her everything would have taken so much longer!!! I thank Maria Liebert and Philipp Kulozik for scientific discussions, extracurricular activities and great times at retreats and conferences. Stefan Kleinsorg was a smart and enthusiastic Bachelor's student. I enjoyed working with him and his results contributed directly to this project. I of course thank all other current and previous members of the Molecular Metabolic Control Department – it was great to get to know you all so well! You all made it a pleasure to come to work every morning. I also thank the DKFZ Genomics and Proteomics core facility, Dr. Barbara Leuchs from the AAV core facility, the genomics department at the University Clinic in Mannheim and Dr. Karin Müller-Decker for helping me with my experiments.

I thank Prof. Rainer Zawatzky, Prof. Suat Özbek and Prof. Rüdiger Hell for reading and evaluating my thesis.

Finally I would like to thank my parents, Steven, Louisa and especially Isabelle for supporting me during the last three years.

You were all a great help!

INDEX

1.	ABSTRACT	1
2.	ZUSAMMENFASSUNG	2
3.	INTRODUCTION	3
3.1	Metabolic Disorders	3
3.1.1.	Obesity	3
3.1.2.	The Metabolic Syndrome, insulin resistance and Type 2 diabetes mellitus	5
3.1.3.	Cancer cachexia	7
3.2	Lipid metabolism	8
3.2.1.	Liver lipid metabolism	8
3.2.2.	Lipoprotein metabolism and dyslipidemia	9
3.3	Cellular signalling	12
3.3.1.	Transcriptional regulation	12
3.3.2.	Transducin beta like 1 and transducin beta like 1 related	14
4.	AIM OF THE STUDY	17
5.	RESULTS	18
5.1	TSC22D4 is a novel TBL1 and TBLR1 interaction partner	18
5.1.1.	Luminescence-based mammalian interactome mapping (LUMIER) screen for novel TBL1 and TBLR1 interacting proteins	18
5.1.2.	Verification of the interaction between TSC22D4 and TBL1 / TBLR1 by Flag co-immunoprecipitation	22
5.1.3.	TSC22D4 interacts directly with the TBL1 / TBLR1 WD40 domains	23
5.2	Analysis of hepatic TSC22D4 expression in mouse disease models	25
5.2.1.	TSC22D4 is expressed ubiquitously throughout the mouse body	25
5.2.2.	TSC22D4 expression is not changed upon fasting	26
5.2.3.	TSC22D4 expression is not changed in the New Zealand Obese mouse model	27

5.2.4.	TSC22D4 expression is reduced in leptin deficient mice	27
5.2.5.	TSC22D4 expression is reduced in high fat diet fed mice	28
5.3	Hepatic TSC22D4 knock down leads to elevated serum triglyceride levels in C57BL/6J mice	30
5.3.1.	Liver specific TSC22D4 knock down using RNA interference	30
5.3.2.	Phenotypic analysis of TSC22D4 deficient C57BL/6J mice	32
5.3.2.1.	Body weight, liver weight, body fat and lean mass	32
5.3.2.2.	Hepatic glycogen and circulating glucose, insulin and ketone bodies	32
5.3.2.3.	Hepatic and serum lipids and steroids	34
5.3.3.	TSC22D4 deficient mice display elevated circulating VLDL triglycerides	36
5.3.4.	Hepatic triglyceride levels are deregulated in the fasted state	37
5.3.5.	VLDL production is increased upon TSC22D4 knock down	39
5.3.5.1.	VLDL clearance is not changed upon TSC22D4 knock down	39
5.3.5.2.	Hepatic VLDL production is enhanced in TSC22D4 deficient mice	40
5.3.5.3.	Lipogenic gene expression is induced in TSC22D4 deficient mice	41
5.3.6.	Whole genome expression profiling in TSC22D4 deficient mice	44
5.3.7.	Acute TSC22D4 knock down affects insulin signalling, but not glucose or insulin tolerance	45
5.3.8.	TSC22D4, TBL1 and TBLR1 triple deficiency leads to severe hypertriglyceridemia	47
5.3.9.	Micro RNA mediated TSC22D4 knock down using adeno-associated virus	50
5.4	TSC22D4 over expression reduces circulating VLDL triglyceride levels in C57BL/6J mice	52
5.4.1.	Hepatic TSC22D4 over expression in fasted and refed mice	52
5.4.1.1.	Effects of TSC22D4 over expression on body composition	53
5.4.1.2.	Effects of TSC22D4 over expression on hepatic lipid metabolism	54
5.4.2.	Fatty acid synthase is repressed by TSC22D4	56
5.4.3.	Semi-endogenous co-immunoprecipitation	57

5.4.4.	Hepatic TSC22D4 restoration in obese mice	58
5.5	TSC22D4 and cancer cachexia	61
5.5.1.	TSC22D4 is elevated in mouse models of wasting and cachexia	61
5.5.1.1.	TSC22D4 is induced by a methionine and choline deficient diet	61
5.5.1.2.	TSC22D4 levels correlate with weight loss in cachectic mice	62
6.	DISCUSSION	64
6.1	TSC22D4 interacts directly with TBL1/TBLR1	65
6.2	TSC22D4 represses VLDL secretion	67
6.3	TSC22D4 in health and disease	70
6.3.1.	TSC22D4 and obesity	70
6.3.2.	TSC22D4 and carcinogenesis	71
6.3.3.	TSC22D4 and cancer cachexia	72
6.4	Summary and outlook	72
7.	MATERIAL	74
7.1	Instruments	74
7.2	Consumables	76
7.3	Chemicals and reagents	77
7.4	Commercial kits	80
7.5	Research diets	81
7.6	Solutions and buffers	81
7.7	Molecular components	84
7.8	Cell lines	85
7.9	Software	86
8.	METHODS	87
8.1	Molecular Biology	87
8.1.1.	Agarose gel electrophoresis	87
8.1.2.	Extraction of DNA from agarose gels	87

8.1.3.	Restriction analysis of DNA fragments or plasmids	87
8.1.4.	Polymerase chain reaction (PCR)	87
8.1.5.	Ligation	88
8.1.6.	Chemical transformation of Escherichia coli	89
8.1.7.	Plasmid preparation	89
8.1.8.	DNA sequencing	90
8.1.9.	RNA isolation from tissue samples	90
8.1.10.	RNA isolation from cell samples	90
8.1.11.	RNA isolation using the RNeasy Mini purification kit	91
8.1.12.	cDNA synthesis	91
8.1.13.	Quantitative Real-Time PCR	91
8.1.14.	Gene expression profiling	92
8.2	Cell Biology	92
8.2.1.	Cultivation of Human Embryonic Kidney (HEK), HEK293A and HEK293T cells	92
8.2.2.	Cultivation of Hepa1c1 mouse hepatoma cells	93
8.2.3.	Cell culture and transient transfection assays	93
8.2.4.	Primary hepatocyte experiments	94
8.3	Animal experiments	95
8.3.1.	General procedures	95
8.3.2.	Hepatic VLDL release	95
8.3.3.	VLDL clearance	96
8.3.4.	Intravenous lipid load test	96
8.3.5.	Glucose tolerance test	96
8.3.6.	Insulin tolerance test	97
8.3.7.	Acute insulin signalling	97
8.4	Biochemistry	97
8.4.1.	Luminescence-based mammalian interactome mapping (LUMIER)	97

8.4.2.	Preparation of protein extracts from liver samples	98
8.4.3.	SDS-PAGE analysis and immunoblotting	99
8.4.4.	Determination of free fatty acid levels	99
8.4.5.	Serum ketone body measurement	100
8.4.6.	Isolation of hepatic lipids	100
8.4.7.	Determination of triglyceride levels	100
8.4.8.	Cholesterol measurement	101
8.4.9.	Blood glucose measurements	101
8.4.10.	Insulin measurement	101
8.4.11.	LPL activity	102
8.4.12.	Fast protein liquid chromatography (FPLC)	102
8.4.13.	Co-Immunoprecipitation	102
8.4.14.	GST-Pulldown	103
8.4.15.	Histochemistry (Hematoxylin and Oil red O).	103
8.4.16.	Plasmids and RNA interference	103
8.5	Virology	104
8.5.1.	Cloning of adenoviruses	104
8.5.2.	Virus harvest using the Freeze-and-Thaw-method	105
8.5.3.	Caesium chloride gradient	105
8.5.4.	Virus titration	106
8.5.5.	AAV Production	106
8.5.6.	AAV purification	107
8.6	Statistical Analysis	109
9.	GLOSSARY	110
10.	FIGURE LEGEND	113
11.	REFERENCE LIST	116
11.1	Internet sources	126

1. ABSTRACT

Metabolism is defined as the sum of all biochemical reactions taking place in any given system at a specific point in time. Deregulation of metabolic balance in the human body can thereby have severe consequences in regard to health and well-being. In mammals, proper storage and distribution of lipids in and between tissues is essential for the maintenance of energy homeostasis. Abnormally high levels of triglycerides (TG) in the blood (“hypertriglyceridemia”) represent a hallmark of disorders such as the Metabolic Syndrome, type 2 diabetes and atherosclerosis. Indeed, hypertriglyceridemia has been identified as an important risk factor for long-term diabetic complications, whilst hypotriglyceridemia occurs in patients suffering from a tumour-associated wasting condition known as cachexia.

In this study, we identify the hepatic transforming growth factor-beta 1 stimulated clone (TSC)-22 D4 as a critical molecular determinant of systemic lipid homeostasis and lipoprotein metabolism. Using a large-scale luminescence based mammalian interactome (LUMIER) screen, TSC22D4 was identified as an as-yet unknown interaction partner of the TBL1/TBLR1 transcriptional co-factor complex. TSC22D4 was found to be down-regulated under conditions of diet-induced obesity and induced in cancer cachexia. Liver-specific ablation of TSC22D4 in mice triggered serum hyperlipidemia through the induction of lipogenic gene expression in the liver and an associated increase in the release of TG-rich very-low-density-lipoprotein (VLDL) particles. Conversely, restoration of TSC22D4 in obese mice led to reduced VLDL release and TG accumulation in the liver.

TSC22D4 expression levels were found to inversely correlate with the degree of weight loss in a mouse model of cancer cachexia. In future, it will be interesting to investigate if the induction of hepatic TSC22D4 activity represents a cause or protective consequence in the onset of tumour-associated cachexia. In this regard, TSC22D4 may serve as a molecular marker for disease progression and prognosis in patients.

2. ZUSAMMENFASSUNG

Der Stoffwechsel umfasst die Summe aller biochemischen Reaktionen, die zu einer bestimmten Zeit in einem Organismus stattfinden. Ist das metabolische Gleichgewicht im menschlichen Körper gestört, hat dies schwerwiegende Auswirkungen auf die Gesundheit und die Lebensqualität. Dabei, ist die effiziente Speicherung und der geregelte Transport von Lipiden zwischen verschiedenen Geweben bei der Koordination des Energiehaushalts von großer Bedeutung. Erhöhte Triglyzeridspiegel im Blut sind ein Kennzeichen des metabolischen Syndroms. Sie treten vermehrt bei Typ 2 Diabetes und Arteriosklerose auf. Während Hypertriglyzeridämie ein wichtiger Risikofaktor bei chronisch diabetischen Komplikationen ist, tritt Hypotriglyzeridämie hingegen vor allem bei Krebskachexiepatienten auf.

In dieser Arbeit zeigen wir, dass das Gen ‘Transforming growth factor-beta 1 Stimulated Clone (TSC)-22 D4’ ein wichtiger molekularer Schalter in der Regulation des Lipidstoffwechsels darstellt. Mit Hilfe eines Hochdurchsatzverfahrens wurde eine Interaktion zwischen TSC22D4 und den transkriptionellen Kofaktoren TBL1 und TBLR1 identifiziert. Die Expression von TSC22D4 ist in diabetischen Mausmodellen reduziert und bei Krebskachexie erhöht. Leberspezifische Knock-Down-Studien in Mäusen führten zur Induktion der Lipogenese, erhöhten Triglyzeridwerten im Blut und einer verstärkten Sekretion von Lipoproteinen geringer Dichte (VLDL). Überexpression von TSC22D4 in diabetischen Mäusen hingegen, resultierte in reduzierter Lipogenese, geringerer VLDL-Sekretion und einer Akkumulation von Triglyzeriden in der Leber.

Die TSC22D4-Expression korrelierte mit dem Verlust an Körpermengewicht bei einem Mausmodel der Krebskachexie. Zukünftige Forschungen werden zeigen, ob die Induktion der TSC22D4-Aktivität in der Leber eine Ursache, oder eine schützende Konsequenz bei der Pathogenese der tumorassoziierten Kachexie darstellt. In diesem Zusammenhang könnte TSC22D4 als Marker für Progression und Prognose bei Krebspatienten dienen.

3. INTRODUCTION

In the past century, biotechnology and translational medical research have made great advances. Previously deadly diseases are manageable and subsequently people are living to a much higher age. This progress has however not only led to demographic problems, but also given rise to new health issues. Aging diseases, such as type 2 diabetes are becoming increasingly prevalent, especially as excess caloric intake and reduced exercise are common in our developed world. While it is important to educate the population on how to prevent the onset of metabolic disorders, mainly through a healthy life style, it is also necessary to understand the underlying molecular and physiological processes. Metabolic signalling and transcriptional control thereby represent potent switches in the natural or pharmacological control and regulation of a healthy metabolic state. This dissertation will therefore focus on novel regulatory components of liver physiology.

3.1 Metabolic Disorders

3.1.1. Obesity

During evolution, mammals have acquired intricate mechanisms to absorb, process and store nutrients. The ability to build energy depots for times of low food availability has thereby been essential for the survival and development of complex organisms (1). Undoubtedly, even today a large part of the world wide population, especially in western Africa, suffers from undernutrition and is heavily reliant on these energy depots (2). In recent years however, a new metabolic problem has become increasingly obvious. Excessive calorie intake, in combination with a sedentary life style, has led to an obesity pandemic in developed and developing countries (Fig. 1). Globally, overweight and obesity cause more deaths than undernutrition. Current estimates from the World Health Organization (WHO) suggest that in 2008, 1.5 billion adults were overweight and 500 million were considered obese, representing 10% of the population. What seems even more

alarming is that, today 43 million children under the age of 5 are estimated to be overweight (I).

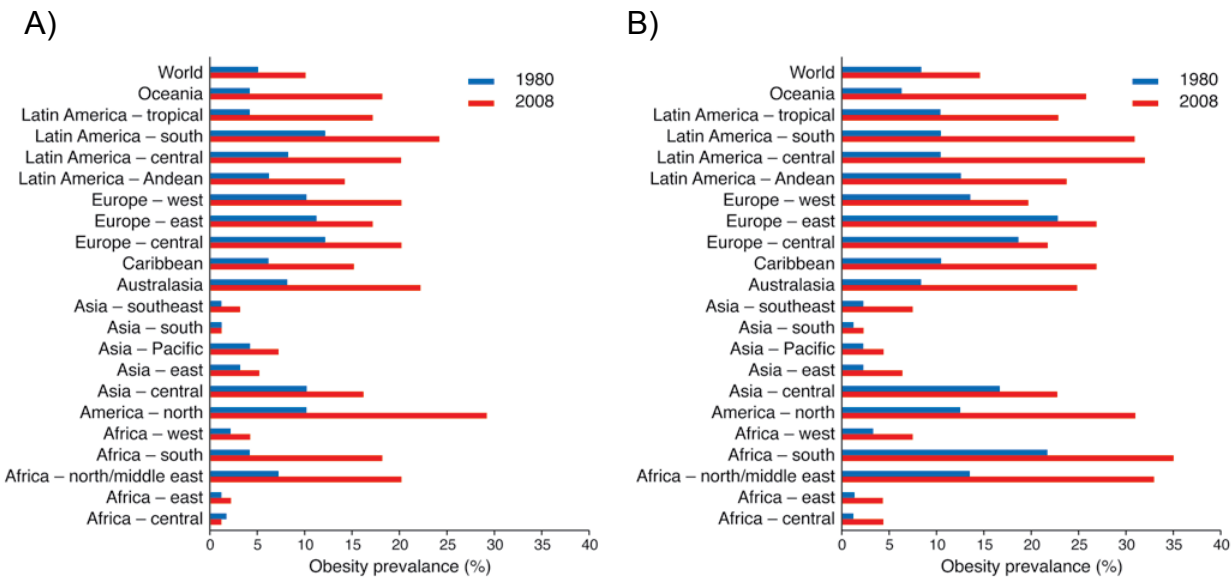


Fig. 1: Increase in obesity incidence. Prevalence of obesity in men (A) and women (B) in 1980 (blue) and 2008 (red). Taken from Ahima 2011.

An individual is considered overweight if his or her body mass index (BMI = weight [kg]/(height [m])²) is above 25 and obese if the BMI is higher than 30. Several medical conditions are associated with obesity. The permanent over-supply of food particularly favours the development of insulin resistance, type 2 diabetes mellitus, hypertension, organ damage, atherosclerosis and cardiovascular disease (3). Apart from these ‘traditional’ metabolic diseases, the link between cancer and obesity is also becoming increasingly evident. Hormones and growth factors, such as insulin, are hypersecreted and induce cell proliferation. In particular, liver, breast and colon cancer incidence are highly associated with excess body weight (4,5).

Obesity has many underlying social and genetic causes. Today large parts of the population consume processed, energy-dense food with low nutritional value. In combination with a sedentary lifestyle and low energy expenditure, the effects on the body are deleterious. Whilst extremely rare monogenic conditions do exist, in most cases obesity stems from a combination of environmental and genetic factors. Many susceptibility genes have been discovered and described in great detail. However, individual susceptibility genes only account for a small portion of obesity cases, since the genetic basis is multigenic and combinatorial. Nevertheless, by understanding the

mechanisms by which such genes function, it will be possible to develop medical intervention strategies to prevent the onset of obesity at an early stage (1,6,7).

3.1.2. The Metabolic Syndrome, insulin resistance and Type 2 diabetes mellitus

Visceral obesity is the primary indicator for a loosely defined condition known as the Metabolic Syndrome or Syndrome X. Apart from central obesity, the Metabolic Syndrome is characterized by dyslipidemia, hypertension, hyperglycaemia and chronic low-grade inflammation. The condition is, amongst other things, associated with cardiovascular disease, type 2 diabetes mellitus, hepatic steatosis and gall stone disease. Individuals suffering from the Metabolic Syndrome have a 5-fold higher risk of developing non-insulin dependent type 2 diabetes mellitus (8,9).

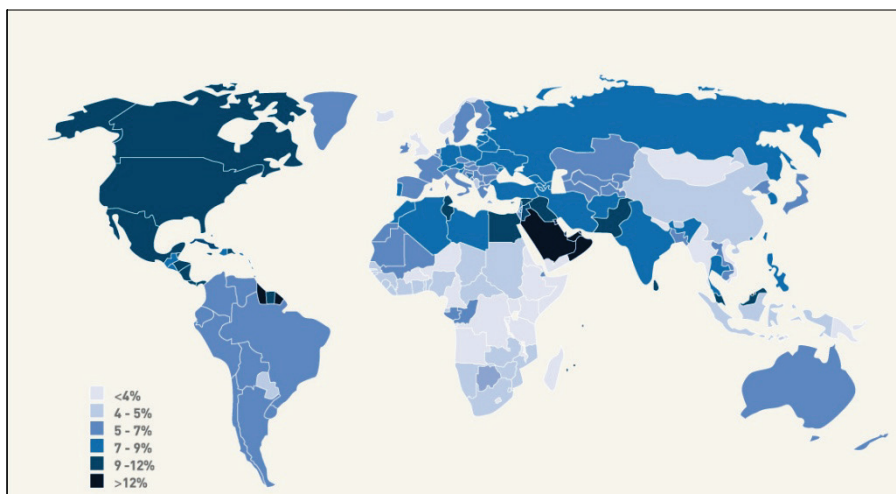


Fig. 2: Prevalence of diabetes 2010. Global incidence of type 2 diabetes mellitus in the year 2010. Taken from (II).

Patients suffering from type 1 diabetes mellitus are generally not obese. They have an autoimmune disease that destroys the pancreatic β -cells required to produce the peptide hormone insulin. Subsequently, they are absolutely dependent on injected insulin to regulate glucose homeostasis (10). The majority of diabetes patients (~90%) suffer from non-insulin dependent type 2 diabetes mellitus, a condition in which the β -cells are initially healthy. The disease, which is tightly associated with obesity and the Metabolic Syndrome, is characterized by insulin resistance of peripheral organs such as the brain, muscle, liver and adipose tissue. As in the case of obesity, the incidence and economic burden are increasing dramatically (Fig. 2) and

what was once considered an aging disease is now commonly being diagnosed in children (11-13).

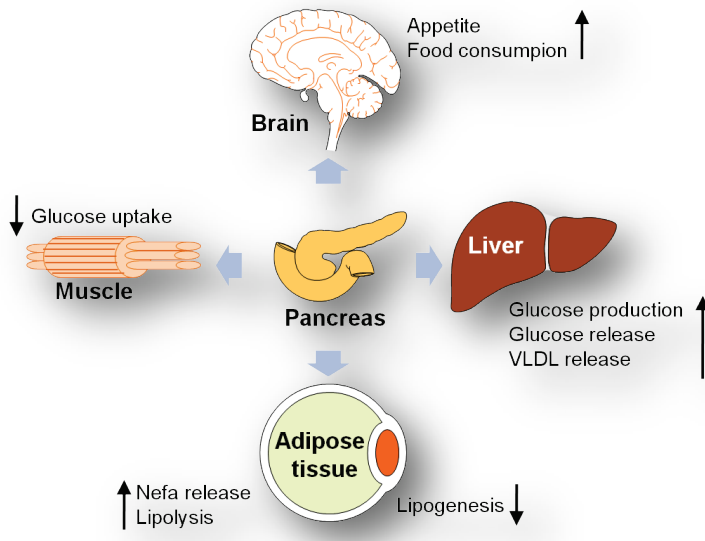


Fig. 3: Obesity and insulin resistance. Insulin resistance leads to elevated lipid release by liver and adipose tissue. Excess glucose is produced by the liver and glucose uptake by muscle is impaired. Elevated serum glucose and lipid levels further aggravate the overall condition.

It is important for the body to maintain normoglycemia, with blood glucose levels in a physiological range (~ 5 mM). Glucose metabolism is regulated by insulin and its antagonist glucagon. After food consumption, the pancreatic β -cells sense the elevation in blood glucose via low affinity Glut2 glucose transporters and subsequently release insulin. The hormone induces signalling cascades, resulting in glucose uptake by muscle, fat and liver and inhibition of hepatic glucose production (gluconeogenesis) and release. At the same time, it inhibits triglyceride (TG) break down (lipolysis) in adipose tissue and instead promotes the conversion of glucose to lipids (lipogenesis). If, upon fasting or exercise, blood glucose levels sink below a threshold, insulin is no longer secreted and instead glucagon is released by pancreatic α -cells. Glucagon induces glucose production and secretion by the liver (14). In the case of insulin resistance, this tightly regulated circuit is compromised. Postprandial and fasting glucose and fatty acid levels are elevated, leading to the release of more and more insulin. Insulin signalling is blunted, muscle and liver inefficiently import and convert glucose and hyperglycaemia occurs due to the reduced inhibition of gluconeogenesis. Lipolysis is not inhibited in adipose tissue, leading to the release of non-esterified free fatty acids. These circulating fatty acids then accumulate in the liver, where they are converted to TGs and induce hepatic steatosis (Fig. 3). All these processes subsequently accelerate the manifestation of severe insulin resistance. At

first, the pancreas can compensate for reduced insulin sensitivity by releasing more insulin, but over time the capacity is exhausted and patients develop full-blown type 2 diabetes mellitus, making them dependent on injected insulin (15).

3.1.3. Cancer cachexia

Cancer and immune suppressing diseases, such as AIDS, induce major changes on whole body glucose, lipid and protein metabolism (16,17). Many cancer entities are indeed accompanied by a condition known as cachexia (*Greek ‘kakos hexis’* meaning bad condition). Cancer cachexia is characterized by severe weight loss, primarily due to lean muscle and adipose tissue wasting, bad prognosis and a reduced quality of life. Pancreatic and lung cancer are particularly often associated with cachexia and the condition is responsible for approximately 20% of all cancer related deaths (18).

Although cachexia patients suffer from appetite loss, anorexia cannot fully explain the observed weight loss, as food supplementation does not stop progression. In healthy individuals, resting energy expenditure (REE) accounts for up to 70% of energy consumption. REE is strongly increased in cachectic patients. This is in part due to increased expression of so-called uncoupling proteins (UCPs) in muscle and adipose tissue. These mitochondrial membrane components relieve the membrane potential before oxidative phosphorylation can take place. This process leads to the production of heat rather than energy in the form of adenosine triphosphate (ATP). Indeed, in recent years it has been shown that energy storing white adipose tissue can be transformed into energy-consuming brown-like adipose tissue in a process known as browning. The transformation results in a depletion of energy and body mass (19). In addition, lipolysis is induced in cachectic individuals' adipose tissue and the released free fatty acids in turn are fed into futile cycles such as the hepatic Cori cycle, leading to further calorie consumption (20). Muscle mass is also greatly reduced in cachexia, as protein synthesis is inhibited and protein breakdown is enhanced. The catabolic effects, in particular ubiquitin dependent proteolysis, thereby seem to be rate limiting (21). Although most focus in cachexia research has been on muscle and adipose tissue, the liver is also important in the manifestation of the disease. It serves as a sink for the fatty acids released from adipose tissue. Subsequently the liver accumulates fat and reduces *de novo* TG secretion (22).

Taken together, cachexia represents a complex pro-inflammatory metabolic disorder affecting systemic glucose, lipid and protein metabolism. There are, as of now, few therapeutic options to treat the disease, making it necessary to investigate the condition in more detail (21,23).

3.2 Lipid metabolism

3.2.1. Liver lipid metabolism

The liver is the largest internal organ and crucial for the regulation and distribution of carbohydrates, lipids and proteins. Apart from hepatocytes (~ 80% of cells), the liver contains immune reactive macrophages (Kupffer cells), natural killer cells (pit cells), endothelial cells and pericytes (stellate cells). It is supplied with blood via the portal vein, which transports nutrients as well as waste products, such as hormones or drugs. The liver is the designated organ for the production and release of bile acids, cholesterol and specific serum proteins, such as albumin. One of the liver's primary functions is the regulation of glucose metabolism. Postprandial insulin signals for excess glucose to be transported into hepatocytes and stored in the form of glycogen. At times of need, these stores are utilized to maintain normoglycemia (24,25).

Systemic lipid metabolism is largely coordinated by the liver. Fatty acids are taken up by transporters (e.g. CD36) on the membranes of hepatocytes, in proportion to their concentration in the serum. Within the cell, they are bound by fatty acid binding proteins and either oxidized or processed to form neutral lipids. Fatty acid oxidation (β -oxidation) takes place in the mitochondria, or in the case of very long chain fatty acids, the peroxisomes. During this process, fatty acids are broken down into acetyl-CoA molecules which are then fed into the citric acid cycle, or used to synthesize steroids, such as cholesterol. Incomplete β -oxidation results in the production of ketone bodies as an alternate energy source. The liver is not only capable of breaking down fatty acids, but is also important for fatty acid and TG biosynthesis. After two

acetyl-CoA molecules have been linked, forming malonyl-CoA, a sequence of condensation reactions takes place, ultimately resulting in the biogenesis of long chain fatty acids. These molecules are then linked to glycerol, forming TGs, which are either stored in the liver or released into the blood stream as components of very low density lipoprotein particles (VLDL) (26-28).

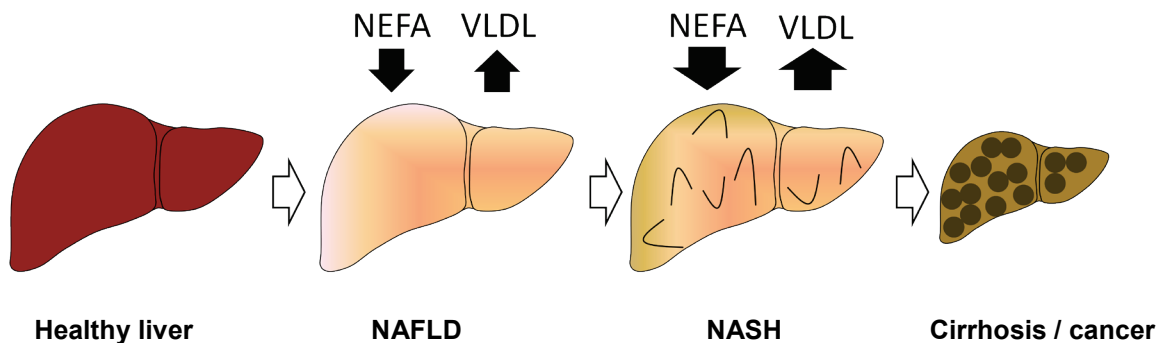


Fig. 4: Progression of fatty liver disease. In obesity and insulin resistance, the liver accumulates increasing amounts of fat, as non-esterified free fatty acid (NEFA) uptake is increased and very low density lipoprotein (VLDL) secretion is reduced. This first leads to the development of non-alcoholic fatty liver disease (NAFLD), then to non-alcoholic steatohepatitis (NASH) and in many cases finally to liver cirrhosis and cancer.

Obesity and type 2 diabetes mellitus not only deregulate hepatic glucose, but also lipid metabolism. Due to increased lipolysis in adipose tissue, more non-esterified free fatty acids are imported into the liver and inhibit insulin signalling. As insulin resistance also induces hepatic lipogenesis, the balance of lipid influx versus lipid efflux is disturbed and fat accumulates within hepatocytes. Indeed, non-alcoholic fatty liver disease (NAFLD) is common amongst diabetes patients and represents a hallmark of the Metabolic Syndrome. In many cases, NAFLD leads to scarring of the liver, non-alcoholic steatohepatitis (NASH) and ultimately liver cirrhosis or failure (Fig. 4). As mentioned above, the liver also acts as a sink for lipids released by adipose tissue in cancer cachexia, again inducing hepatic steatosis (22,29,30).

3.2.2. Lipoprotein metabolism and dyslipidemia

TGs and cholesterol are transported through the blood stream by macromolecular complexes known as lipoprotein particles. Their surface is composed of amphipathic phospholipids, which surround a core, containing hydrophobic TGs and cholesterol esters. The particles are classified according to their density, which in combination

with the apolipoprotein composition, determines their further fate. Whilst there are several sub-categories, lipoprotein particles are generally classed in the four major categories stated below (Tab. 1) (31).

Lipoprotein species	Abbreviation	Primary apolipoprotein	Triglyceride content [%]	Cholesterol content [%]
High density	HDL	ApoA I-V	~ 7.5	~ 20
Low density	LDL	ApoB100	~ 7.5	~ 45
Very low density	VLDL	ApoB100	~ 70	~ 7.5
Chylomicrons	Chylo.	ApoB48	~ 90	~ 5

Tab. 1: Characteristics of different lipoprotein species (Adapted from Ginsberg et al. 2004).

Chylomicrons are lipoprotein particles which contain TGs and cholesterol originating from food. They are produced by the intestine and provide muscle and adipose tissue with energy. Their major protein component is apolipoprotein B (ApoB) 48, an isoform containing 48% of the full-length ApoB coding sequence. Once they have been depleted of TGs, their remnants are taken up by the liver (32). Very low density lipoproteins (VLDL) have a similar structure, but are synthesized endogenously by the liver and released into the blood stream. VLDL assembly takes place in the endoplasmatic reticulum (ER) and is strictly regulated by TG availability and regulatory proteins such as microsomal TG transport protein (MTP). During biosynthesis of full length ApoB100, the main protein component of VLDL, TGs and cholesterol are added to the particles, which are then secreted by the liver (33). Circulating VLDL is hydrolyzed by lipoprotein lipase (LPL), providing adipose tissue and muscle with energy in the form of fatty acids. Consequently, the density of the particles increases, apolipoproteins are exchanged and low density lipoprotein particles (LDL) are formed and recycled by the liver. Excess cholesterol is removed from the periphery by high density lipoprotein particles (HDL) that originate from the liver. In a process referred to as reverse cholesterol transport, these particles scavenge cholesterol and deliver it to the liver for processing. Uptake is primarily performed by low density lipoprotein receptor (LDLR) that has high affinity for apoprotein E (ApoE), a component integrated into HDL and LDL (34,35).

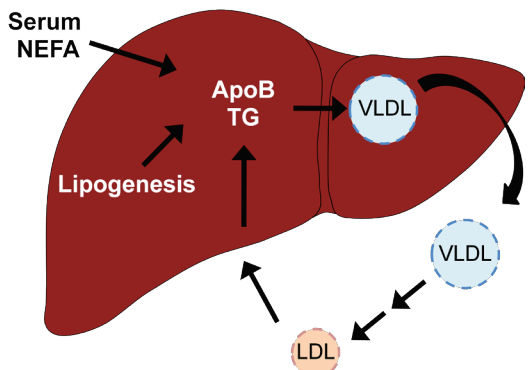


Fig. 5: Very low density lipoprotein metabolism. Very low density lipoprotein (VLDL) particles are generated in the liver. Output is coordinated by apolipoprotein B (ApoB) synthesis, intracellular triglyceride (TG) content, the rate of lipogenesis and import of non-esterified free fatty acids (NEFA) and low density lipoprotein (LDL) particle remnants from the serum. All these stimuli are increased in obesity and type 2 diabetes mellitus. Adapted from Ginsberg et al. 2004.

Dyslipidemia describes a pathogenic condition characterized by deregulated, usually elevated, blood lipid content. In obese and insulin resistant individuals, lipoprotein metabolism is disturbed, primarily due to increased VLDL secretion by the liver. This is most likely due to elevated serum fatty acid levels, excess TGs resulting from enhanced hepatic lipogenesis and increased uptake of TG containing chylomicron and VLDL remnants (Fig. 5). Indeed, insulin resistant patients display a characteristic pro-atherogenic lipoprotein profile defined by elevated LDL and VLDL TG levels in combination with reduced HDL content. Such a profile not only accelerates the onset of insulin resistance, but also favours the manifestation of cardiovascular disease and atherosclerosis (36,37). Over time, excess VLDL is processed by cholesteryl-ester transfer protein (CETP). TGs and cholesterol are thereby exchanged between VLDL and HDL, leading to a reduction of 'good', cholesterol scavenging HDL and an accumulation of 'bad' small dense cholesterol containing LDL particles. These LDL particles are pathogenic, due to their reduced affinity for hepatic lipoprotein transporters, a higher capacity of binding to arterial walls and increased susceptibility to oxidation (38,39). Oxidized LDL can no longer be cleared by the liver. Instead, it is removed by macrophages via phagocytosis. Due to their morphology, the resulting cells are referred to as foam cells. Over time they enter and accumulate in the arterial wall and form atherosclerotic plaques due to an inflammatory response. Consequently, blood flow is reduced, increasing the risk of infarctions in the heart, brain or other vital organs (40).

3.3 Cellular signalling

3.3.1. Transcriptional regulation

The ability to recognize external signalling molecules and to coordinate a precise intracellular response has been a prerequisite for the evolution of multi-cellular life. Over time, complex cellular machinery encompassing cell-surface receptors, activators, enzymes and substrates has evolved and become essential for relaying extracellular messages to intracellular effectors. Dynamic formation of signal-dependent protein structures, rapid signal transduction via preassembled multi-protein complexes, sub-cellular localization and temporal availability, have thereby proven to be crucial for efficient signalling (41). Signals are transmitted by numerous mechanisms, predominantly leading to conformational changes or protein modifications. Phosphorylation of proteins, for example, may deem them accessible for interaction partners or render them functionally active. Once a signal has reached the nucleus, it often induces changes in the cell's transcriptional profile. This process is primarily governed by transcription factors that bind directly to DNA. The mammalian genome contains almost 1000 individual transcription factors that, in combination with the basal transcriptional machinery, DNA binding factors, chromatin remodelling complexes, co-factors and histone modifying enzymes, precisely regulate gene expression (42,43).

Nuclear receptors are a subset of transcription factors that are activated by ligand binding and act as a direct link between the extracellular environment and gene expression. The ligands are small molecules such as steroid hormones, bile acids or lipids. They enter the cell and its nucleus via diffusion or translocation. As far as we know, the human genome encodes 48 nuclear receptors. All of them have a characteristic structure, consisting of an N-terminal activation domain, a conserved central DNA-binding domain and a C-terminal ligand binding domain (44). Nuclear receptors have precise tissue-specific expression patterns and only bind to prototypic DNA sequences (response elements), usually upstream of a target gene's promoter (45). Due to their tissue-specificity and their crucial relevance in governing energy metabolism, nuclear receptors have long been in the focus of biomedical research.

Synthetic peroxisome proliferator activated receptor (PPAR) γ ligands (rosiglitazones) effectively counteract insulin resistance and dyslipidemia. However, as rosiglitazones have severe side-effects other nuclear receptors are being investigated as potential drug targets. The PPAR δ ligand GW501516, for example, has shown very promising results regarding systemic glucose and lipid homeostasis and is currently being tested in phase I clinical trials (46).

Nuclear receptors and transcription factors do not act alone in controlling gene expression, but instead are components of large multi-protein regulatory complexes. These complexes regulate DNA accessibility and subsequently transcriptional capacity. Chromatin structure depends on DNA methylation status, chromatin composition and the presence of histone modifications. By adding or removing specific residues to histone tails, chromatin remodelling enzymes determine how densely or loosely chromatin is packed. In this context, histone deacetylation leads to tightly packed inaccessible chromatin and histone hyperacetylation loosens the structure and facilitates transcription (47). Chromatin remodelling enzymes are recruited to the vicinity of DNA by co-regulators that induce transcriptional activation (co-activators) or repression (co-repressors). Nuclear receptor co-repressor (N-CoR) and silencing mediator for retinoid and thyroid hormone receptors (SMRT) are two prototypical co-repressors with high sequence homology (48,49). Both contain a bipartite nuclear receptor interaction domain, but can also interact with conventional transcription factors. The co-repressors are at the centre of large multi-protein complexes containing the enzymatic component histone deacetylase (HDAC) 3. By removing acetyl residues from histone tails, this enzyme uncovers positively charged surfaces that interact with the negatively charged DNA and compress the chromatin structure (Fig. 6). N-CoR and SMRT bind unligated nuclear receptors, thereby inhibiting transcription. When a ligand binds to the nuclear receptor, the co-repressor is dismissed and co-activators and histone acetyl transferases (HAT) interact with the nuclear receptor. Subsequently chromatin is remodelled into the loose, accessible form (Fig. 6). Often, active mechanisms such as phosphorylation or ubiquitin dependent dismissal are required to enable the switch from a repressive to an active state. This process is known as de-repression. Nuclear receptors and co-regulators have been implicated in the development of several metabolic disorders

and cancer entities, making them attractive targets when trying to understand and combat these diseases (42,50,51).

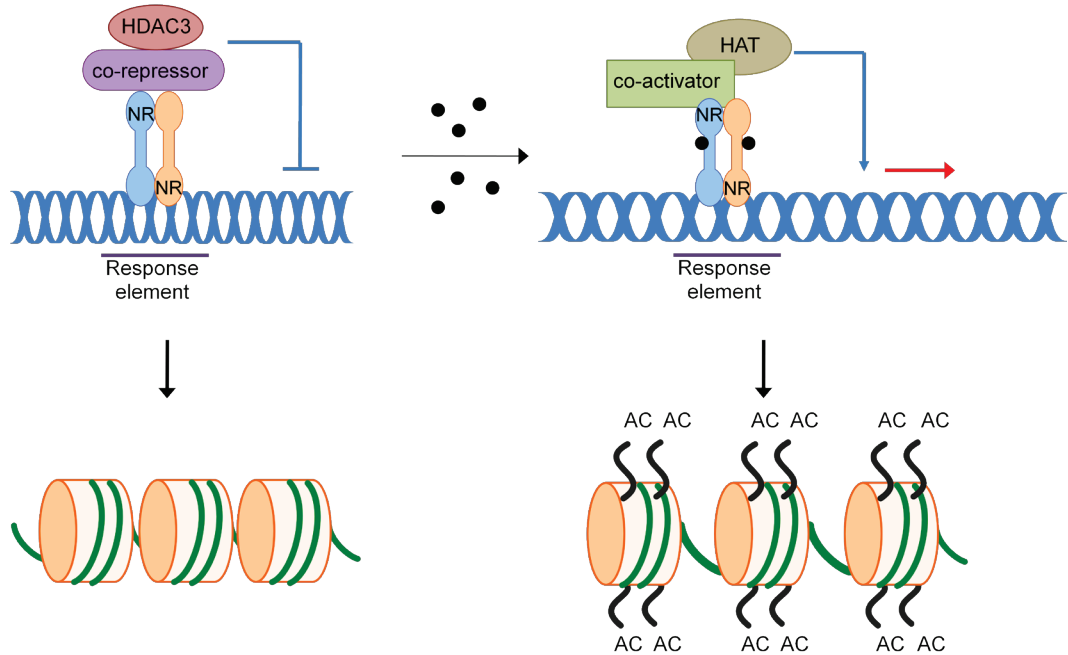


Fig. 6: Transcriptional control. Unligated nuclear receptors (NR) are bound to co-repressor complexes that recruit histone deacetylase (HDAC) 3, leading to hypoacetylated, tightly packaged DNA. Upon ligand binding, the co-repressive structures are dismissed. Co-activators and histone acetyl transferases (HAT) are recruited, leading to hyperacetylated (AC), accessible chromatin.

3.3.2. Transducin beta like 1 and transducin beta like 1 related

Transducin beta like 1 (TBL1) is a gene located on the human X-chromosome. It was initially described in the context of sensorineural deafness, a hearing disorder that occurs primarily in middle aged men and is associated with deletions in the TBL1 gene (52,53). TBL1 shares almost 90% sequence homology with another protein, transducin beta like 1 related (TBLR1). Structurally, both proteins possess an N-terminal LisH domain, followed by an F-Box domain and six C-terminal WD40 repeats which form a propeller structure. TBL1 and TBLR1 directly interact with the N-CoR/SMRT N-termini via their LisH domains and are involved in the repression of gene expression (54). The co-repressors interact with histones H2A, H3 and H4, making them accessible for HDAC3, which is also incorporated in the N-CoR/SMRT complex. Subsequently, histones are hypoacetylated and transcription is repressed (55-57). Interestingly, TBL1 and TBLR1 are not only required for repression, but also

for signal-dependent dismissal of co-repressors and subsequent activation of gene expression. Both proteins serve as E3 ubiquitin ligases that recruit E2 ubiquitin conjugating enzymes, such as UbcH5-E2, leading to ubiquitination and ultimately degradation of co-repressors by the proteasome. Furthermore, TBL1 and TBLR1 have been shown to actively recruit co-activators including Rip140 and CBP, hence their description as nuclear receptor co-repressor / co-activator exchange factors (58) (Fig. 7).

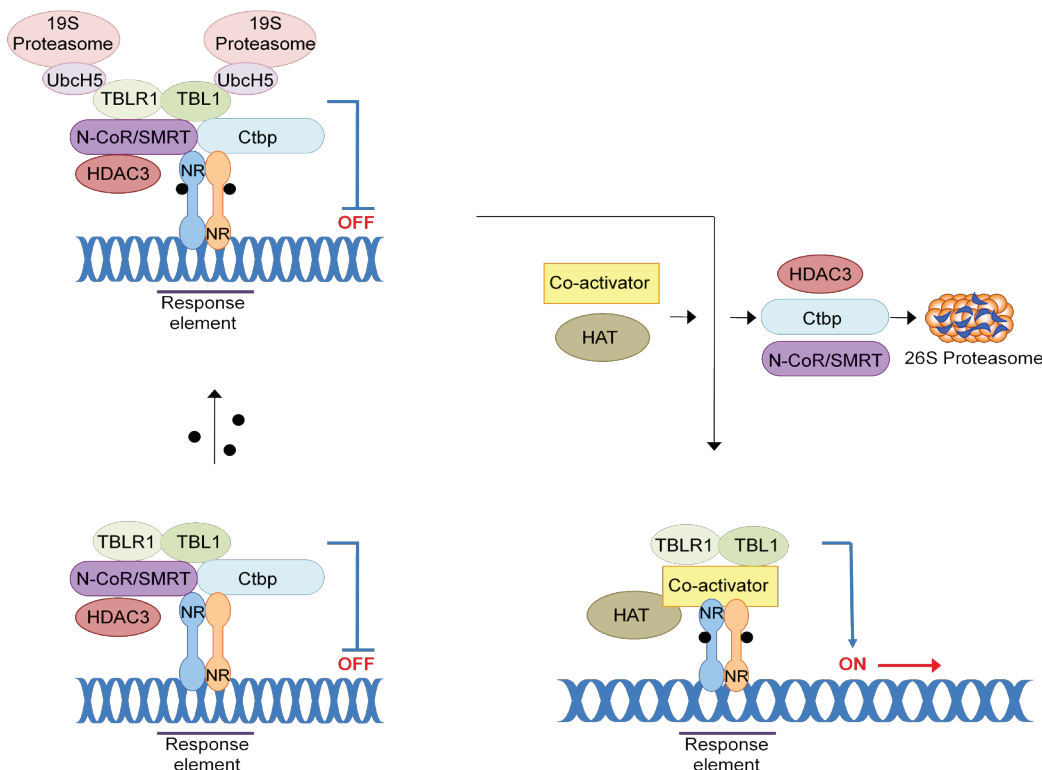


Fig. 7: Nuclear receptor co-repressor / co-activator exchange factors TBL1 and TBLR1. Unligated nuclear receptors (NR) are associated with co-repressor complexes containing N-CoR/SMRT, Ctbp, HDAC3, TBL1 and TBLR1. Upon ligand binding, TBLR1 recruits the E2 ubiquitin conjugating enzyme UbcH5 to N-CoR/SMRT. TBL1 targets the same enzyme to Ctbp. UbcH5 interacts with the 19 S proteasome and subsequently, the co-repressor complexes are dismissed and degraded by the 26 S proteasome. TBL1 and TBLR1 then actively recruit co-activator complexes and histone acetyl transferases (HAT).

Initially TBL1 and TBLR1 were considered to be functionally redundant. Recent studies have however shown that they have distinct functions, primarily regulated by phosphorylation sites specific to one or the other protein. In this regard, TBLR1 for example seems to be the ubiquitin ligase required for de-repression of N-CoR/SMRT, whilst TBL1 is required to dismiss the co-repressor C-terminal-binding protein (Ctbp) (Fig. 7). Many genes are repressed by both N-CoR/SMRT and Ctbp at the same time,

implementing a dual checkpoint to be passed during signal dependent gene activation (59). Nuclear receptors are not the only transcription factors regulated by TBL1 and TBLR1. Several other pathways, including the canonical wnt signalling cascade have also been linked to the two co-factors. Indeed, TBL1 and TBLR1 have been shown to recruit the wnt associated protein β -catenin to hypoacetylated target gene promoters and facilitate gene expression driven by the transcription factor TCF. The direct interaction with TBL1 and TBLR1 furthermore protects β -catenin against ubiquitin dependent proteasomal degradation, as the binding site for E2 ubiquitin conjugating enzymes is hidden. Wnt signalling promotes cell proliferation and can induce tumour formation, implying that TBL1 and TBLR1 may be involved in this process (60-62).

It was recently shown that TBL1 and TBLR1 play a crucial role in the regulation of hepatic lipid metabolism. Mice lacking the two proteins in their livers develop severe hypertriglyceridemia and hepatic steatosis, as *de novo* lipogenesis in the liver is increased and β -oxidation is reduced (63). To understand the mechanisms underlying this phenotype in more detail, it is necessary to identify and investigate proteins that interact with TBL1 and TBLR1 in the liver.

4. AIM OF THE STUDY

The Metabolic Syndrome affects a large part of the world wide population and its prevalence is ever increasing. In recent years it has become more and more evident that both environmental and genetic parameters influence the integrity of transcriptional networks that are crucial in maintaining a healthy metabolic status. The precise molecular mechanisms are however still largely enigmatic.

The aim of this study was to perform a luminescence-based mammalian interactome mapping (LUMIER) screen and discover novel interaction partners of TBL1 and TBLR1, two proteins known to play important roles in the regulation of liver lipid homeostasis. After identifying and confirming a new TBL1 / TBLR1 interaction partner, we intended to functionally characterize the relevance of this novel target gene by employing *in vivo* loss and gain of function studies. Furthermore, the regulation of the novel TBL1 / TBLR1 interacting protein was to be investigated in various models of metabolic stress and dysfunction. The experimental design is described in Fig. 8.

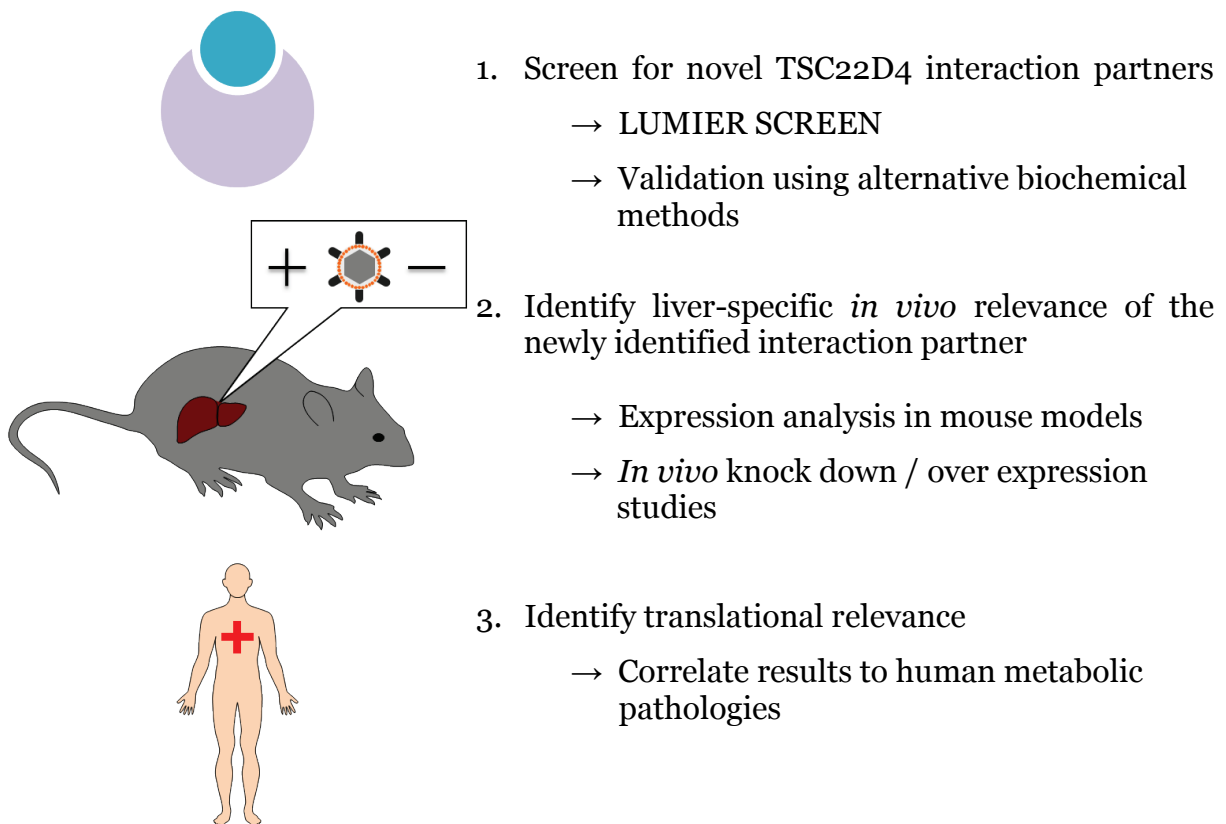


Fig. 8: Experimental design overview

5. RESULTS

5.1 TSC22D4 is a novel TBL1 and TBLR1 interaction partner

5.1.1 Luminescence-based mammalian interactome mapping (LUMIER) screen for novel TBL1 and TBLR1 interacting proteins

Both TBL1 and TBLR1 have been shown to play important roles in hepatic lipid metabolism (63). In this regard, liver-specific ablation of either protein leads to the development of hepatic steatosis and hypertriglyceridemia. Further, TBL1 expression is not only reduced in diabetic animal models, but also inversely correlates with liver TG content in humans suffering from non-alcoholic steatohepatitis (NASH).

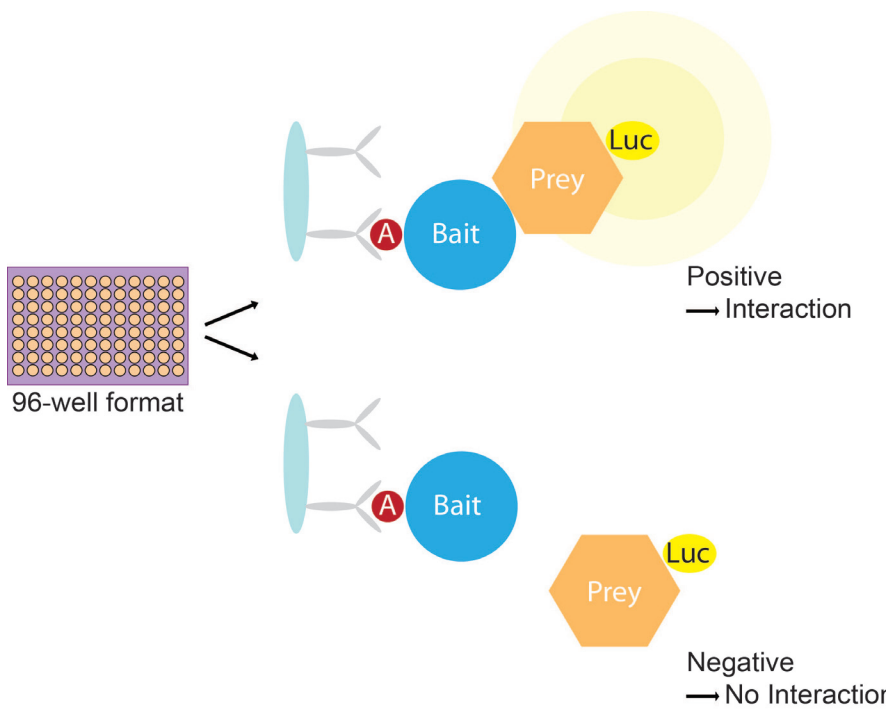


Fig. 9: Luminescence-based mammalian interactome mapping (LUMIER). Prey proteins were cloned into a reporter construct expressing Renilla Luciferase and co-transfected into HEK293T cells with a library of Protein-A tagged nuclear proteins in a 96 well format. Positive protein-protein interactions resulted in measurable luciferase activity above background after protein purification using IgG coated magnetic beads. If no interaction took place, the luciferase-tagged bait was lost during washing and no signal above background was detected.

In order to further investigate the precise mechanisms by which TBL1 and TBLR1 partake in transcriptional control and the regulation of metabolic processes, it is important to identify and characterize their associated proteins. To this end, a luminescence-based mammalian interactome mapping (LUMIER) screen was employed to identify novel TBL1 and TBLR1 interaction partners. Using this high

throughput co-immunoprecipitation procedure, it was possible to rapidly screen for protein-protein interactions in a mammalian system (64). HEK293T cells were co-transfected with Renilla Luciferase-tagged TBL1 or TBLR1 and a library of 605 different nuclear proteins fused to a Protein-A tag. After cell lysis and purification of the Protein-A-tagged bait using IgG beads, positive interactions were identified by measuring the luciferase signal, after the addition of luciferin. Only if the bait and prey proteins interacted, could luminescence be detected. The well characterized interactions between FOS and JUN, as well as TBL1 and TBLR1, served as positive controls, for assay integrity. A model for the experimental set-up employed in this study is shown in Fig. 9.

The luciferase signals resulting from the positive control reactions were significantly above background, demonstrating that true interactions could be detected using the LUMIER method (Fig. 10A). These values also served as references when judging the results obtained during screening and determining cut-off values, above which an interaction was considered to be likely. Luciferase-tagged TBL1 co-precipitated with several members of the nuclear protein library, resulting in luminescence signals significantly above background. The strongest interactions were observed with the proteins CRTC1, MAFK, NRF1, RRM2, RYBP TRIM27, TRIM32, TSC22D1, TSC22D4, VGLL1, WRNIP1 and ZFP36L2 (in alphabetical order). The highest luciferase signal was thereby detected after co-transfection of tagged TBL1 and TGF β stimulated clone (TSC) 22 domain family, member 4 (TSC22D4; Fig. 10A).

To verify the obtained results, the assay was repeated several times with the twelve top scoring candidate proteins. In all cases a strong interaction between TSC22D4 and TBL1 was detected (Fig. 10B). Indeed, the TBL1-TSC22D4 interaction consistently delivered stronger signals than both the FOS-JUN and the TBL1-TBLR1 positive control assays, indicating that this interaction is true and worthy of further investigation.

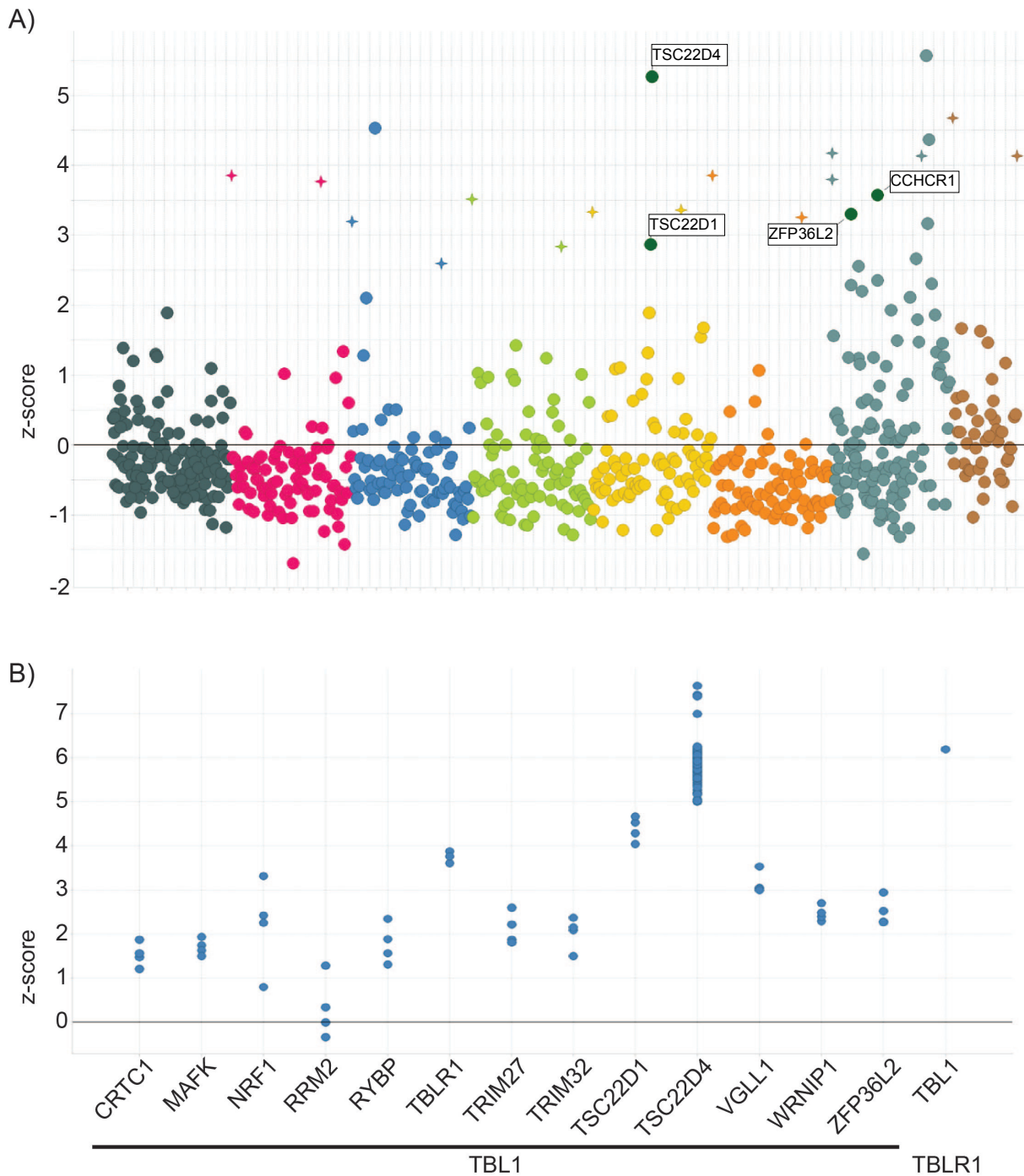


Fig. 10: Novel TBL1 interaction partners were identified by LUMIER screen. LUMIER assays were performed with luciferase-tagged TBL1 and an array of 605 different nuclear protein expression constructs. The Y-axis represents z-scores and colours indicate individual 96-well plates. Stars represent TBL1- TBLR1 binding as a positive control. Selected hits, including the interaction between TBL1 and TSC22D4, are labeled (A). The top hits resulting from the TBL1-screen were re-assessed and the interaction between TBL1 and TSC22D4 was verified in several independent experiments. Each blue spot represents an individual assay (B).

Next, the LUMIER screen was performed using luciferase-tagged TBLR1 as prey and the same library of Protein-A tagged nuclear proteins as bait. As TBL1 and TBLR1 share over 90% protein sequence homology (65), it is likely that they posses certain common interaction partners. As expected, a strong interaction between TBLR1 and TSC22D4 was observed in the screen. The obtained luciferase signals were again significantly higher than those resulting from the positive controls, strengthening the notion that TSC22D4 is incorporated in complexes harbouring TBL1 and TBLR1 (Fig. 11).

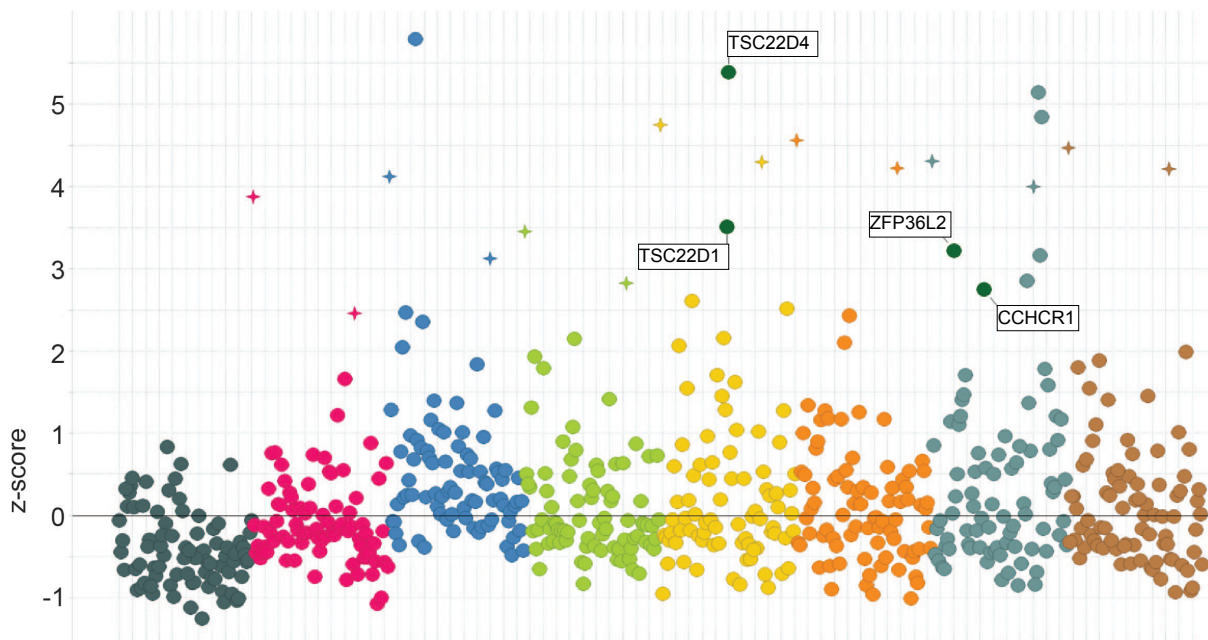


Fig. 11: Novel TBLR1 interaction partners were identified by LUMIER screen. LUMIER assays were performed using luciferase-tagged TBLR1 and a library consisting of 605 nuclear proteins. The Y-axis represents z-scores and colours indicate individual 96-well plates. Stars represent TBL1- TBLR1 binding as a positive control. Selected hits, including the interaction between TBLR1 and TSC22D4, are labeled.

Little is known about the *in vivo* characteristics and tissue-specific importance of TSC22D4 and no studies have so far described this gene in a metabolic context. The protein has however, like TBL1 and TBLR1, been shown to be involved in transcriptional repression (66), making it an interesting candidate for further *in vivo* analysis. Before investigating the functional relevance of TSC22D4, it was however first necessary to further verify the interaction with TBL1 and TBLR1 using multiple biochemical methods.

5.1.2. Verification of the interaction between TSC22D4 and TBL1 / TBLR1 by Flag co-immunoprecipitation

Flag co-immunoprecipitation studies were performed to prove that the newly identified interaction between TBL1, TBLR1 and TSC22D4 was true. In this setting, it was important to use different affinity tags to those used in the LUMIER assays, to exclude that the Renilla Luciferase and Protein-A polypeptide sequences had influenced heterodimer formation and led to false positive results during screening. HEK293 cells were co-transfected with Flag-tagged TBL1, Flag-tagged TBLR1 or the Flag-tag alone in combination with Myc-tagged TSC22D4. After cell lysis, the Flag-tagged proteins were immunoprecipitated using an anti-Flag affinity resin. Only in the presence of the Flag-TBL1 or Flag-TBLR1 fusion-proteins, was it possible to co-precipitate Myc-TSC22D4, supporting the notion that TSC22D4 and TBL1 / TBLR1 interact with one another (Fig. 12).

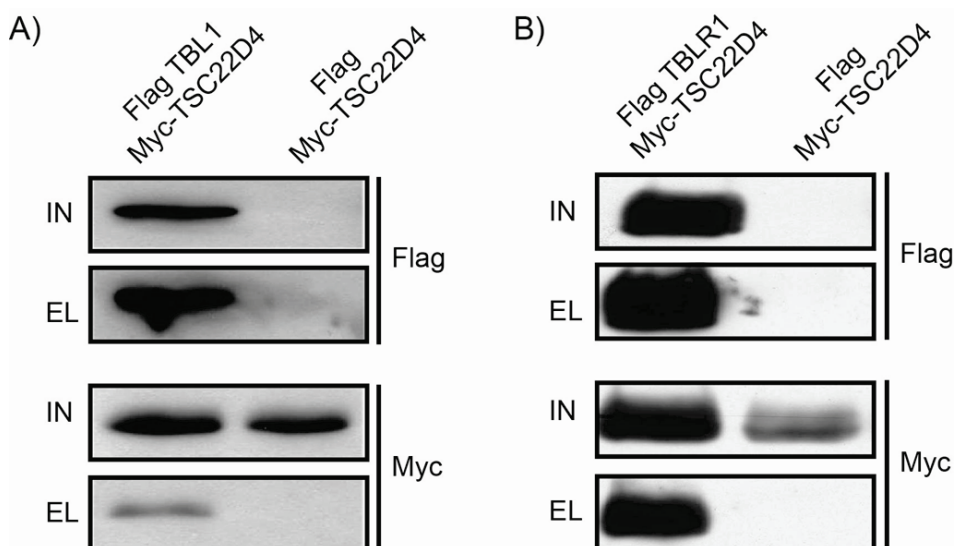


Fig. 12: TSC22D4 co-precipitates with TBL1 and TBLR1 in Flag co-immunoprecipitation studies. For co-immunoprecipitation studies, HEK293 cells were transfected with Myc-TSC22D4 and a vector encoding either the control Flag peptide, Flag-TBL1 (**A**) or Flag-TBLR1 (**B**). Affinity purification was performed with an anti-Flag antibody. Bound proteins were resolved by SDS-PAGE and subsequently detected by Western blot. IN: Input; EL: Elution.

5.1.3. TSC22D4 interacts directly with the TBL1 / TBLR1 WD40 domains

Both LUMIER assays and Flag co-immunoprecipitation studies do not clearly distinguish between direct and indirect protein-protein interactions. As experiments are performed in the presence of all proteins expressed in the cell line of choice, it cannot be excluded that specific cellular proteins are required to link the identified novel interaction partners. GST-pull down assays were carried out to investigate whether the interaction between TSC22D4, TBL1 and TBLR1 is of direct nature, or if further components are required for their association. These experiments are performed *in vitro*, meaning that further cellular proteins are not present in the reaction mix and only direct interactions can be detected. One protein partner is fused to a GST-tag, expressed in bacteria and affinity purified using a glutathione matrix. The other protein of interest is *in vitro* transcribed and translated in the presence of ^{35}S -radiolabeled methionine. The two proteins are subsequently incubated together. After purification on a glutathione matrix via the GST-tag, it is possible to detect the radiolabeled protein by autoradiography, if the proteins directly interact and co-precipitate.

First, the GST-peptide alone (negative control), GST-tagged full length TBL1 and the TBL1 LisH, F-Box and WD40 domains were incubated with radiolabeled full-length TSC22D4. Whilst no signal could be detected in the negative control lane, full-length GST-TBL1 did pull-down TSC22D4. This was also the case for the WD40 domain, but not the isolated LisH or F-Box domains (Fig. 13).

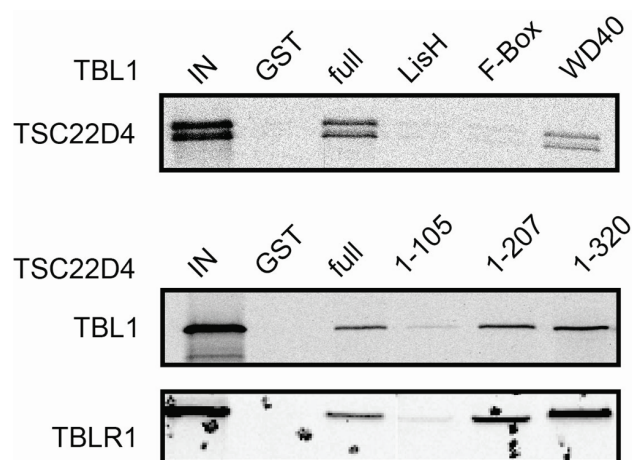


Fig. 13: TSC22D4 interacts directly with TBL1 and TBLR1. GST-pulldown assays were performed with full length or truncated versions of TSC22D4, TBL1 or TBLR1 fused to GST and GST alone as a negative control. GST fusion proteins were incubated with radiolabeled *in vitro* translated full length TBL1, TBLR1 or TSC22D4 protein. Bound proteins were resolved by SDS-PAGE and visualized by autoradiography. Input lanes represent 20% of the input. IN: Input.

In order to map the interaction in more detail, the experiment was then performed in reverse orientation. GST-tagged TSC22D4, or GST-tagged deletion constructs, consisting of the N-terminal 105, 207 or 320 amino acids were incubated with 35 S-radiolabeled full-length TBL1. No signal was detected in the negative control assay, in which TBL1 was incubated with the GST peptide alone. As expected, full-length GST-TSC22D4 successfully pulled down full-length radiolabeled TBL1. When TBL1 was incubated solely with the N-terminal 105 amino acids of TSC22D4, no interaction was observed, whilst the longer deletion constructs were sufficient to precipitate the interaction partner (Fig. 13), indicating that the sequence between amino acids 105 and 207 is crucial for the interaction to take place.

To assess if TBLR1 also directly interacts with TSC22D4, or if TBL1 may act as an intracellular bridging protein, we incubated radiolabeled TBLR1 with full-length GST-TSC22D4 or one of the three TSC22D4 deletion constructs. Again, we observed that the full-length proteins interacted and that the TSC22D4 domain ranging from amino acids 105 to 207 was required for the effective interaction (Fig. 13). The TSC22D4 N-terminus alone did not suffice.

In summary, these data demonstrate a direct interaction between the TBL1 / TBLR1 C-terminal WD40 domains and the TSC22D4 mid-domain (amino acids 105 to 207) (Fig. 14). As both TBL1 and TBLR1 are known to play important roles in liver metabolism (63), we decided to further investigate the functional relevance of their novel interaction partner, TSC22D4, in regard to its potential involvement in the pathogenesis of, or protection against, metabolic disorders.

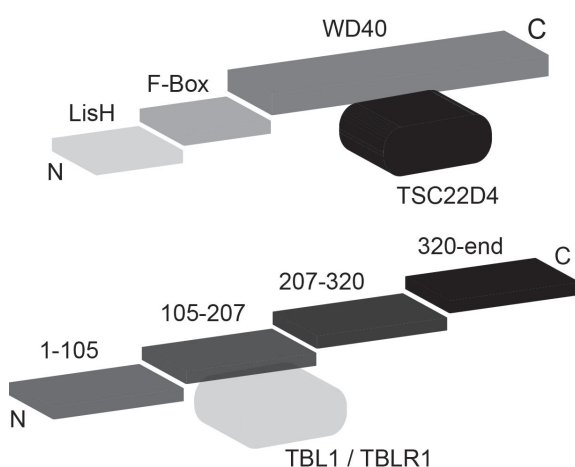


Fig. 14: Mapping the interaction between TSC22D4, TBL1 and TBLR1. Model of the direct interaction between the mid-domain of TSC22D4, ranging from amino acids 105 to 207 and the TBL1 / TBLR1 WD40 domain.

5.2 Analysis of hepatic TSC22D4 expression in mouse disease models

5.2.1. TSC22D4 is expressed ubiquitously throughout the mouse body

In order to investigate the expression of TSC22D4, TBL1 and TBLR1 throughout the body, we analyzed the presence of all three proteins in various mouse tissues by Western blot. This analysis served as a reference when deciding which organ to focus on in future *in vivo* experiments. TSC22D4 was expressed in all tissues analyzed, albeit at varying levels (Fig. 15 panel 1). Expression was particularly high in the liver and inguinal fat, both important tissues for the regulation of energy metabolism.

TBL1 and TBLR1 were however not present in all organs. Interestingly, in some tissues both proteins were mutually expressed, whilst only one of the highly related proteins seemed to be translated in others, indicating that the two genes are not functionally redundant, but have tissue specific functions. Concerning metabolically important organs, TBL1 was expressed to a higher extent in liver, pancreas and brown adipose tissue (BAT), whilst in abdominal fat TBLR1 was almost exclusively expressed (Fig. 15 panel 2, 3).

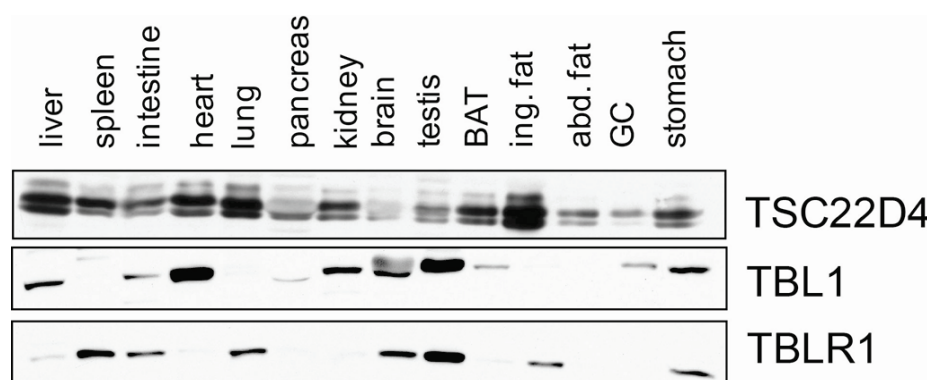


Fig. 15: Tissue specific expression of TSC22D4, TBL1 and TBLR1.
Protein lysates from mouse liver, spleen, intestine, heart, lung, pancreas, kidney, brain, testis, brown adipose tissue (BAT), inguinal fat, abdominal fat, gastrocnemius muscle (GC) and stomach were assessed in regard to TSC22D4, TBL1 and TBLR1 expression. Proteins were separated by SDS-PAGE and subsequently detected by Western blot using TSC22D4, TBL1 and TBLR1 antibodies

As TSC22D4 is highly expressed in the liver and its novel interaction partners TBL1 and TBLR1 have been shown to be deregulated in diabetic and pre-diabetic settings (63), liver samples taken from mouse models of metabolic stress and disease conditions were assessed in regard to TSC22D4 expression.

5.2.2. TSC22D4 expression is not changed upon fasting

During fasting, blood sugar levels fall, insulin secretion by the pancreas is inhibited and the pancreatic alpha cells, which are located in the islets of Langerhans, produce the hormone glucagon to maintain normoglycemia. Glucagon can bind to hepatocytes via the glucagon receptor and stimulate glycogen breakdown (glycogenolysis), glucose production (gluconeogenesis) and consequently glucose release from the liver. Upon feeding, external glucose is made available and subsequently pancreatic glucagon release is suppressed, whilst insulin secretion is induced. In obesity, this tightly regulated circuit is impaired and glucose is also released from the liver in the fed state, leading to hyperglycaemia (14).

To test if TSC22D4 expression is regulated in response to nutritional restriction, mice were fasted for 24 hours. After starvation, one group of animals was sacrificed immediately and the other mice were fed for 6 hours. Hepatic TSC22D4 mRNA expression was determined by quantitative PCR (Fig. 16). There was no change in TSC22D4 mRNA levels in response to fasting or refeeding, indicating that food restriction does not act as a signal controlling the expression.

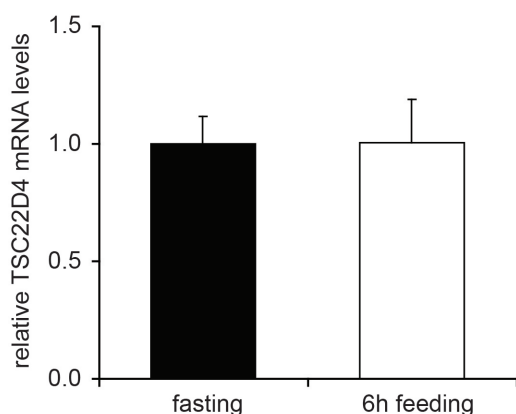


Fig. 16: TSC22D4 expression is not regulated by fasting. RNA was extracted from the livers of mice fasted for 24 hours and either directly sacrificed, or refed for 6 hours after fasting. (n=6), (means ± SEM).

5.2.3. TSC22D4 expression is not changed in the New Zealand Obese mouse model

Mouse models of obesity and type 2 diabetes are commonly used to investigate the relevance of specific genes and external factors in metabolism. The New Zealand Obese (NZO) mouse represents a polygenic model of diabetes. The strain originally resulted from spontaneous mutations during breeding of lean New Zealand Black (NZB) mice. As several genes are responsible for the diabetic phenotype displayed by these animals, they model the development of the Metabolic Syndrome in humans very well. The mice are characterized by a high birth weight, glucose intolerance and hypertension (67). To assess if TSC22D4 expression is influenced by the obese phenotype, hepatic RNA was isolated and the abundance of TSC22D4 mRNA was assessed. A difference in TSC22D4 expression could not be detected (Fig. 17).

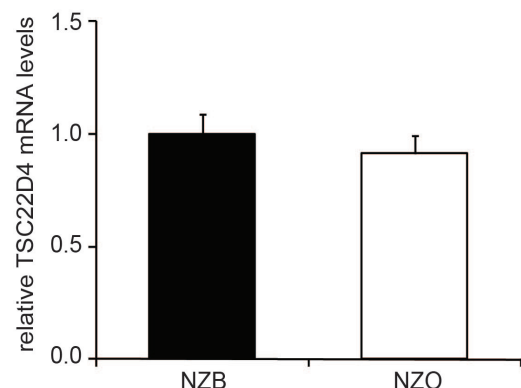


Fig. 17: TSC22D4 expression is not changed in New Zealand Obese mice. RNA was extracted from the livers of lean New Zealand Black (NZB) and diabetic New Zealand Obese (NZO) mice. TSC22D4 expression was subsequently determined by quantitative PCR. (n=6), (means ± SEM).

5.2.4. TSC22D4 expression is reduced in leptin deficient mice

In the fed state, the hormone leptin is secreted by adipocytes and transported to the hypothalamus via the blood stream. In the brain, it serves as a neuroendocrine signal for satiety and leads to appetite suppression. Furthermore, leptin regulates the metabolic rate via central mechanisms. Homozygous loss of function mutations in the leptin gene as observed in ob/ob mice (Lep^{ob}), lead to hyperphagia, hyperglycaemia, hyperinsulinemia and subsequently severe obesity and pre-diabetes (68). TSC22D4 gene expression was analyzed in random fed ob/ob and control wild type mice. mRNA levels were significantly (~40%) reduced in the ob/ob mice compared to the

wild type controls, indicating that TSC22D4 could be linked to the onset of obesity (Fig. 18).

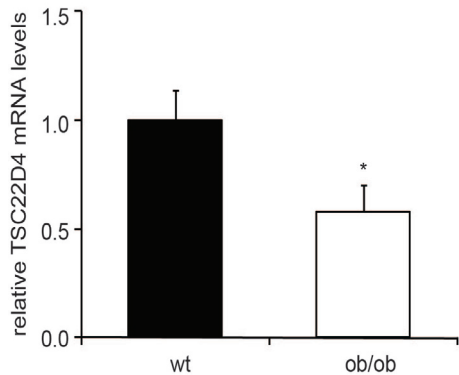


Fig. 18: TSC22D4 expression is reduced in leptin deficient ob/ob mice. RNA was extracted from the livers of lean control and obese ob/ob mice. TSC22D4 expression was subsequently determined by quantitative PCR. (n=4), (means \pm SEM). (*) indicates significance; $p \leq 0.05$.

5.2.5. TSC22D4 expression is reduced in high fat diet fed mice

The majority of type 2 diabetes cases in the human population result from reduced energy expenditure and excessive caloric intake, as associated with a sedentary lifestyle and a diet rich in fat and sucrose. The consumption of excess fat thereby leads to increased fat accumulation throughout the body. Fat is stored in adipose tissue and ectopically in organs, such as the liver, leading to tissue damage. Over time, obese individuals develop glucose intolerance and ultimately type 2 diabetes mellitus (3).

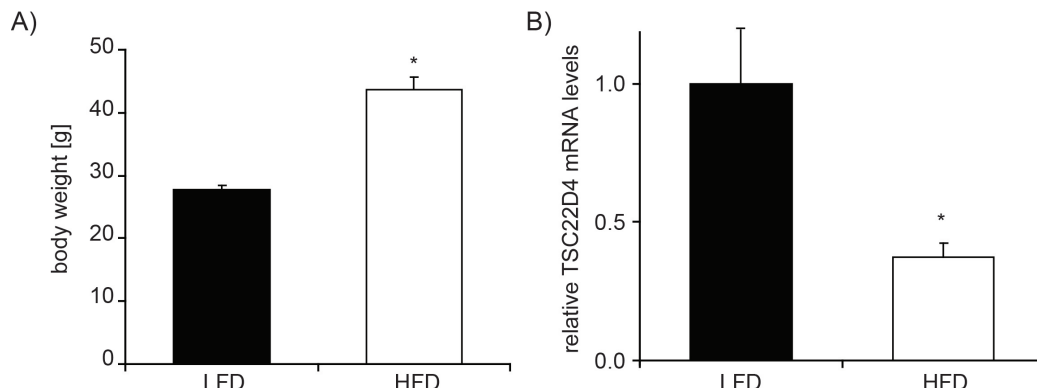


Fig. 19: TSC22D4 expression is reduced in mice upon a high fat diet. Mice were fed a control low fat diet (LFD) or a high fat diet (HFD). Their weight was determined after 9 weeks on the respective diet (**A**). RNA was extracted from the livers of these mice and TSC22D4 expression was subsequently determined by quantitative PCR (**B**); (n=4), (means \pm SEM). (*) indicates significance; $p \leq 0.05$.

The onset of obesity can be modelled by feeding mice a high fat diet over the course of several weeks. On such a diet, the animals gain weight quickly and develop hyperglycaemia, hyperinsulinemia and hypertension (69). TG content increases in the adipose tissue, blood and liver whilst energy expenditure and activity decrease. To assess the consequences concerning TSC22D4 expression, mice were fed either a high fat diet containing 60% energy from fat or a control low fat diet containing 10% energy from fat over a 9 week period. The mice consuming the high fat diet put on significantly more weight (Fig. 19 A) and developed hyperglycaemia (data not shown). Hepatic TSC22D4 expression levels were determined after the mice had been sacrificed (Fig. 19 B). TSC22D4 expression was significantly (~60%) lower in mice fed the high fat diet, further strengthening the notion that TSC22D4 may be involved in the development of obesity and the Metabolic Syndrome.

Consistent with the elevation of counter-regulatory hormonal pathways in insulin resistance, particularly adrenal glucocorticoids (14), chronic exposure of wild-type mice to the anti-inflammatory synthetic steroid dexamethasone for 3 weeks also triggered the inhibition of TSC22D4 mRNA levels (Fig. 20). Glucocorticoids stimulate gluconeogenesis in the liver by binding to the glucocorticoid receptor. Due to their anti-inflammatory properties they are often used as medication to treat inflammatory conditions. A side effect of chronic exposure is however the development of diabetes and hypertension, as they induce an elevation of blood glucose levels (70,71).

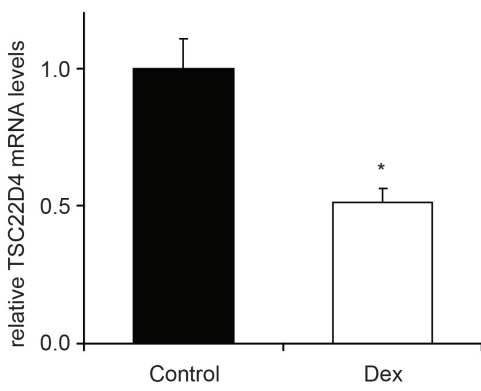


Fig. 20: TSC22D4 expression is reduced in glucocorticoid treated mice. RNA was extracted from the livers of mice injected with 1.2 mg/kg dexamethasone (Dex) intraperitoneally every day for 3 weeks. Control mice received an equal volume saline. TSC22D4 expression was subsequently determined by quantitative PCR. (n=4), (means \pm SEM). (*) indicates significance; $p \leq 0.05$.

Taken together, these results suggest that hepatic TSC22D4 is specifically down-regulated in metabolic stress conditions, as associated with insulin resistant obesity. To further address the role of TSC22D4 in this context, functional experiments

needed to be performed in which TSC22D4 expression was artificially decreased or enforced in the livers of wild type mice.

5.3 Hepatic TSC22D4 knock down leads to elevated serum triglyceride levels in C57BL/6J mice

Adenoviral vectors are commonly used to genetically manipulate mammalian cells, or whole organs. Vectors expressing short hairpin RNAs (shRNA) targeting specific sequences for degradation by the RNA induced silencing complex (RISC) are easy to generate and it is possible to produce large titres, ranging up to 1×10^{12} infectious units per ml. Several different mammalian cell types can be transduced by adenovirus expressing the constitutively active U6-polymerase III promoter. After the shRNA transgene has been transcribed, it forms a stem loop structure which is processed by the cellular RNA interference (RNAi) machinery. During this process, the loop structure is removed and a mature RNAi construct is produced (72). Tail vein injection of adenovirus into mice largely results in the infection of liver cells, as the virus is transported directly to the liver's capillary system. This approach has the advantage that liver specific gene function can be investigated, as other tissues are hardly affected by the transgene. Experiments using adenovirus need to be performed in a specific time window, as the viral genes (especially E2 and E4) expressed after infection lead to an immune response that clears the vector after approximately 14 days. The ideal time point for phenotypic analysis has been shown to be 7 days post infection (71).

5.3.1. Liver specific TSC22D4 knock down using RNA interference

Specific shRNA sequences targeting TSC22D4 were cloned into the Invitrogen pENTR-DEST vector. Their knock down efficiency was tested by co-transfected Hepa 1c1 cells with the shRNAs and a TSC22D4 over expression construct. TSC22D4 depletion was then analyzed by Western blot (data not shown). The most promising sequence was sub-cloned into the second generation Invitrogen pAD-BLOCK-IT vector. The vector contained the majority of the viral genome, but lacked the E1 and

E3 genes required for viral replication (safety feature). Virus was produced by transfecting HEK293A cells, which expressed the missing genes in trans. The resulting replication incompetent adenovirus was purified using the caesium chloride method (71). In order to investigate the effects of reduced TSC22D4 expression in the livers of C57BL/6J mice, 1×10^9 viral particles expressing either a scrambled shRNA sequence (control), or the sequence targeting the TSC22D4 mRNA were administered via the tail vein. Mice were given free access to food and considered random fed. Seven days after injection the animals were sacrificed. Liver, gastrocnemius muscle, kidney and inguinal fat were collected and shock frozen. TSC22D4 knock down efficiency was assessed at RNA level by quantitative PCR and at protein level by Western blot. RNA levels were reduced by approximately 60% (Fig. 21 A). TSC22D4 protein levels (Fig. 21 B) were also significantly lower in the TSC22D4 knock down group than in the control shRNA treated subgroup. To test the tissue specificity of the knock down, TSC22D4 protein expression was also assessed in skeletal muscle and kidney. Expression remained unaffected in both organs (Fig. 21 B). As the viral construct had effectively knocked down TSC22D4, the mice were subsequently thoroughly analyzed in regard to the resulting phenotype. Systemic, as well as, organ specific effects on glucose and lipid metabolism were thereby investigated.

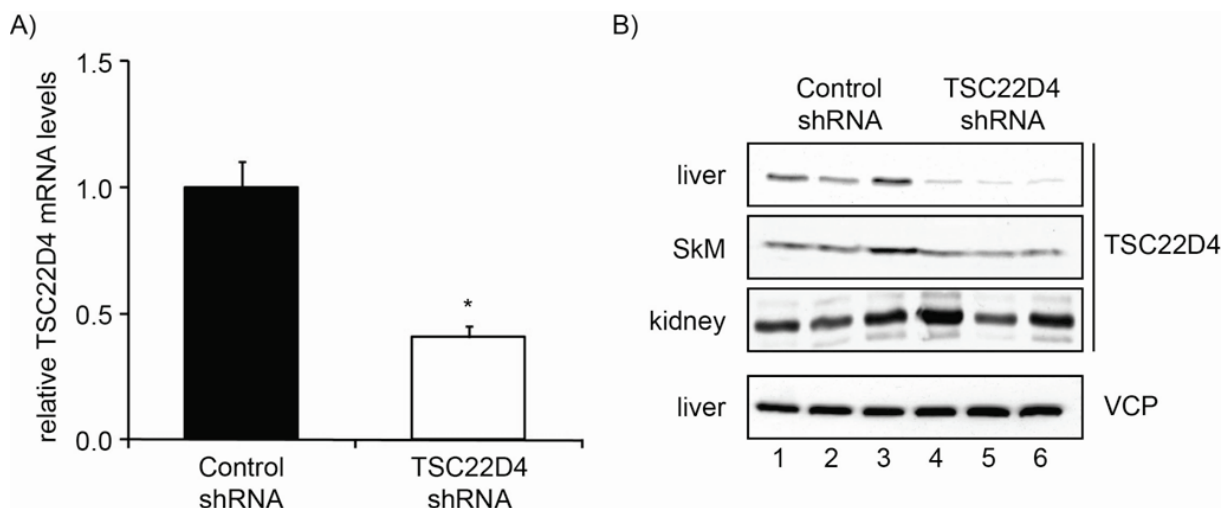


Fig. 21: shRNA mediated knock down of TSC22D4 mRNA and protein. Quantitative PCR analysis of liver RNA extracts from representative control or TSC22D4 shRNA adenovirus-injected C57BL/6J mice 7 days after injection (**A**). Western blot of liver, gastrocnemius skeletal muscle (SkM) and kidney extracts from representative control (lanes 1-3) or TSC22D4 (lanes 4-6) shRNA adenovirus-injected C57BL/6J mice 7 days after injection using TSC22D4 and VCP antibodies (**B**); (n>7), (means ± SEM). (*) indicates significance; p ≤ 0.05.

5.3.2. Phenotypic analysis of TSC22D4 deficient C57BL/6J mice

5.3.2.1. Body weight, liver weight, body fat and lean mass

To assess if TSC22D4 deficiency acutely affects total body weight or fat distribution, mice were weighed before the sacrifice. Furthermore, their body composition was assessed using an Echo MRI body composition analyzer. This device is capable of determining total fat mass, as well as lean mass, consisting of mainly muscles, tendons and connective tissues. No changes in either body weight (Fig. 22 A), fat mass (Fig. 22 C), or lean tissue mass (Fig. 22 D) were measurable 7 days after TSC22D4 shRNA delivery. Liver weight, as determined during preparation of the mice also remained unchanged by TSC22D4 knock down (Fig. 22 B).

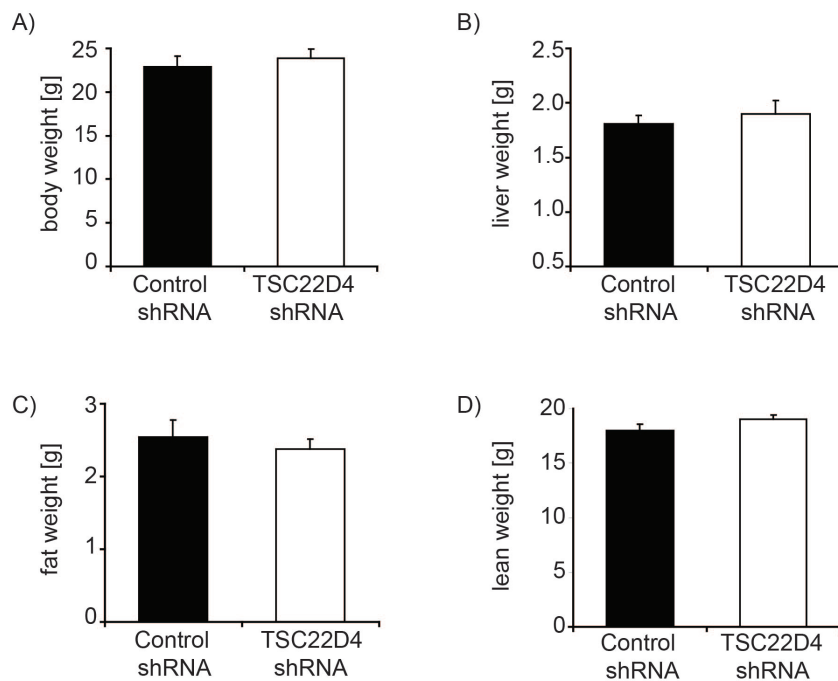


Fig. 22: Body weight and composition are not affected by hepatic TSC22D4 knock down. Body weight (A), liver weight (B), fat (C) and lean (D) mass of mice treated with control or TSC22D4 shRNA adenovirus were determined 6-7 days after infection; ($n \geq 7$), (means \pm SEM).

5.3.2.2. Hepatic glycogen and circulating glucose, insulin and ketone bodies

After consuming food, glucose is taken up into the blood stream and serves as an energy source for the brain. Excess glucose is however stored in the liver, where it is converted to the starch like polymer glycogen. At times in which dietary energy is not available, for example during sleep periods, these stores are utilized to maintain normoglycemia and guarantee energy availability to the brain. This balance in glucose metabolism is tightly regulated by insulin (14). In order to investigate the role

of TSC22D4 in glucose metabolism, blood glucose levels and hepatic glycogen stores were analyzed. Whilst blood glucose remained unaffected (Fig. 23 A), a slight increase in glycogen content was measured in random fed TSC22D4 deficient mice (Fig. 23 B). In line with this observation, serum insulin levels were slightly, albeit not significantly, elevated (Fig. 23 C). In conclusion, these results show that glucose metabolism was not significantly affected by TSC22D4 depletion.

Energy deficiency in the brain has severe consequences for the whole body and keeping this organ nourished is of highest priority. If, during prolonged fasting, blood glucose levels are not sufficient to supply the brain with energy, ketone bodies serve as an alternative energy source. These substances are produced by the liver and are by-products of beta oxidation (fatty acid breakdown). Acetyl-CoA serves as the substrate and the process is known as ketogenesis. In the brain, ketone bodies are broken down to acetyl-CoA and fed into the citric acid cycle to produce energy (73). Levels of circulating ketone bodies remained unaffected by TSC22D4 knock down (Fig. 23 D). In conclusion, these results show that glucose metabolism was not significantly affected by TSC22D4 depletion.

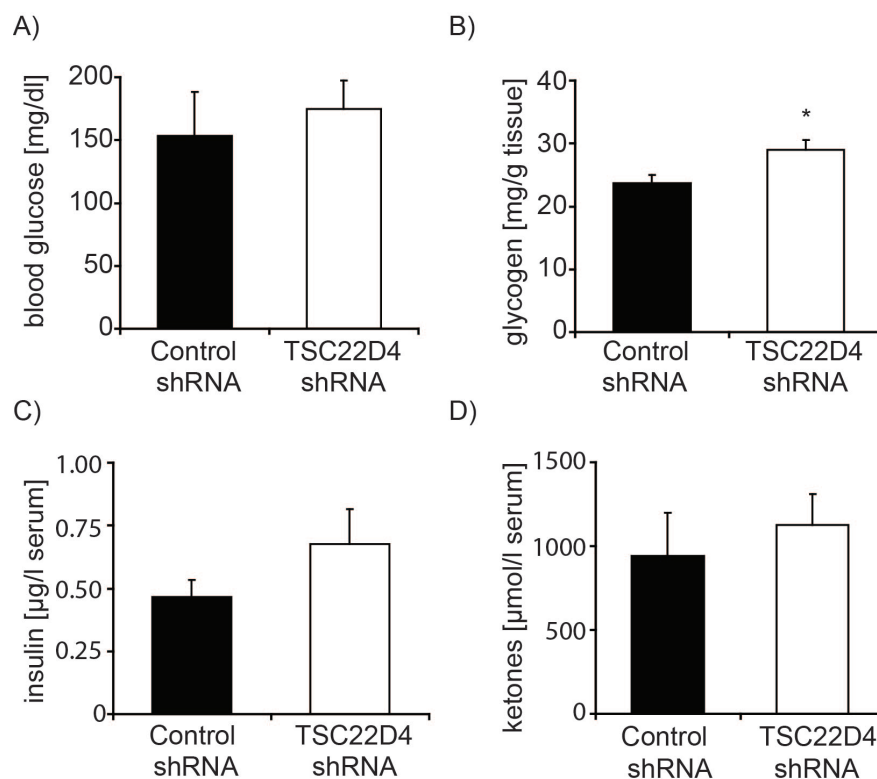


Fig. 23: Glucose, glycogen insulin and ketone body levels upon TSC22D4 knock down. Blood glucose (A), hepatic glycogen (B), serum insulin (C) and ketone bodies (D) were determined in mice treated with control or TSC22D4 shRNA adenovirus 7 days after injection; ($n \geq 7$), (means \pm SEM). * indicates significance; $p \leq 0.05$.

5.3.2.3. Hepatic and serum lipids and steroids

After sacrificing the mice, lipids were isolated from the livers in order to investigate the effects of TSC22D4 on lipid and steroid metabolism. Non-esterified free fatty acids (NEFA) are imported into the liver via lipoprotein particles, esterified and used for the production of TGs and as a substrate for beta oxidation (74). Hepatic and serum NEFA levels were determined using a commercial kit. Whilst a mild decrease was observed in the liver (Fig. 24 A), serum NEFA levels were unaffected by TSC22D4 knock down (Fig. 24 B).

A)

B)

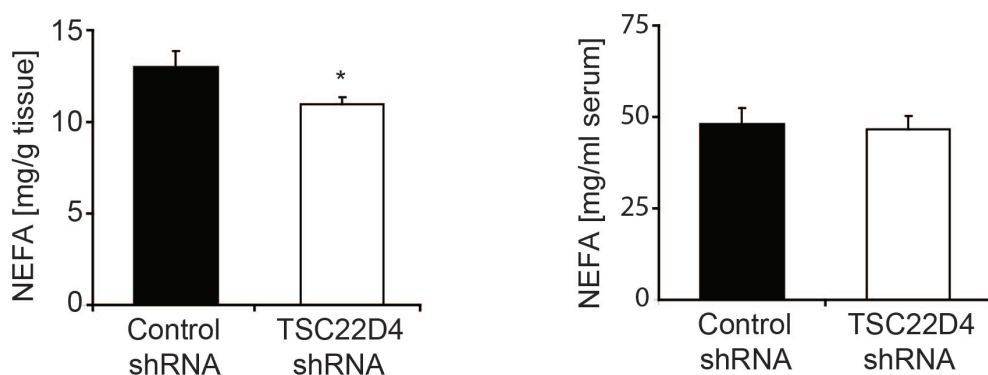


Fig. 24: Liver non-esterified fatty acids are slightly reduced upon TSC22D4 knock down. Liver (A) and total serum (B) non-esterified fatty acid (NEFA) content was determined from mice treated with control or TSC22D4 shRNA adenovirus 7 days after infection; ($n \geq 7$), (means \pm SEM). (*) indicates significance; $p \leq 0.05$.

Cholesterol is a steroid that is produced by the liver and subsequently transported throughout the periphery by lipoprotein particles. It is an important component of cellular membranes and also a necessary substrate for the production of hormones and bile acids. Elevated cholesterol levels are however associated with metabolic complications, such as atherosclerosis and cardiovascular disease (75). Hepatic and serum cholesterol content were determined using a commercial kit. Whilst TSC22D4 knock down did not change liver cholesterol content (Fig. 25 A), circulating cholesterol was slightly, but significantly, elevated, hinting towards an involvement of TSC22D4 in the metabolism of lipoprotein particles (Fig. 25 B).

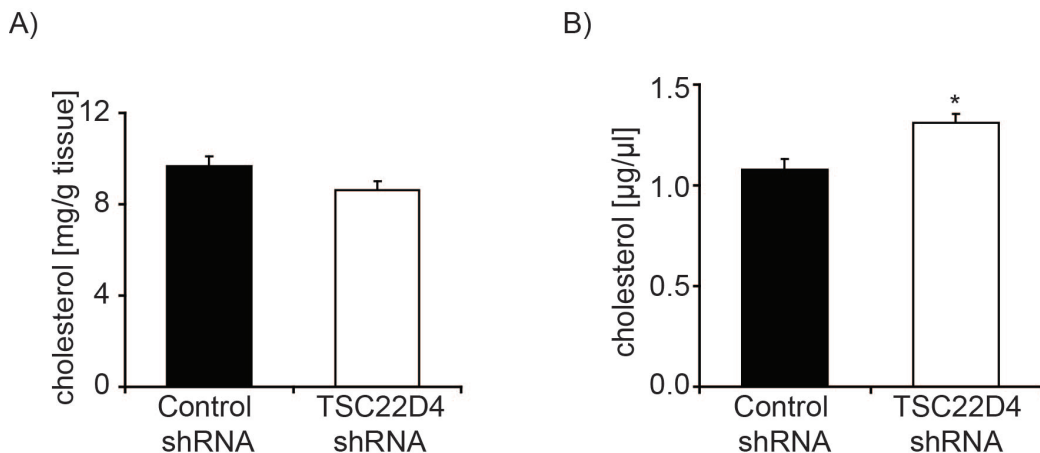


Fig. 25: Serum, but not hepatic cholesterol levels are elevated upon TSC22D4 knock down. Liver (A) and total serum (B) cholesterol content was determined from mice treated with control or TSC22D4 shRNA adenovirus 7 days after infection; ($n \geq 7$), (means \pm SEM). (*) indicates significance; $p \leq 0.05$.

TGs are either taken up by the intestine or produced by and stored in the liver. When required, they are released from the liver and transported throughout the body by lipoprotein particles, providing energy to adipose and muscle tissue. Elevated TG levels in the liver (hepatice steatosis), as associated with the Metabolic Syndrome, lead to liver fibrosis and ultimately cancer. Excessive blood TG levels (hypertriglyceridemia) are associated with cardiovascular diseases (27,76). To assess if TG trafficking is deregulated in the absence of TSC22D4, hepatic and serum TG levels were determined using a commercial kit. Whilst hepatic TG stores were significantly decreased by TSC22D4 knock down (Fig. 26 A), serum TGs were markedly elevated more than 2-fold (Fig. 26 B), indicating disrupted TG trafficking either to or from the liver.

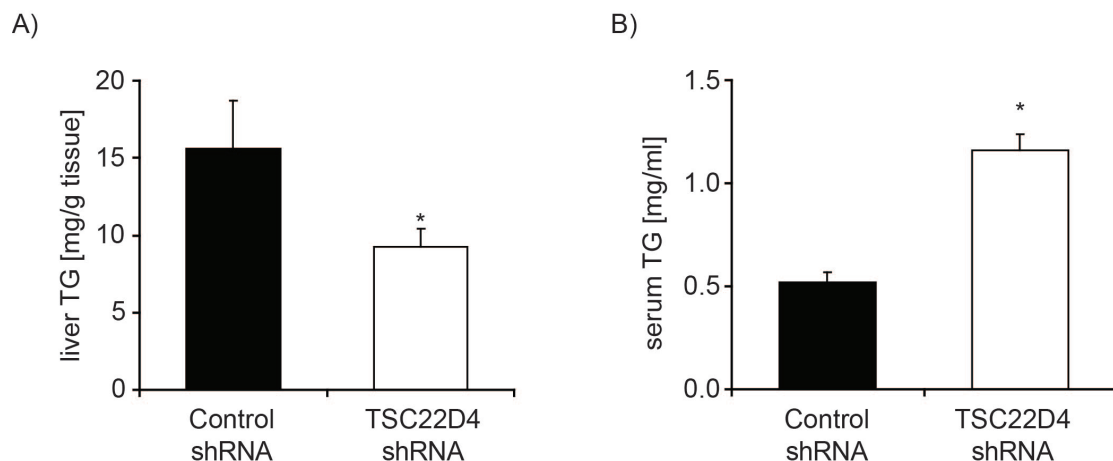


Fig. 26: Hepatic triglycerides are reduced, whilst serum triglycerides are elevated upon TSC22D4 knock down. Liver (A) and total serum (B) triglyceride (TG) content was determined from mice treated with control or TSC22D4 shRNA adenovirus 7 days after infection; ($n \geq 7$), (means \pm SEM). (*) indicates significance; $p \leq 0.05$.

5.3.3. TSC22D4 deficient mice display elevated circulating VLDL triglycerides

Generally TGs are released by the liver and transported as components of multi-protein complexes known as very low density lipoprotein (VLDL) particles. Elevated VLDL levels are associated with increased risk of diabetes, cardiovascular diseases, heart attacks and strokes and contribute significantly to the Metabolic Syndrome (36). As an increase in serum TG levels was observed in mice after TSC22D4 knock down, we analyzed the different lipoprotein species in regard to their TG and cholesterol content. To this effect, total serum was fractionated by size exclusion using fast protein liquid chromatography and a Superose 6 10/300 GL column. As larger particles migrate through the matrix quicker than denser ones, it is possible to separate the lipoproteins according to size. VLDL particles are collected first, followed by low density (LDL) and finally high density (HDL) lipoprotein particles.

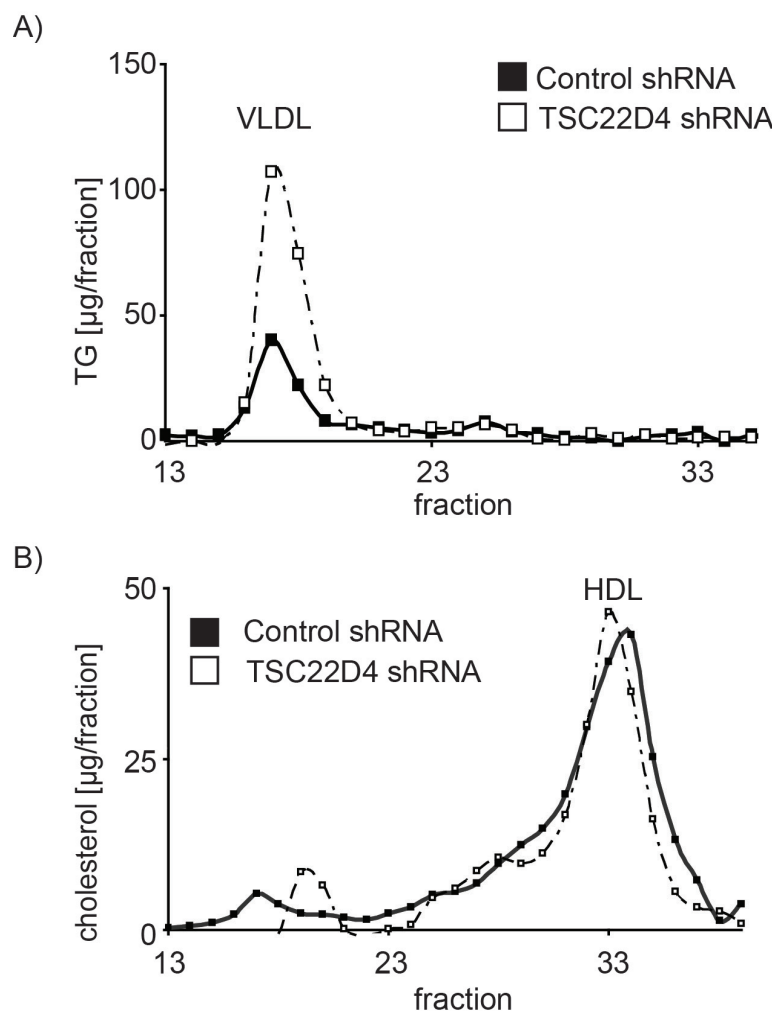


Fig. 27: VLDL triglycerides are elevated in TSC22D4 deficient mice. Lipoprotein-associated serum triglyceride (TG) (**A**) and cholesterol (**B**) levels as measured by fast protein liquid chromatography (FPLC). Serum from mice treated with either control or TSC22D4 shRNA adenovirus was pooled 7 days after infection and applied to a Superose 6 10/300 GL column; ($n \geq 7$).

Indeed, the observed increase in serum TGs could be attributed to the VLDL fraction, as the corresponding peak (fraction number 17) was significantly higher (Fig. 27 A) than in the control group. Hardly any TGs were measured in the HDL fraction. HDL particles mainly transport cholesterol. No clear differences in the lipoprotein profile could be seen concerning the distribution of cholesterol within the HDL fraction (fraction number 33) upon TSC22D4 knock down (Fig. 27 B).

5.3.4. Hepatic triglyceride levels are deregulated in the fasted state

As mice are nocturnal animals, they primarily consume food in the dark period. Therefore, when they are fasted overnight, this represents quite severe starvation and leads to considerable metabolic stress. Interestingly, hepatic and serum TG stores are significantly elevated in this situation (personal observation). The increased hepatic TG content upon fasting is probably due to uptake of more NEFA after their higher release from adipose tissue. Subsequently more VLDL may be secreted by the liver in an effort to provide the periphery with TGs as a source of energy. The precise mechanism underlying this phenomenon is however so far not known. To investigate if TSC22D4 plays a role in the fasting, or immediate refeeding response, 12 mice were injected with the TSC22D4 or control shRNA adenovirus. Six days after injection, their food was withdrawn in the evening. The following morning, six mice were sacrificed in the starved state, whilst the other mice were refed for precisely 6 hours before they were prepared.

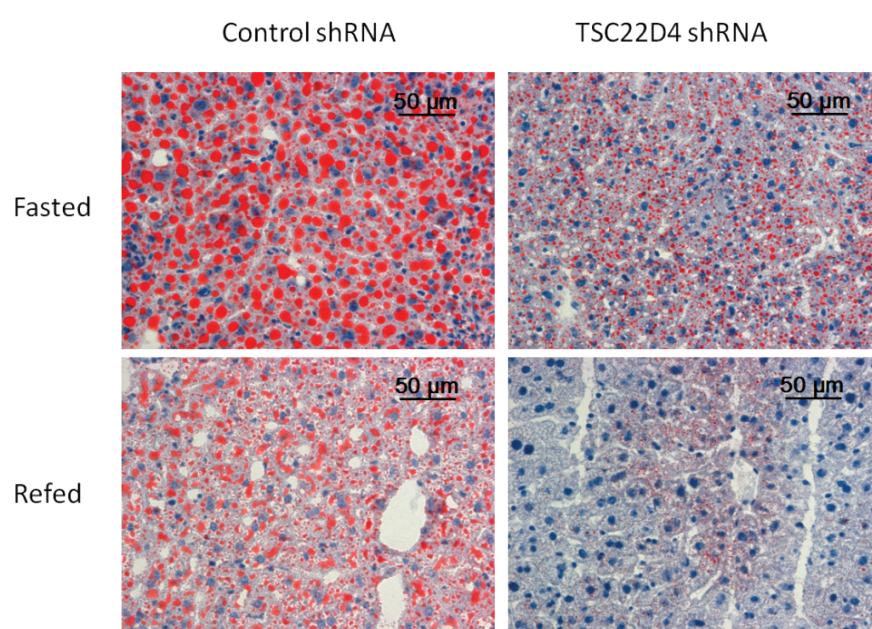


Fig. 28: Hepatic triglycerides are strongly reduced in TSC22D4 deficient mice. Liver sections from representative C57BL/6J mice, either fasted for 16 hours or refed for 6 hours, 7 days after injection of either control or TSC22D4 shRNA adenovirus. Lipids were stained red using Oil Red O.

Liver sections were stained with Oil Red O, a fat soluble dye that specifically stains neutral TGs. As expected, hepatic TGs accumulated in the fasted state in control mice and were reduced by feeding. TSC22D4 knock down resulted in a significant decrease in liver TG content in both the fasted and refed state. Hardly any TGs were visible in refed TSC22D4 deficient mice (Fig. 28).

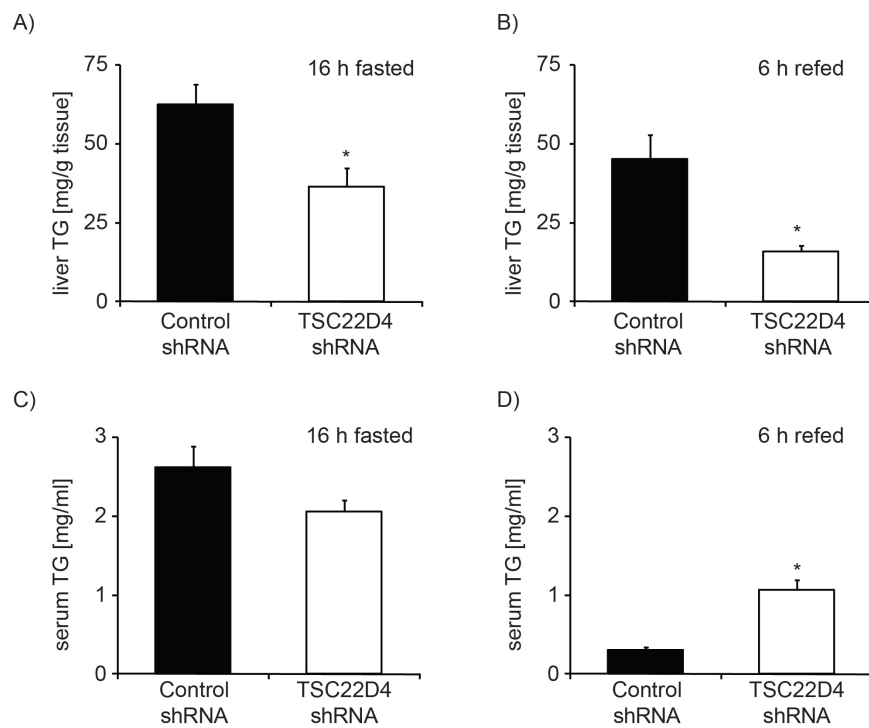


Fig. 29: Fasting liver triglycerides are reduced in TSC22D4 deficient mice. Liver triglyceride (TG) content was determined from 16 hour fasted (**A**) and 6 hour refed (**B**) mice, treated with control or TSC22D4 shRNA adenovirus 7 days after infection. Total serum TGs were determined in the same mice (**C, D**); ($n \geq 7$), (means \pm SEM). (*) indicates significance; $p \leq 0.05$.

The observed decrease in hepatic TG content in both fasted and refed TSC22D4 knock down animals was also determined by colorimetric assay (Fig. 29 A, B). Concerning TG release by the liver, no differences were observed in the already high total fasting serum TG levels (Fig. 29 C). Upon refeeding, however, TSC22D4 deficient mice had significantly higher circulating TGs than their control shRNA treated counterparts (Fig. 29 D). In this context, FPLC analysis revealed that this elevation can be attributed to an increase in the VLDL peak in fed TSC22D4 deficient mice (Fig. 30 A, B).

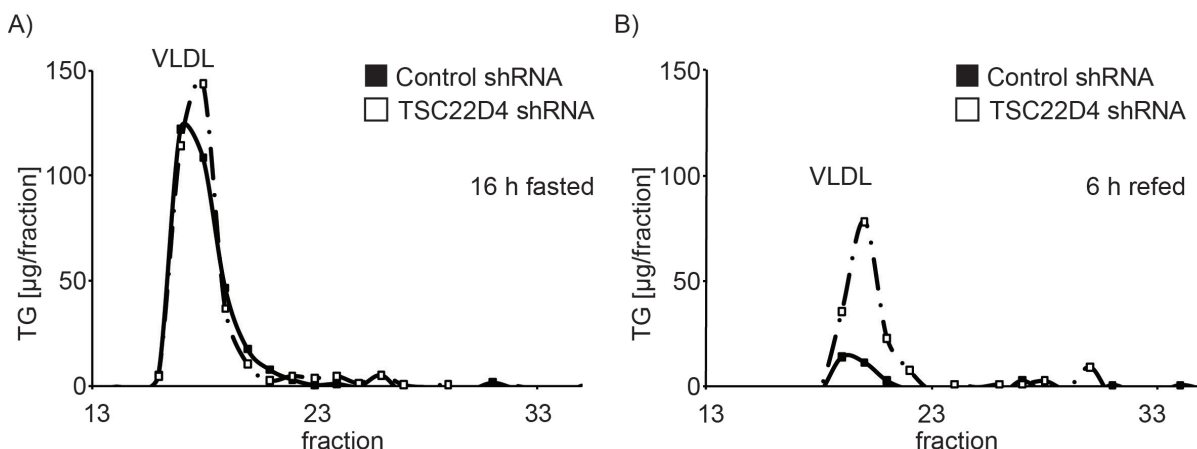


Fig. 30: TSC22D4 knock down elevates circulating VLDL triglyceride levels in the fed, but not the fasted state. Lipoprotein-associated serum triglyceride (TG) levels as measured by fast protein liquid chromatography (FPLC). Serum from 16 hour fasted (**A**) or 6 hour refed (**B**) mice treated with either control or TSC22D4 shRNA adenovirus was pooled 7 days after infection and applied to a Superose 6 10/300 GL column; (n≥7).

5.3.5. VLDL production is increased upon TSC22D4 knock down

The observed changes in hepatic and serum TG levels could either be due to reduced VLDL clearance in the periphery or increased lipogenesis and VLDL secretion by the liver. Individual studies were applied to assess these possible mechanisms.

5.3.5.1. VLDL clearance is not changed upon TSC22D4 knock down

Lipoprotein lipase (LPL) is the enzyme required for VLDL-TG hydrolysis enabling uptake of NEFA into muscle and adipose tissue. The protein is mainly expressed in white adipose tissue and skeletal muscle, where it is attached to the capillaries. By hydrolyzing TGs into three free fatty acids and one monoacylglycerol, LPL provides energy (fatty acids) which is either stored in the adipose tissue, or consumed by muscle (77). Reduced LPL activity would result in an increased VLDL TG content in the blood stream. To investigate if LPL activity was affected by hepatic VLDL knock down, the enzyme was isolated from white adipose tissue. A subsequent activity assay was performed using radiolabeled glyceryl tri-[¹⁴C] oleate. No significant changes were observed in LPL activity upon TSC22D4 knock down (Fig. 31 A), indicating that this is not the mechanism underlying the observed phenotype.

Excess VLDL particles can be cleared by the liver to prevent accumulation in the blood stream. Specific receptors, expressed on the membranes of hepatocytes

mediate this process. To test if this form of clearance was affected by TSC22D4 knock down, mice were fasted for 4 hours and injected purified human VLDL via the tail vein. Blood was taken at distinct time points and human Apolipoprotein B (ApoB) levels in the serum were determined using an enzyme-linked immunosorbent assay (ELISA) that specifically recognizes the human and not the murine protein isoform. Clearance was slightly improved in TSC22D4 deficient mice as these animals removed the human protein from the blood stream quicker (Fig. 31 B). The difference was however rather small and could not explain the observed phenotype, as improved clearance would prevent, rather than induce, serum hypertriglyceridemia. Possibly, VLDL clearance is improved upon TSC22D4 knock down as a compensatory mechanism to counteract elevated serum TG levels.

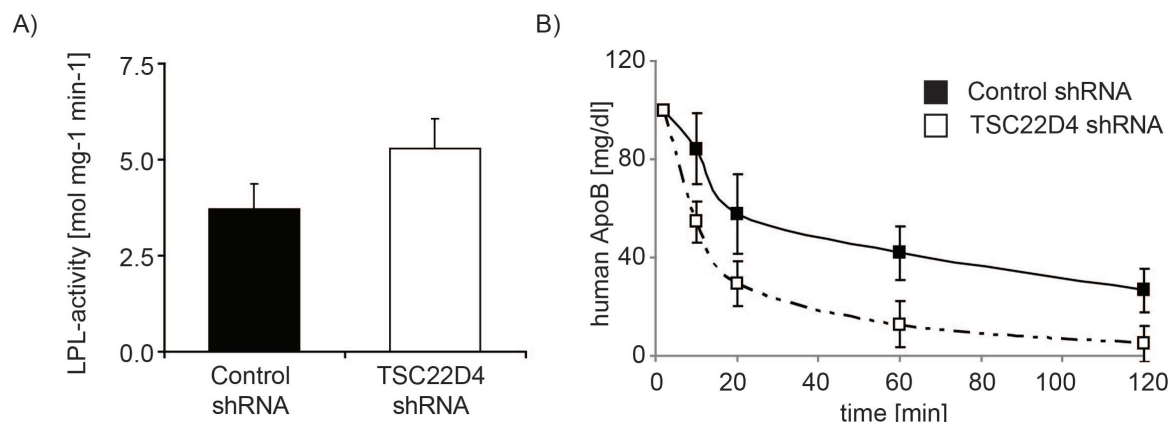


Fig. 31: TSC22D4 knock down does not reduce VLDL clearance from the blood stream. White adipose tissue lipoprotein lipase (LPL) activity was determined in C57BL/6J mice treated with control or TSC22D4 shRNA adenovirus (**A**). Clearance of human ApoB from serum of control or TSC22D4 shRNA adenovirus-injected C57BL/6J mice was determined 7 days after injection. 20 μ g of human VLDL were injected into each animal and serum samples were taken at the indicated time points. Human ApoB levels were determined by human-specific ELISA (**B**); (means \pm SEM, n \geq 6).

5.3.5.2. Hepatic VLDL production is enhanced in TSC22D4 deficient mice

A VLDL production assay was performed to address if changes in VLDL release by the liver could account for the increase in circulating serum VLDL TG levels in TSC22D4 deficient mice. Animals were injected with the non-ionic detergent tyloxapol, leading to a complete inhibition of peripheral LPL (78). Subsequently, all VLDL particles released by the liver accumulated in the blood stream over time. Blood was drawn at specific time points after tyloxapol administration and TG levels were determined colorimetrically. Indeed, TSC22D4 knock down led to a significantly

increased VLDL secretion rate. Over time, about 25% more VLDL particles were released by TSC22D4 deficient mice, which can explain the elevated serum TG levels after knock down (Fig. 32 A).

ApoB is the main protein component of VLDL particles (33). If VLDL secretion is amplified, subsequently, more ApoB protein is required for VLDL assembly. To investigate if hepatic ApoB levels were affected by TSC22D4 knock down, Western blots were performed using liver protein lysates from control and TSC22D4 deficient mice. Increased ApoB protein levels were observed in mice after TSC22D4 knock down, further strengthening the hypothesis that VLDL production is induced in the absence of TSC22D4 (Fig. 32 B).

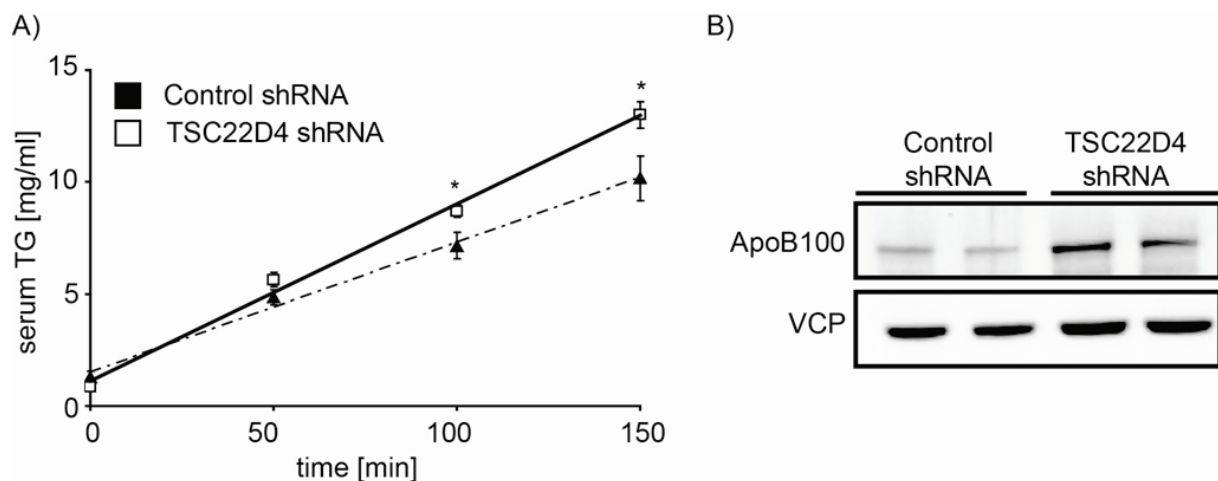


Fig. 32: TSC22D4 knock down leads to increased VLDL secretion by the liver. Hepatic very-low-density lipoprotein (VLDL) release in control or TSC22D4 shRNA adenovirus injected wild-type C57BL/6J mice 7 days after injection. Time after tyloxapol injection indicated (A). Hepatic apolipoprotein B (ApoB) protein levels in representative control or TSC22D4 shRNA adenovirus-injected C57BL/6J mice were determined by Western blot 7 days after injection using ApoB and VCP antibodies (B); (n=6), (means \pm SEM). (*) indicates significance; $p \leq 0.05$.

5.3.5.3. Lipogenic gene expression is induced in TSC22D4 deficient mice

As serum VLDL levels were elevated in TSC22D4 deficient mice, it was likely that TG biosynthesis in the liver (lipogenesis) was increased to account for the higher requirements. Quantitative real time PCR was used to investigate the expression of key lipogenic genes using cDNA produced from hepatic RNA extracts. The investigated genes and a short description of their hepatic function are listed in Tab. 2.

Gene name	Abbreviation	Function
ATP-citrate lyase	Acly	Acetyl CoA synthesis
Acetyl-CoA carboxylase	Acc1	Conversion of acetyl CoA to malonyl CoA
Fatty acid synthase	Fasn	Fatty acid elongation
Stearoyl-CoA desaturase-1	Scd1	Production of desaturated fatty acids
Sterol regulatory element-binding protein 1	Srebp1	Transcription factor regulating lipogenic gene expression
Lipin1	Lipin1	Involved in VLDL production
Peroxisome proliferator-activated receptor alpha	Ppara	Transcription factor regulating hepatic lipid metabolism

Tab. 2: List of analyzed genes involved in hepatic lipid metabolism and lipogenesis.

All lipogenic genes analyzed were strongly up-regulated in livers of random fed C57BL/6J mice lacking TSC22D4, indicating that not only VLDL release, but also *ne-novo* TG biosynthesis and VLDL production were enhanced (Fig. 33).

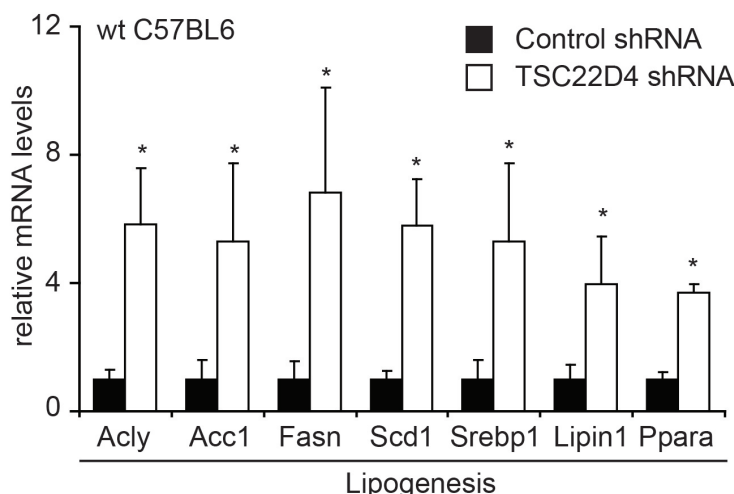


Fig. 33: Expression of lipogenic genes is upregulated in TSC22D4 deficient mice. Quantitative PCR analysis of ATP citrate lyase (Acly), acetyl-coenzyme A carboxylase 1 (Acc1), fatty acid synthase (Fasn), stearoyl-CoA desaturase-1 (Scd1), sterol regulatory element-binding protein-1c (Srebp1), Lipin1 and peroxisome proliferator-activated receptor α (Ppara) mRNA levels in livers of control or TSC22D4 shRNA adenovirus-injected wild-type C57BL/6J mice 7 days after injection; ($n \geq 7$), (means \pm SEM). (*) indicates significance; $p \leq 0.05$.

To investigate if other metabolic processes in the liver were affected by TSC22D4 knock down, the expression of genes involved in bile acid metabolism [src-homology protein 1 (Shp1), cholesterol 7 alpha-hydroxylase (Cyp7a1)], VLDL clearance [receptor-related protein (Lrp), low-density lipoprotein receptor (Ldlr), lipolysis stimulated lipoprotein receptor (Lsr)] and lipoprotein inhibition [apolipoprotein C 1 (Apoc1), apolipoprotein C 2 (Apoc2), apolipoprotein A 1 (Apoa1), angiopoietin-like 3 (Angptl3), angiopoietin-like 4 (Angptl4)] was assessed (Fig. 34 A-B). No significant changes in the expression of these genes were observed, indicating that the effects on gene expression were specific to lipogenesis.

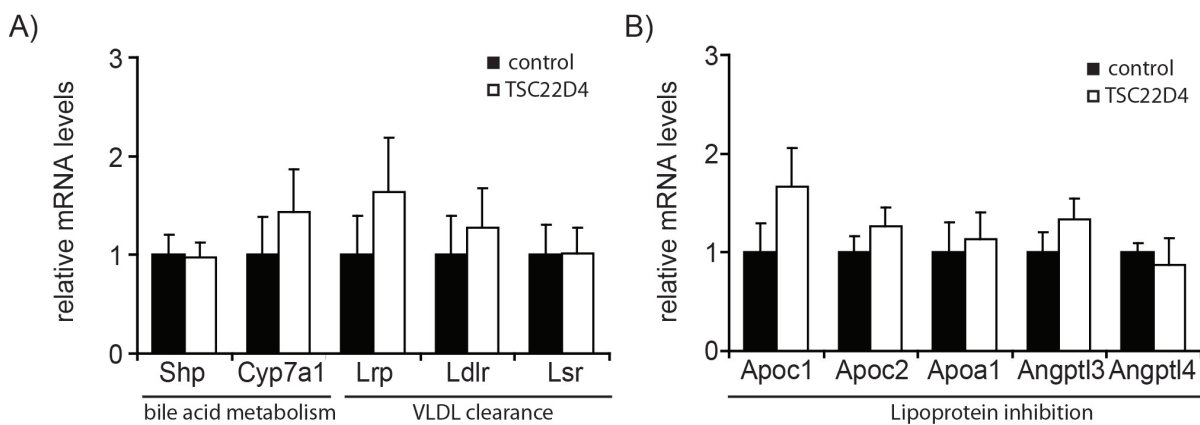


Fig. 34: Expression of genes involved in bile acid metabolism, VLDL clearance and lipoprotein processing is not affected by TSC22D4 knock down. Quantitative PCR analysis of src-homology protein 1 (Shp1), cholesterol 7 alpha-hydroxylase (Cyp7a1), lipoprotein receptor-related protein (Lrp), low-density lipoprotein receptor (Ldlr) and lipolysis stimulated lipoprotein receptor (Lsr) mRNA levels in livers of control or TSC22D4 shRNA-injected wild-type C57BL/6 mice (**A**). Quantitative PCR analysis of apolipoprotein C 1 (Apoc1), apolipoprotein C 2 (Apoc2), apolipoprotein A 1 (Apoa1), angiopoietin-like 3 (Angptl3), angiopoietin-like 4 (Angptl4) mRNA levels in livers of control or TSC22D4 shRNA-injected wild-type C57BL/6J mice (**B**); (n≥7), (means ± SEM). (*) indicates significance; p ≤ 0.05.

The liver not only contains hepatocytes, but also several other cell types, including quiescent pericytes (stellate cells) immune reactive macrophages (Kupffer cells), fibroblasts, and blood cells. To assure that the observed effects on lipogenic gene expression were hepatocyte specific, primary hepatocytes were isolated from C57BL/6J mice and cultivated *in vitro*. The isolated hepatocytes were then transduced using adenovirus expressing either control, or TSC22D4 shRNA. Lipogenic gene expression was analyzed. Several lipogenic genes, including Acly, Scd1 and Ppara were also up regulated in this *ex-vivo* setting (Fig. 35), indicating that TSC22D4 knock down induces lipogenic gene expression in hepatocytes in a cell-autonomous manner.

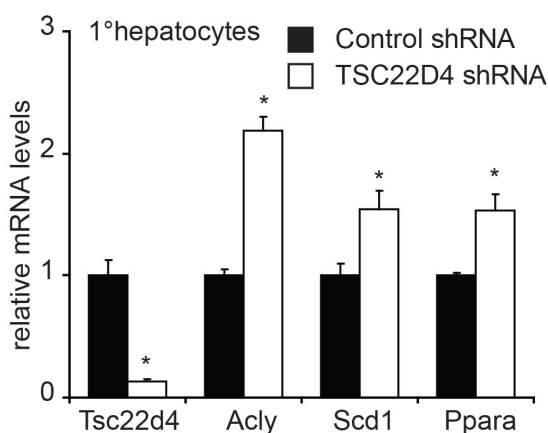


Fig. 35: Lipogenic genes are upregulated in TSC22D4 deficient primary mouse hepatocytes. Quantitative PCR analysis of TSC22D4, ATP citrate lyase (Acly), stearoyl-CoA desaturase-1 (Scd1), peroxisome proliferator-activated receptor α (Ppara) mRNA levels in primary (1°) mouse hepatocytes treated with control or TSC22D4 shRNA adenovirus; (n=3), (means ± SEM). (*) indicates significance; p ≤ 0.05.

5.3.6. Whole genome expression profiling in TSC22D4 deficient mice

To further investigate the consequences of TSC22D4 deficiency concerning hepatic gene expression, microarray analysis was performed using RNA extracts isolated from the livers of random fed control or TSC22D4 deficient mice. The up regulation of the lipogenic genes shown in Fig. 33 was confirmed in this experiment (data not shown). Pathway analysis revealed that biosynthesis of steroids, fatty acid metabolism, fatty acid elongation, adipokine signalling, PPAR signalling, the citrate cycle (tricarboxylic acid cycle) and fatty acid biosynthesis were amongst the pathways which were regulated the strongest in TSC22D4 deficient mice (Fig. 36 A). These results are in line with the observed elevation of serum TGs.

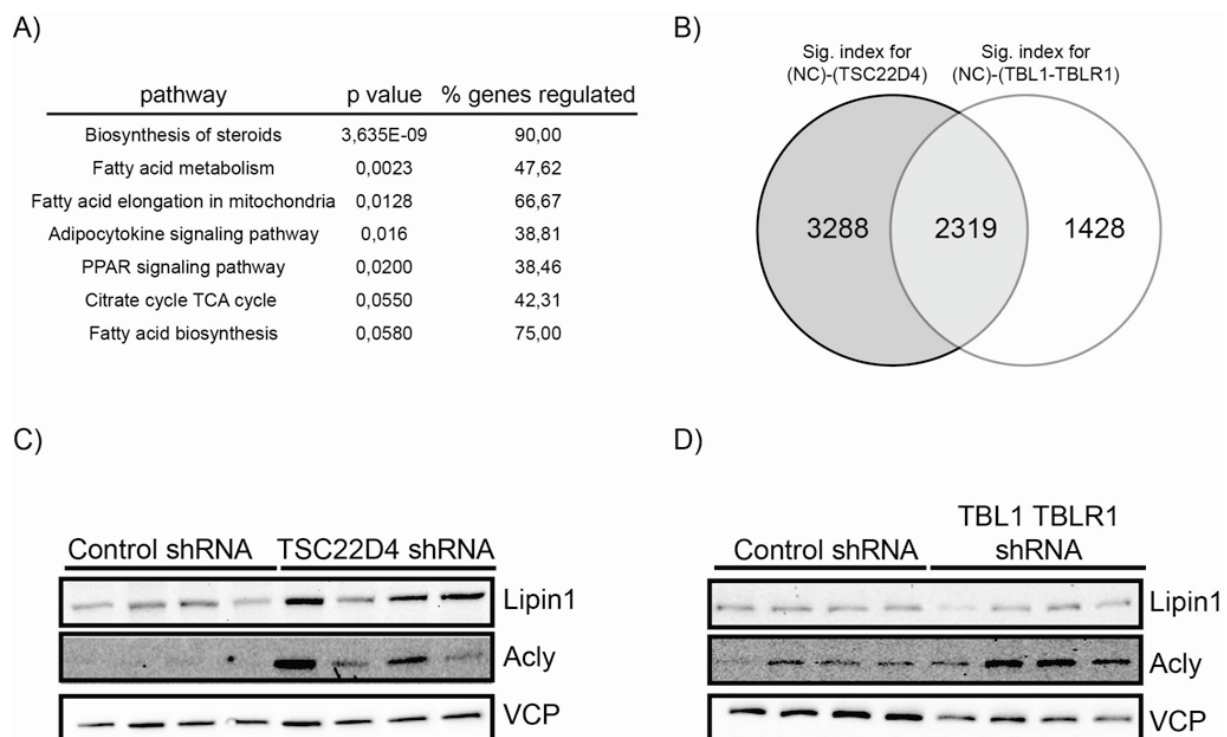


Fig. 36: Hepatic pathway expression analysis of TSC22D4 or TBL1 / TBLR1 deficient livers. Significantly regulated pathways upon hepatic TSC22D4 knock down, as determined by Affymetrix microarray analysis (**A**). Venn diagram displaying the overlap of significantly regulated genes upon TSC22D4 and TBL1 / TBLR1 knock down (**B**). Western blot of liver, extracts from representative control or TSC22D4 shRNA adenovirus-injected C57BL/6J mice 7 days after injection using Lipin1, Acly and VCP antibodies (**C**). Western blot of liver, extracts from representative control or TBL1 and TBLR1 shRNA adenovirus-injected C57BL/6J mice 7 days after injection using Lipin1, Acly and VCP antibodies (**D**). P ≤ 0.05.

The increase in serum TGs and the induction of lipogenesis seen after TSC22D4 knock down had also been described in TBL1 and TBLR1 double deficient mice (63).

Microarrays were performed using liver RNA extracts from these TBL1 / TBLR deficient animals. When comparing the genes regulated by either TSC22D4 or TBL1 / TBLR1 knock down, it was evident that a large portion of the regulated genes overlapped, whilst other genes were only significantly regulated in one of the two experimental settings (Fig. 36 B). This fits with the fact that the absence of TSC22D4 only in part copies the phenotype observed after hepatic TBL1 / TBLR1 double knock down. Both groups of mice display increased lipogenesis, but TSC22D4 deficient mice have reduced hepatic TG stores, whilst TBL1 / TBLR1 knock down animals have highly steatotic livers. It has furthermore been shown that TG secretion is not changed in TBL1 / TBLR1 deficient animals (63).

Western blot analyses of Acly and Lipin1 protein expression were performed using hepatic protein extracts from random fed TSC22D4 or TBL1 / TBLR1 deficient mice. Acly, a gene primarily involved in lipogenesis was, as expected, up regulated in both settings. Lipin1, a gene required for VLDL release, was however only up regulated upon TSC22D4 knock down. (Fig. 36 C, D). These results emphasize that TSC22D4, TBL1 and TBLR1 only in part have directly overlapping functions, primarily concerning lipogenesis.

5.3.7. Acute TSC22D4 knock down affects insulin signalling, but not glucose or insulin tolerance

In both humans and mice, over time, increased circulating TG levels are known to cause insulin resistance and ultimately contribute to the development of type 2 diabetes (79). As shRNA mediated knock down of TSC22D4 led to a marked increase in serum TG levels, we decided to investigate the consequences of the resulting hypertriglyceridemia in regard to glucose tolerance and insulin sensitivity.

Mice were injected with adenovirus expressing the control or TSC22D4 specific shRNA. One week after injection, an intravenous glucose tolerance test (GTT) was performed to investigate if the capacity to handle glucose was altered by TSC22D4 knock down. For this cause, a bolus of glucose (10 µl of a 20% solution / g mouse weight) was injected intraperitoneally and blood sugar levels were monitored over time. No differences could be observed in clearance of the externally infused glucose,

indicating that glucose tolerance is not acutely affected by short-term TSC22D4 deficiency (Fig. 37 A).

In a second experiment, an intravenous insulin tolerance test (ITT) was performed to address the effects regarding insulin sensitivity. After insulin administration, blood glucose levels quickly decreased in both the control and the TSC22D4 knock down group. They then recovered within 2 hours. No major differences were observed between the TSC22D4 deficient and the control mice, indicating that insulin tolerance was also not acutely affected (Fig. 37 B).

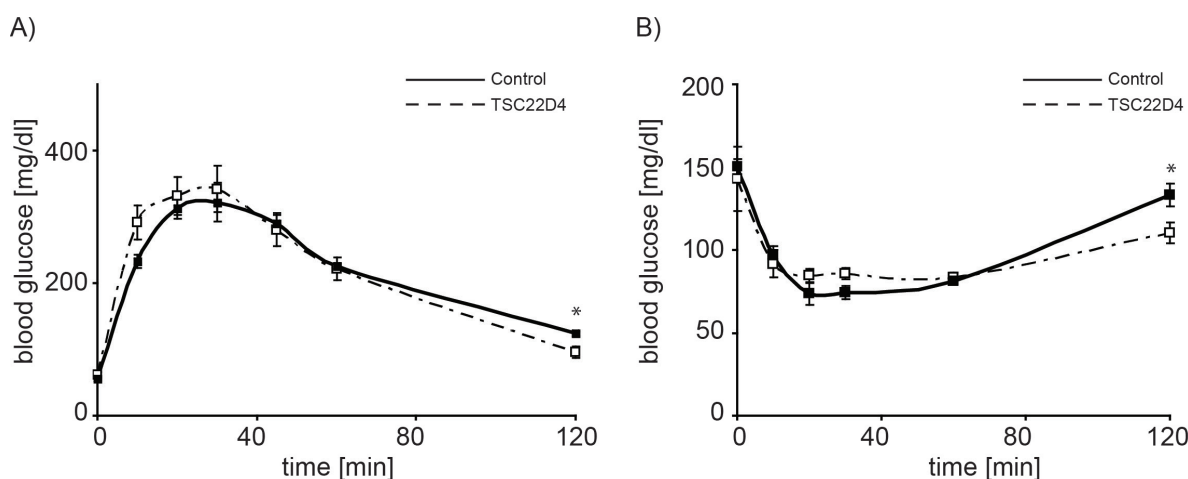


Fig. 37: Glucose tolerance and insulin sensitivity are not affected by TSC22D4 knock down. Glucose tolerance test (GTT) (A) and insulin tolerance test (ITT) (B) in control or TSC22D4 shRNA adenovirus-injected C57BL/6J mice 7 days after injection; (means \pm SEM). $P \leq 0.05$, * indicates significance.

One week of TSC22D4 deficiency had not sufficed to induce systemic glucose intolerance, or insulin resistance. We therefore investigated the sensitivity of the insulin signalling cascade at the molecular level. Control or TSC22D4 deficient mice were injected either PBS, or 1U/kg insulin and prepared precisely 10 min after injection. Hepatic insulin signalling was subsequently assessed by analysing protein kinase B (PKB=AKT) and glycogen synthase kinase 3 (GSK3) activity, as determined by their phosphorylation status.

No differences could be seen in the basal, non-stimulated state. The insulin induced phosphorylation of both AKT and GSK3 was, however, blunted in TSC22D4 deficient mice, representing the first step in the development of insulin resistance in these

animals (Fig. 38). It is plausible that over time, this defect in insulin sensitivity could favour the development of systemic insulin resistance and the Metabolic Syndrome.

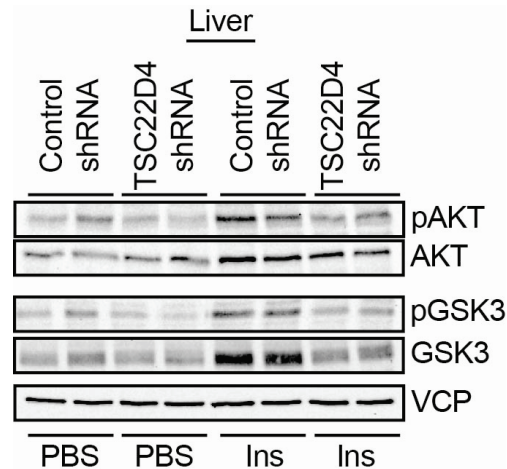


Fig. 38: Insulin signaling is blunted in TSC22D4 deficient mice. Western blot of liver extracts from representative control or TSC22D4 shRNA adenovirus-injected C57BL/6J mice 7 days after injection using AKT (AKT=PKB, Protein Kinase B), phospho AKT (pAKT), GSK3 (Glycogen Synthase Kinase 3), phospho GSK3 (pGSK3) and VCP antibodies. Animals were either injected with PBS or 1U/kg body weight insulin 10 min prior to sacrifice. Mice were analyzed in the fed state (n=3).

5.3.8. TSC22D4, TBL1 and TBLR1 triple deficiency leads to severe hypertriglyceridemia

TSC22D4 has been shown to directly physically interact with TBL1 and TBLR1. On the one hand, the absence of each one of the three proteins alone induces significant hypertriglyceridemia. In contrast however, TBL1 and TBLR1 deficiency favour liver steatosis, whilst TSC22D4 knock down reduces hepatic TG stores. The question therefore arose, as to the consequences of TSC22D4, TBL1 and TBLR1 triple deficiency. To address this point, we acutely knocked down either, TSC22D4 alone, TBL1 and TBLR1 in combination, or all three genes at once using 1×10^9 infectious units of each virus. In all cases the total titre was adjusted to 3×10^9 using adenovirus expressing the control shRNA. Mice injected with control virus served as one control, whilst a second control group consisted of mice injected PBS instead of adenovirus.

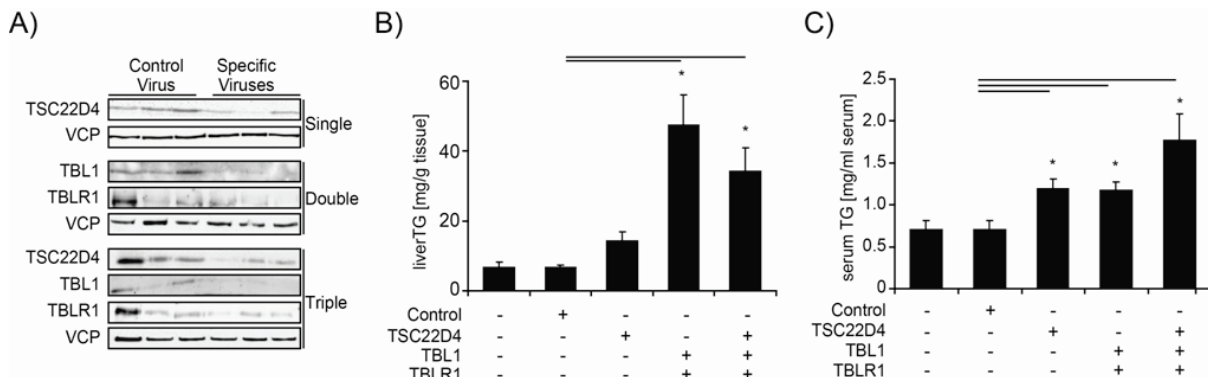


Fig. 39: TSC22D4, TBL1 and TBLR1 triple deficient mice have elevated serum and liver triglycerides. Western blot of liver extracts from fed representative control, TSC22D4, TBL1 and TBLR1 or TSC22D4, TBL1, TBLR1 shRNA adenovirus-injected C57BL/6J mice 7 days after injection using TSC22D4, TBL1, TBLR1 and VCP antibodies (A). Liver (B) and serum (C) triglyceride (TG) content in the same mice as in a; (means \pm SEM, n \geq 6). P < 0.05, * indicates significance.

Knock down efficiency was not as strong as in past experiments (Fig. 39 A). Nevertheless, the severe hepatic steatosis associated with TBL1 / TBLR1 double knock down (63) was observed, but only slightly reduced by additional TSC22D4 deficiency (Fig. 39 B). Serum hypertriglyceridemia was seen upon TSC22D4 single knock down and TBL1 / TBLR1 double knock down. Serum TG levels were even further increased in the TSC22D4, TBL1, TBLR1 triple deficient mice (Fig. 39 C). Although the consequences did not seem additive, TSC22D4 / TBL1 / TBLR1 triple knock down did have very severe effects on circulating TG levels. No differences were observed between the control virus injected mice and PBS treated mice, indicating that the observed phenotypes did not result from off-target viral effects.

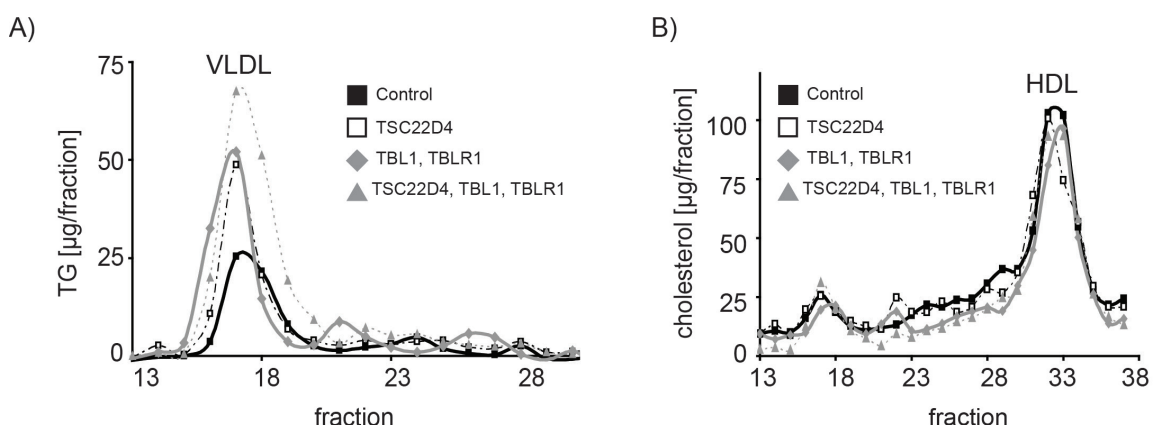


Fig. 40: TSC22D4, TBL1 and TBLR1 triple deficient mice have elevated VLDL triglycerides. Lipoprotein-associated serum triglyceride (TG) (A) and cholesterol (B) levels as measured by fast protein liquid chromatography (FPLC). Pooled serum from control, TSC22D4, TBL1 and TBLR1 or TSC22D4, TBL1, TBLR1 shRNA adenovirus-injected C57BL/6J mice was applied to a Superose 6 10/300 GL column 7 days after injection; (n=6).

Indeed, FPLC analysis revealed that the increased amounts of serum TGs detected upon TSC22D4 single, TBL1, TBLR1 double and TSC22D4, TBL1, TBLR1 triple deficiency were in all cases located in the VLDL fraction. All three groups had significantly higher VLDL TG peaks than control animals. The corresponding VLDL peaks (fraction 17) resulting from TSC22D4 single and TBL1 / TBLR1 double knock down were comparable, whilst triple knock down led to an even higher VLDL peak (Fig. 4o A). VLDL and HDL (fraction 33) cholesterol levels remained unaffected, as assessed by FPLC (Fig. 4o B).

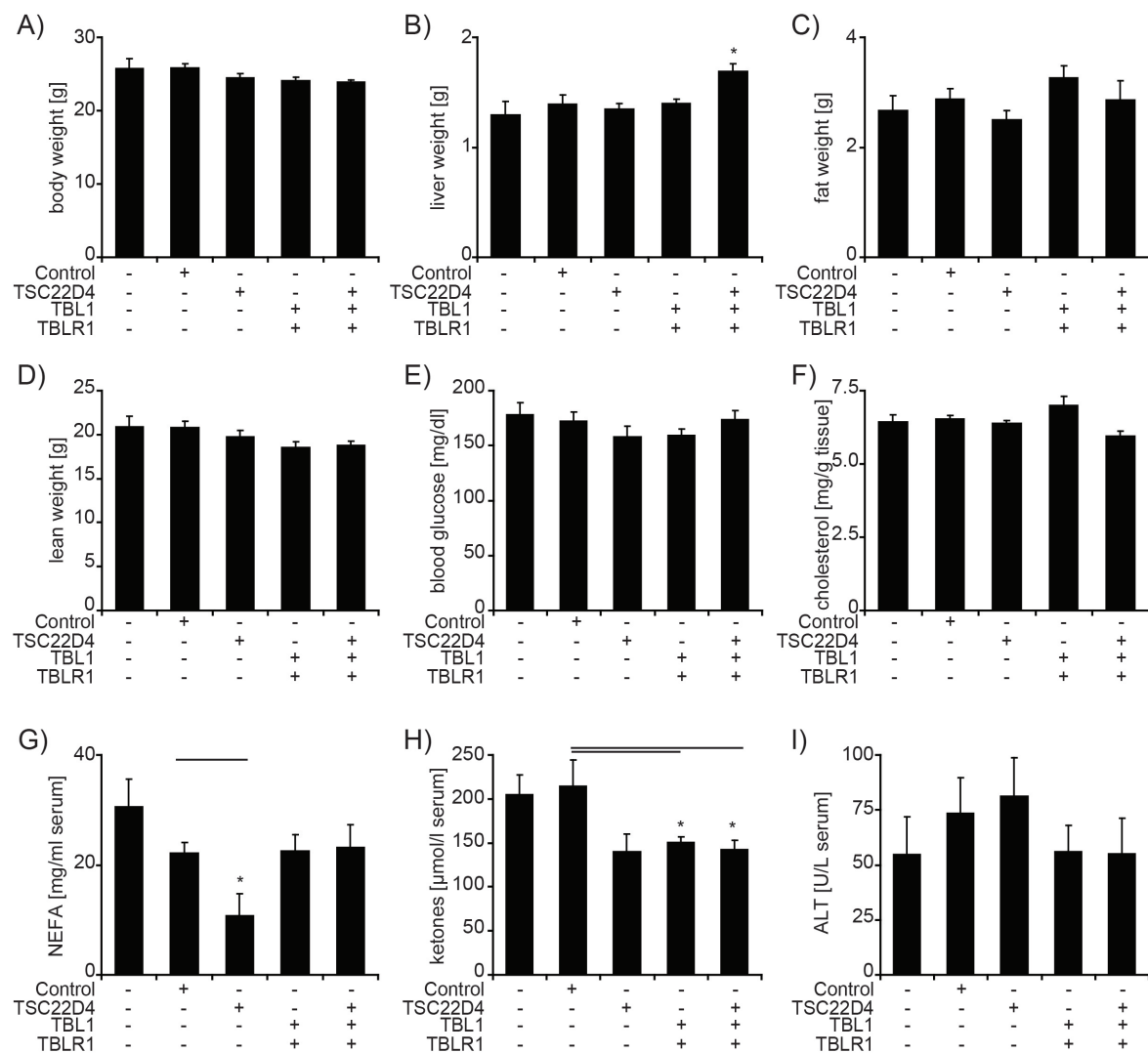


Fig. 41: Phenotypic analysis of TSC22D4, TBL1 and TBLR1 triple deficiency. Body weight (A), liver weight (B), fat weight (C), lean weight (D), blood glucose (E), liver cholesterol (F), serum NEFA (G), serum ketone bodies (H) and serum alanine transaminase (ALT) (I), in PBS, control TSC22D4, TBL1 and TBLR1 or TSC22D4, TBL1 and TBLR1 shRNA adenovirus-injected C57BL/6J mice 7 days after injection (means \pm SEM, n \geq 6). P \leq 0.05, * indicates significance.

Other metabolic parameters were generally not affected by any of the knock down conditions (Fig. 41 A-G). Only ketone body levels were, as expected (63), reduced in response to impeded beta oxidation in the absence of TBL1 and TBLR1 (Fig. 41 H). Serum alanine transaminase levels served as a marker for liver damage. No difference could be observed between PBS or virus treated animals (Fig. 41 I).

5.3.9. Micro RNA mediated TSC22D4 knock down using adeno-associated virus

Adenoviral vectors are known to not only infect hepatocytes, but also other liver cells, including Kupffer macrophages. In order to analyze not only liver, but hepatocyte specific TSC22D4 knock down, an AAV-vector expressing a micro RNA (miRNA) against TSC22D4 was produced. The AAV serotype was designed to preferably infect hepatocytes and the miRNA was under the control of the hepatocyte-specific LP1 promoter, which is not active in Kupffer or stellate cells (63). Transduction using AAV vectors leads to long-term knock down, since the virus does not provoke an immune reaction which would lead to its clearance, as is the case when using adenovirus (80). To investigate if obesity and insulin resistance influence the TSC22D4 deficient phenotype, C57BL/6J mice were put on either a high fat diet containing 60% energy from fat (HFD) or a low fat control diet (LFD) containing only 10% energy from fat for 9 weeks.

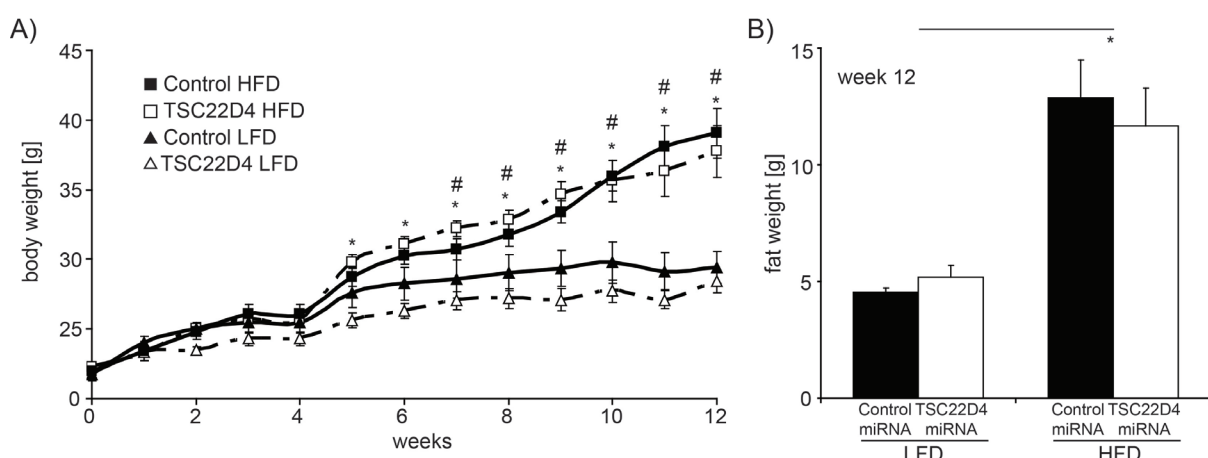


Fig. 42: Weight development of TSC22D4 deficient mice on a high fat diet. C57BL/6J mice injected with an adeno-associated virus (AAV) expressing either a control or a TSC22D4-specific micro RNA (miRNA). 3 weeks after injection, animals were either fed a high fat diet (HFD) containing 60% energy from fat or a control low fat diet (LFD), containing 10% energy from fat (A). Fat mass of the mice was measured after 9 weeks of LFD or HFD feeding (B); (means \pm SEM, $n \geq 4$). $P \leq 0.05$, * indicates significance (TSC22D4 HFD vs. TSC22D4 LFD), # indicates significance (control HFD vs. control LFD).

5×10^{11} infectious units of AAV were administered via the tail vein. Three weeks after infection, half the mice were put on the HFD and the other half were maintained on the LFD. As expected, over time the HFD fed mice put on significantly more weight than their LFD fed counterparts (Fig. 42 A). Their body fat content, as determined by Echo MRI, was also significantly higher after 9 weeks of diet (Fig. 42 B). No differences could be seen between control miRNA and TSC22D4-specific miRNA treated mice in regard to body composition.

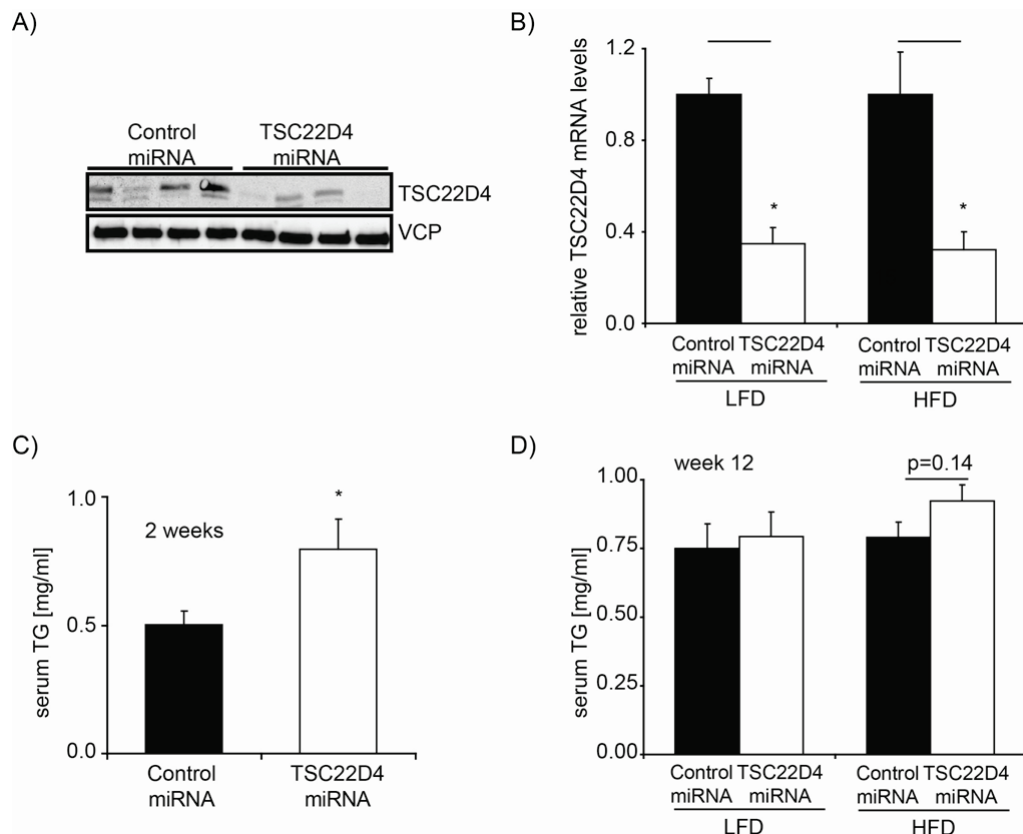


Fig. 43: TSC22D4 knockdown using a miRNA expressing adeno-associated virus. Western blot analysis of liver extracts from mice injected with adeno-associated virus expressing a control or TSC22D4 specific miRNA using TSC22D4 and VCP specific antibodies 12 weeks after injection (**A**). Quantitative PCR analysis of TSC22D4 mRNA levels in livers of control or TSC22D4 miRNA-injected wild-type C57BL/6J mice (**B**). Serum triglyceride (TG) levels in the same mice 14 days after injection (**C**). Serum TG levels in the same mice 12 weeks after injection. Mice were fed either a diet containing 10% energy from fat (LFD), or 60% energy from fat (HFD) for 9 weeks (**D**); means \pm SEM, $n \geq 4$. $P \leq 0.05$, * indicates significance.

After the sacrifice, knock down was assessed by quantitative PCR and Western blot analysis. A decrease in protein abundance was observed (Fig. 43 A) and mRNA levels were reduced by approximately 65 % (Fig. 43 B). During the experiment, blood had been taken from the tail vein every 2 - 3 weeks to investigate serum TG levels over

time. Serum TGs were significantly elevated 2 weeks after infection with virus expressing the TSC22D4 specific-miRNA, copying the phenotype observed in the experiments using shRNA expressing adenovirus (Fig. 43 C). A decisive difference could however no longer be seen 12 weeks after transduction. At this time point, serum TG levels were slightly, albeit not significantly higher in the HFD fed TSC22D4 deficient mice, whilst there was no difference at all between the LFD fed groups (Fig. 43 D).

In summary, these results confirm the involvement of TSC22D4 in the regulation of circulating serum TG levels, but point towards the presence of mechanisms capable of, at least in part, compensating for chronic TSC22D4 deficiency. Possibly other members of the TSC22 family are involved in these compensatory processes, as at least TSC22D1 can interact with TSC22D4.

5.4 TSC22D4 over expression reduces circulating VLDL triglyceride levels in C57BL/6J mice

Having seen that hepatic TSC22D4 deficiency leads to reduced liver TG levels, increased lipogenesis and elevated serum VLDL secretion, we sought to investigate the consequences of enforced TSC22D4 over expression. For this cause, an adenovirus encoding the TSC22D4 cDNA sequence in frame with the Flag peptide under the control of the constitutively active CMV promoter was cloned and produced.

5.4.1. Hepatic TSC22D4 over expression in fasted and refed mice

1×10^9 infectious units of either TSC22D4 over expression virus, or an empty control virus incorporating the CMV promoter were administered to mice via tail vein injection. The mice were sacrificed 7 days after infection. To investigate the effects of starvation, the animals were fasted for 16 hours prior to the day of preparation. Half the mice were sacrificed in the fasted state, whilst the other half were refed for 6 hours.

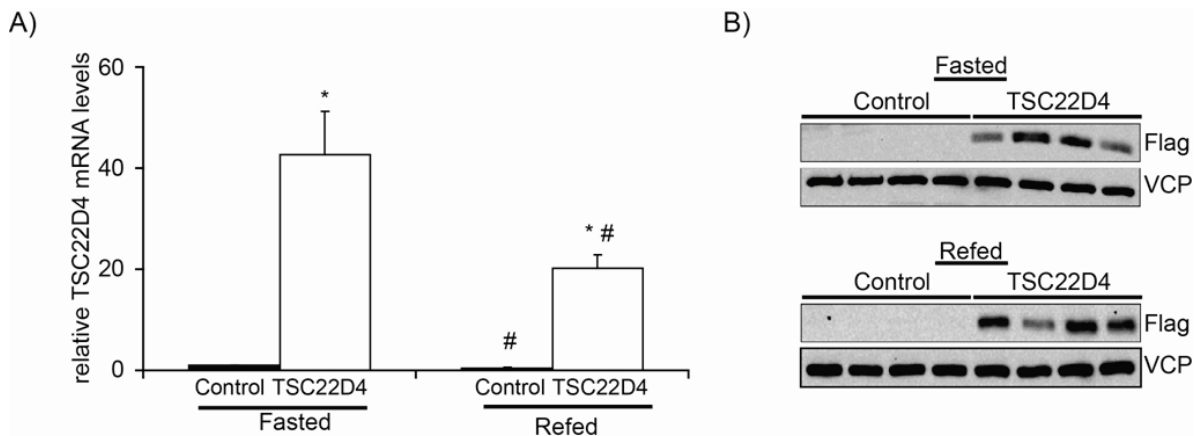


Fig. 44: Hepatic TSC22D4 over expression in fasted and refed mice. Quantitative PCR analysis of TSC22D4 mRNA levels in livers of control or TSC22D4 cDNA adenovirus-injected wild-type C57BL/6J mice. Animals were fasted for 16 hours and refed for 6 hours (**A**). Western blot of liver extracts from representative fasted or refed control or Flag-TSC22D4 cDNA adenovirus-injected C57BL/6J mice 7 days after injection using Flag and VCP antibodies (**B**); (means \pm SEM, $n \geq 4$). $P \leq 0.05$, * indicates significance (control vs.TSC22D4), # indicates significance (fasted vs. refed).

A significant increase in TSC22D4 expression was detected at the mRNA level by quantitative PCR analysis (Fig. 44 A). Approximately 40 times more TSC22D4 mRNA was present in mice treated with the over expression virus. Interestingly, less TSC22D4 expression was observed in the fed compared to the fasted state. This was true for mice treated with the control virus or the TSC22D4 over expressing virus, hinting towards up regulation of TSC22D4 upon fasting, a phenomenon that had previously not been seen. The recombinant TSC22D4 protein was visualized by Western blot using a Flag antibody. A strong signal, corresponding to the recombinant TSC22D4 protein could thereby be visualized (Fig. 44 B).

5.4.1.1. Effects of TSC22D4 over expression on body composition

TSC22D4 over expression induced no major changes concerning body or liver weight in the fasted or refed state (Fig. 45 A). A slight decrease was however measured in TSC22D4 over expressing animals in regard to fat weight (Fig. 45 B, C). Whilst no differences were detectable concerning fasting glucose levels, mice over expressing TSC22D4 had slightly but significantly elevated blood sugar content compared to fed empty virus treated mice (Fig. 45 D).

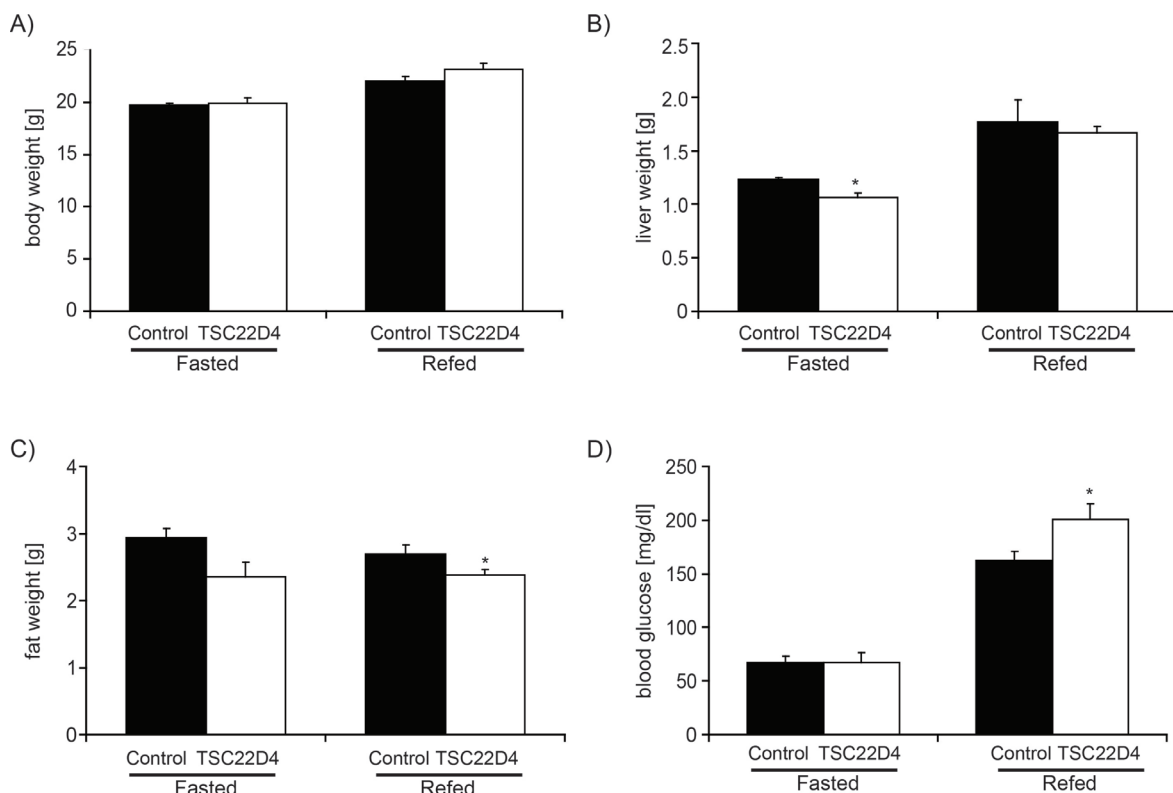


Fig. 45: Body composition of TSC22D4 over expressing mice. Fasting and refeeding body weight (**A**), liver weight (**B**), fat weight (**C**) and blood glucose levels (**D**) in control or Flag-TSC22D4 cDNA adenovirus-injected C57BL/6J mice 7 days after injection; (means \pm SEM, $n \geq 4$). $P \leq 0.05$, * indicates significance (control vs. TSC22D4).

5.4.1.2. Effects of TSC22D4 over expression on hepatic lipid metabolism

As previously observed, liver TG stores were increased in fasted, as compared to refed mice. Upon TSC22D4 knock down, liver TG levels had been significantly reduced. In turn, over expression led to a slight increase in hepatic TG content, particularly in the fasted state (Fig. 46 A). Fasting liver cholesterol levels were also slightly elevated in the TSC22D4 group, there was however no difference in fed animals (Fig. 46 B).

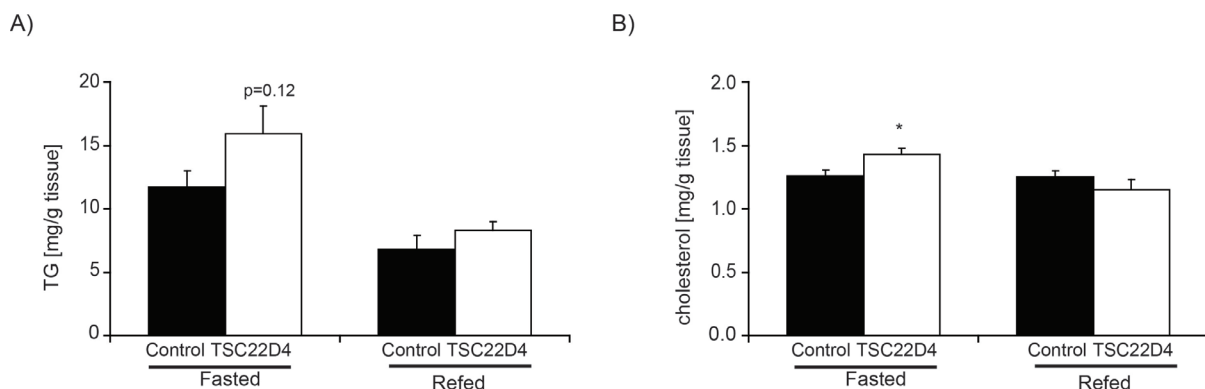


Fig. 46: Hepatic triglycerides and cholesterol in TSC22D4 over expressing mice. Fasting and refeeding triglyceride (TG) (**A**) and cholesterol content (**B**) in livers of control or Flag-TSC22D4 cDNA adenovirus-injected C57BL/6J mice 7 days after injection; (means \pm SEM, $n \geq 4$). $P \leq 0.05$, * indicates significance.

Next, serum VLDL TG and HDL cholesterol levels were analyzed using FPLC. In knock down experiments, the major phenotype had been a marked elevation of circulating serum VLDL levels. Indeed, hepatic TSC22D4 over expression induced the opposite effect. Whilst circulating HDL cholesterol was not affected (Fig. 47 A, B), VLDL TG levels were decreased by TSC22D4 over expression (Fig. 47 C, D). The effect was strongest in fasted mice, where hardly any VLDL peak was detectable. These data increase the evidence that TSC22D4 expression is integral in the regulation of VLDL metabolism.

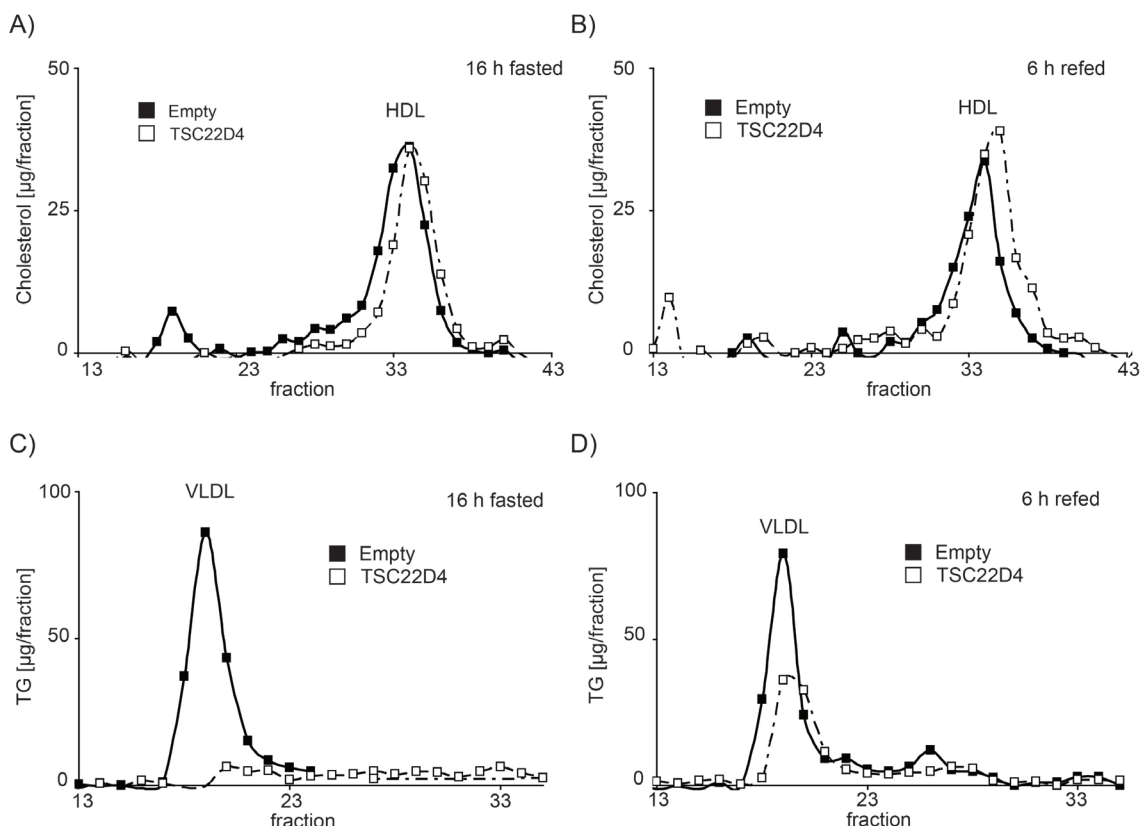


Fig. 47: Serum lipoprotein profiles of TSC22D4 over expressing mice. Lipoprotein-associated serum cholesterol levels as measured by fast protein liquid chromatography (FPLC) in 16 hour fasted (**A**) or 6 hour refed (**B**) mice injected with control or TSC22D4 over expression adenovirus. Lipoprotein-associated triglyceride levels in the same fasted (**C**) and refed (**D**) mice as above; ($n \geq 3$).

To investigate if the phenotype observed concerning hepatic and circulating VLDL TG levels was also reflected at the degree of lipogenic gene expression, mRNA levels of Acly, Acc1, Fasn, Scd1, Srebp1 and Lipin1 were assessed by quantitative real time PCR. No differences could be observed in fasted mice, probably as they are already in a state in which hepatic lipogenesis is generally repressed (Fig. 48 A). Lipogenesis was however significantly blunted upon TSC22D4 over expression in the fed state, indicating once more, that TSC22D4 is required for the proper induction of TG biosynthesis (Fig. 48 B).

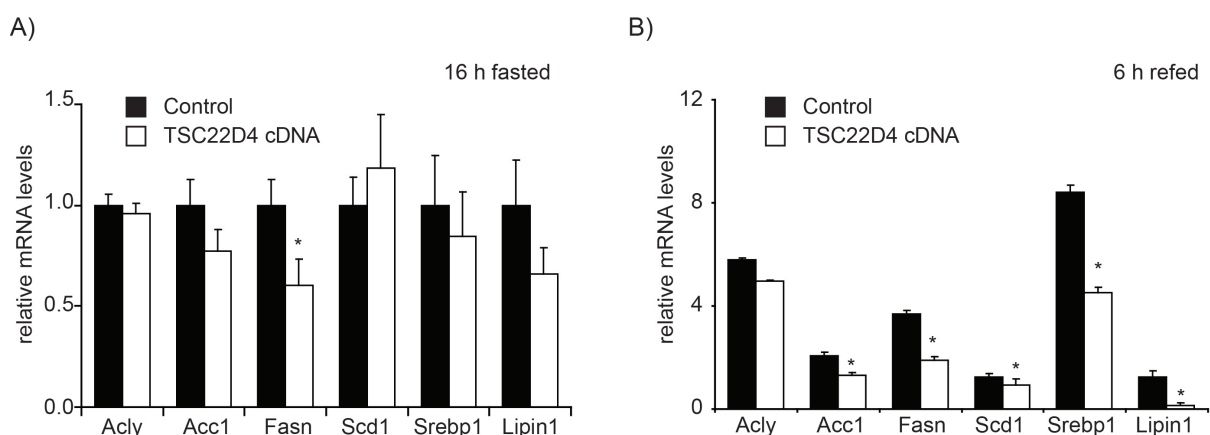


Fig. 48: Lipogenesis is blunted in TSC22D4 over expressing mice. Quantitative PCR analysis of ATP citrate lyase (Acly), acetyl-coenzyme A carboxylase 1 (Acc1), fatty acid synthase (Fasn), stearoyl-CoA desaturase-1 (Scd1), sterol regulatory element-binding protein-1c (Srebp1) and Lipin1 mRNA levels in livers of 16 hour fasted (**A**) or 6 hour refed (**B**) control or TSC22D4 over expression adenovirus-injected wild-type C57BL/6J mice 7 days after injection; (means \pm SEM, $n \geq 4$). $P \leq 0.05$, * indicates significance. Gene expression values are normalized to control 16 h fasted values.

5.4.2. Fatty acid synthase is repressed by TSC22D4

In order to demonstrate the involvement of TSC22D4 in the repression of lipogenesis in an *in vitro* setting, immortalized Hepa 1c1 mouse hepatoma cells were transfected with a vector encoding the fatty acid synthase (FasN) promoter in frame with the luciferase coding sequence. A second construct expressing either Flag peptide as a control, or Flag-TSC22D4 was co-transfected and a third vector encoding β -galactosidase was used to normalize results. As was seen in *in vivo* experiments, TSC22D4 led to a dose dependent repression of FasN promoter activity (Fig. 49). In summary, these data support the hypothesis that TSC22D4 is directly involved in the regulation of lipogenic gene expression.

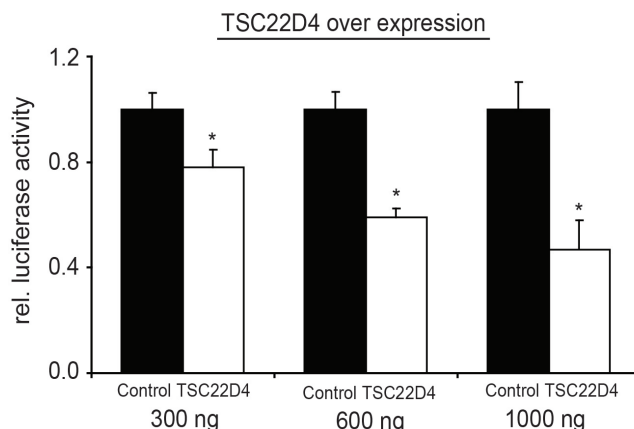


Fig. 49: TSC22D4 represses fatty acid synthase promoter activity. Transient transfection assay of Hepa 1c1 hepatocytes cotransfected with a pGL2_FAS -150bp/-43bp FasN promoter construct and increasing amounts of TSC22D4 cDNA; (means \pm SEM, n \geq 3). P \leq 0.05, * indicates significance.

5.4.3. Semi-endogenous co-immunoprecipitation

Utilizing the presence of the Flag-tagged TSC22D4 protein in mice treated with the TSC22D4 over expression adenovirus, semi-endogenous co-immunoprecipitation studies were performed to verify the hepatic interaction with TBL1/TBLR1. For this purpose, we used anti-Flag agarose and 4 mg of hepatic protein lysate. Indeed, both TBL1 and TBLR1 co-precipitated with Flag-tagged TSC22D4 (Fig. 50), indicating that the observed interaction actually takes place in the liver and that TSC22D4, TBL1 and TBLR1, at least in part mutually contribute to the observed reduction in serum TG levels. As lipogenesis is controlled by all three of the proteins, it is likely that together they are involved in the repression of this process.

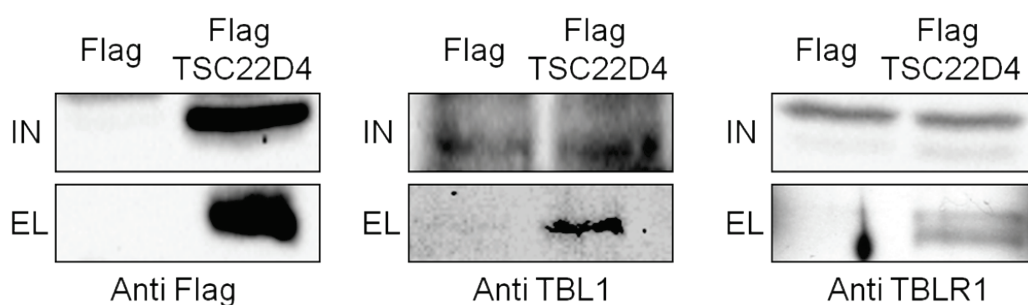


Fig. 50: TBL1 and TBLR1 interact with TSC22D4 in the liver. C57BL/6J mice were infected with either Flag-TSC22D4 or empty control adenovirus. 7 days after injection Flag co-immunoprecipitation studies were performed with 4 mg of liver protein lysate. TBL1 (A) and TBLR1 (B) only co-precipitated in the presence of Flag-TSC22D4. Affinity purification was performed with an anti-Flag antibody. Bound proteins were resolved by SDS-Page and subsequently detected by Western blot. IN: input; EL: elution.

5.4.4. Hepatic TSC22D4 restoration in obese mice

Up until now, we had observed that TSC22D4 over expression leads to the opposite phenotype to TSC22D4 knock down and that mice fed a high fat diet express decreased amounts of TSC22D4 in the liver. The question therefore arose, whether restored TSC22D4 expression in livers of obese mice could counteract the associated pathological hypertriglyceridemia. To address this point, mice were fed either a control diet (LFD) containing 10% energy from fat or a high fat diet (HFD) containing 60% energy from fat for 11 weeks. 10 days prior to sacrifice, 2×10^9 infectious units of empty control or TSC22D4 over expression adenovirus were injected via the tail vein. The degree of obesity and any effects of TSC22D4 on body composition were assessed by weight and EchoMRI measurements. Mice fed the HFD were significantly heavier than LFD fed mice and also had more than double the amount of fat. No differences could however be seen between TSC22D4 over expressing and control mice concerning body composition (Fig. 51 A, B).

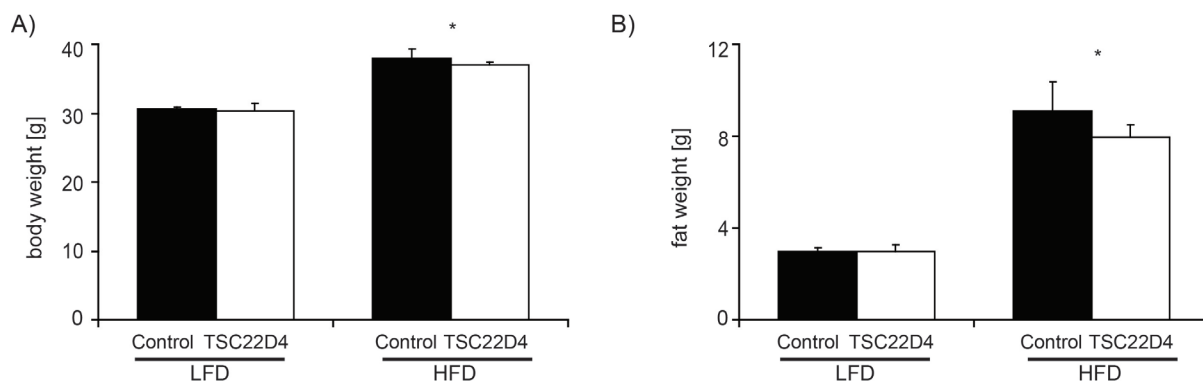


Fig. 51: Body weight and fat content of obese TSC22D4 over expressing mice. Body weight of control or Flag-TSC22D4 cDNA adenovirus-injected C57BL/6J mice 7 days after injection. Mice had previously been fed either a control low fat diet (LFD), or a high fat diet (HFD) for 12 weeks (**A**). Body fat content of the same mice as above (**B**); (means \pm SEM, n=7). P \leq 0.05, * indicates significance (LFD vs. HFD).

Blood glucose levels were determined in fasted and fed mice. In the fasted state, no differences were measurable in lean mice. As expected, obese control mice had higher fasting blood glucose levels than LFD fed mice. Obese TSC22D4 over expressing animals, however, displayed fasting blood glucose levels comparable to those seen in lean individuals (Fig. 52 A). In the fed state, obese control mice again had higher blood glucose levels than lean animals. TSC22D4 over expression did not affect fed

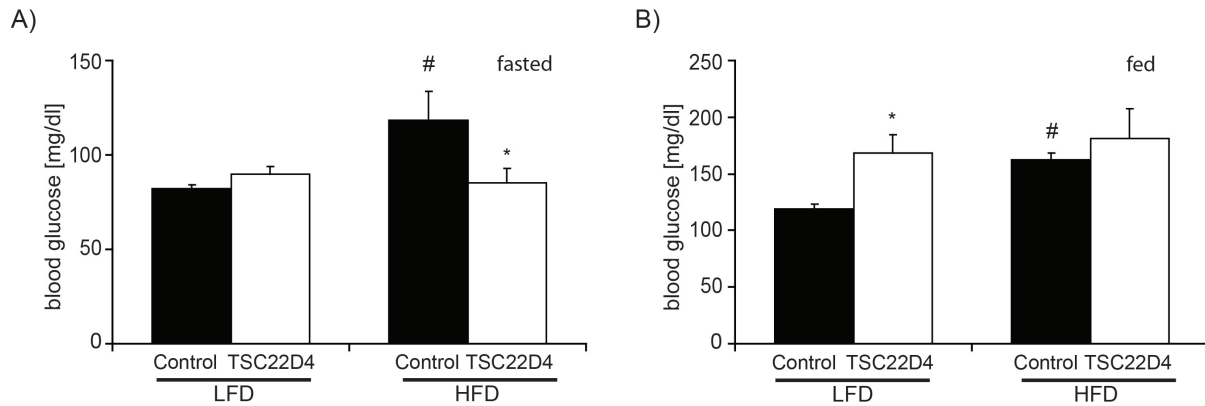


Fig. 52: Fasting and feeding blood glucose levels of obese TSC22D4 over expressing mice.
Fasting (A) or feeding (B) blood glucose levels of control or Flag-TSC22D4 cDNA adenovirus-injected C57BL/6J mice 7 days after injection. Mice had previously been fed either a control low fat diet (LFD), or a high fat diet (HFD) for 12 weeks; (means \pm SEM, n=3). P \leq 0.05, * indicates significance (control vs. TSC22D4). # indicates significance (LFD vs. HFD).

blood glucose levels in obese mice, but did increase levels in lean mice, bringing them into the same range as seen in HFD fed animals, indicating that TSC22D4 over expression affects insulin signalling or glucose handling (Fig. 52 A). Mice were sacrificed in the random fed state. As expected, liver TG levels were elevated in HFD compared to LFD fed mice. In line with previous results, hepatic TG stores were larger in TSC22D4 over expressing mice when compared to their control counterparts (Fig. 53 A). The effect was strongest in lean mice, but a tendency was also visible in obese animals. Liver cholesterol levels were not affected by any of the observed conditions (Fig. 53 B).

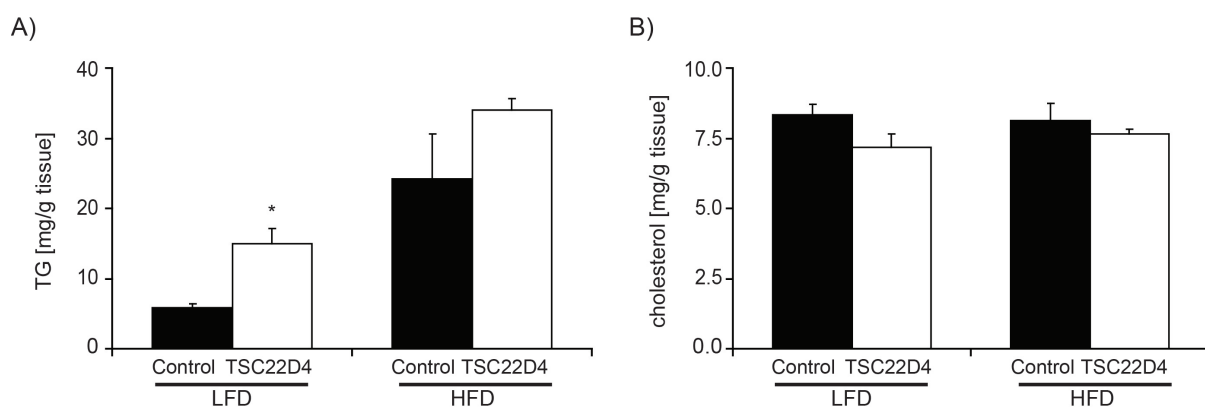


Fig. 53: Hepatic triglycerides and cholesterol in obese TSC22D4 over expressing mice.
Hepatic triglyceride (TG) (A) and cholesterol (B) content of control or Flag-TSC22D4 cDNA adenovirus-injected C57BL/6J mice 7 days after injection. Mice had previously been fed either a control low fat diet (LFD), or a high fat diet (HFD) for 12 weeks; (means \pm SEM, n=3). P \leq 0.05, * indicates significance (control vs. TSC22D4).

Serum cholesterol and TG content in the HFD fed mice were investigated after fractionation by FPLC. TSC22D4 over expression slightly blunted the HDL cholesterol peak, indicating that circulating lipoprotein metabolism was affected (Fig. 54 A). The VLDL TG peak observed in mice treated with control virus was completely absent in TSC22D4 over expressing mice (Fig. 54 B). This result is in line with previous data and strengthens the hypothesis that TSC22D4 is involved in the suppression of VLDL release.

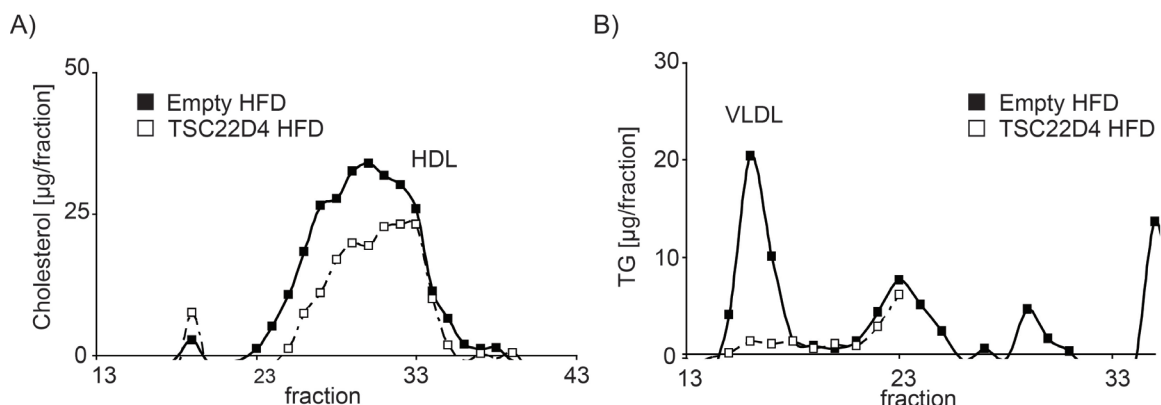


Fig. 54: Serum lipoprotein profiles of obese TSC22D4 over expressing mice. Lipoprotein-associated serum cholesterol (**A**) and triglyceride (TG) (**B**) levels as measured by fast protein liquid chromatography (FPLC). Mice had previously been fed a high fat diet (HFD) for 12 weeks; (n=3).

Taking all the results obtained so far into account, one would expect that the observed decrease in circulating VLDL after TSC22D4 over expression results from defective VLDL secretion. To prove this is the case, a VLDL secretion assay was performed with HFD fed mice treated with control or TSC22D4 over expression adenovirus. In line with the previous observations, VLDL secretion was indeed reduced in these animals (Fig. 55).

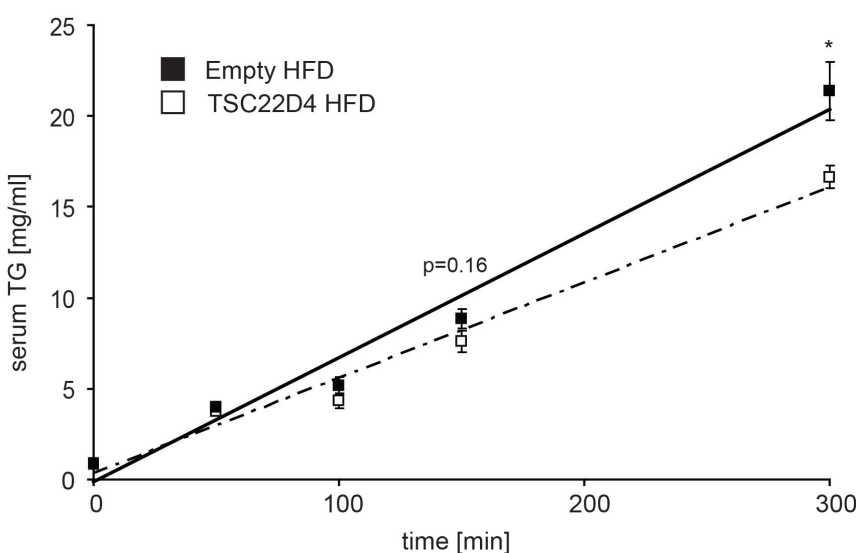


Fig. 55: TSC22D4 over expression leads to decreased VLDL secretion by the livers of obese mice. Hepatic very-low-density lipoprotein (VLDL) release in control or TSC22D4 over expression adenovirus-injected wild-type C57BL/6J mice. Time after tyloxapol injection indicated. Mice had previously been fed a high fat diet (HFD) for 12 weeks; (means \pm SEM, n \geq 4). P < 0.05, * indicates significance.

5.5 TSC22D4 and cancer cachexia

The phenotypes resulting from TSC22D4 knock down and over expression indicate that the gene is involved in the regulation of VLDL release by the liver. Judging from these data, one could speculate that TSC22D4 may play a role in the pathogenesis of tumour-associated cancer cachexia, a condition in which muscle and adipose tissue depots are depleted (81). One characteristic of the early stages of this disease is the development of hepatic steatosis in combination with low levels of circulating serum TGs (22). As this reflects the phenotype observed in mice over expressing TSC22D4, we analyzed mouse models associated with the development of cancer cachexia in regard to TSC22D4 expression.

5.5.1. TSC22D4 is elevated in mouse models of wasting and cachexia

5.5.1.1. *TSC22D4 is induced by a methionine and choline deficient diet*

Mice fed a diet lacking methionine and choline (MCD), develop severe hepatic steatosis and have low serum TG levels. Choline is an important component required for the production of VLDL particles in the liver. Its absence results in defective VLDL assembly (82). Methionine deficiency, on the other hand, severely disrupts protein metabolism. As a consequence, mice lose large amounts of weight and fat content. Whilst this model does not directly reflect cancer cachexia, the conditions do have many similarities, concerning hepatic lipid metabolism and drastic weight loss.

Mice were fed either a control diet or an MCD diet for 4 weeks. Indeed, the MCD-fed animals lost a significant amount of total body (Fig. 56 A) and fat weight (Fig. 56 B) during the course of the diet. As expected, serum TG levels were dramatically decreased (Fig. 56 C) and the livers accumulated large quantities of fat (Fig. 56 D). The expression of the lipogenic genes FasN and Srebp1 was blunted, as had been the case in TSC22D4 over expressing mice (Fig. 56 E). Importantly, TSC22D4 mRNA and protein were strongly up regulated in mice on the MCD diet, hinting towards an involvement in VLDL release under pathological conditions (Fig. 56 F, G).

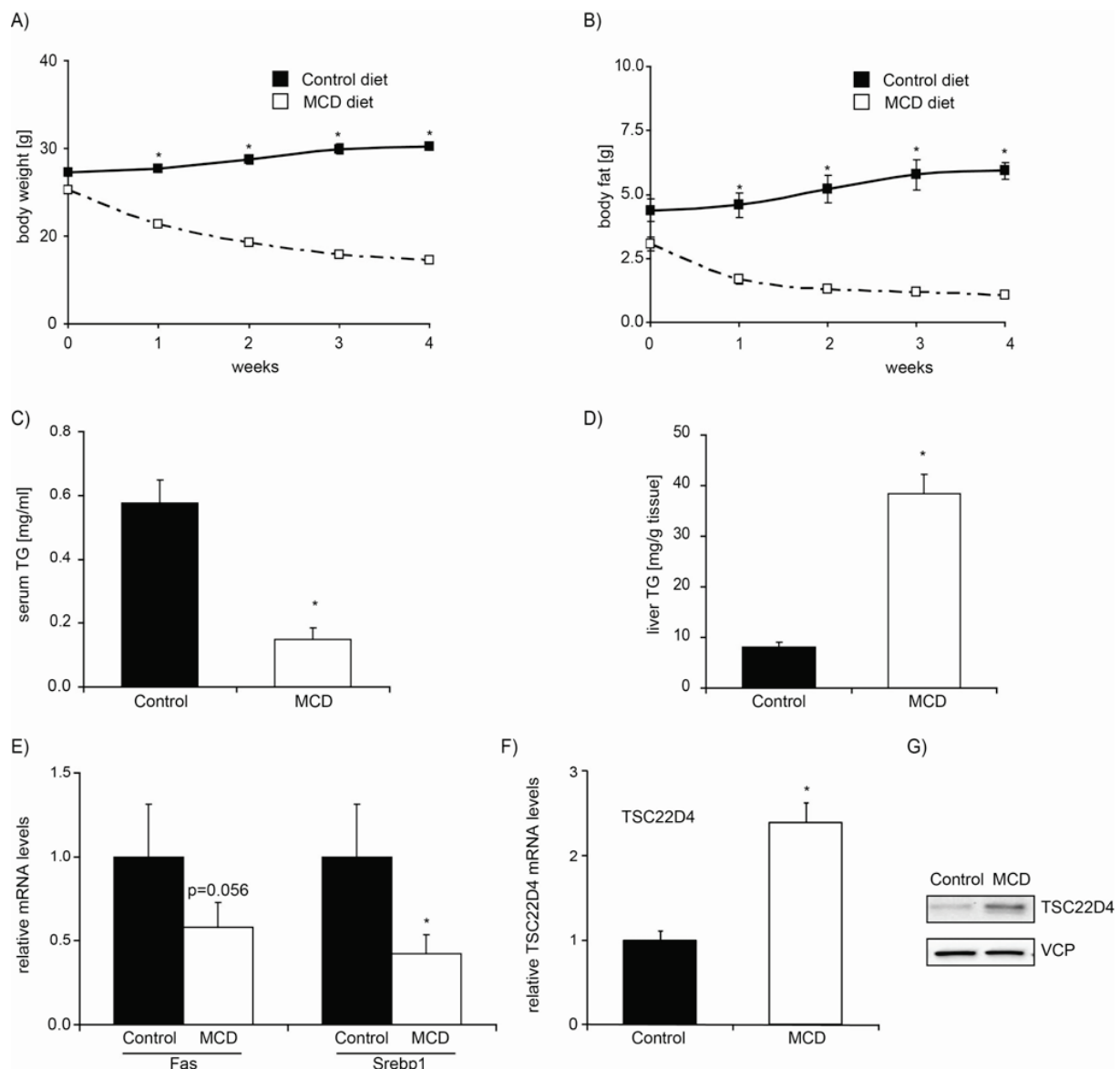


Fig. 56: TSC22D4 is induced by methionine and choline deficiency. Body weight (**A**) and fat content (**B**) of C57BL/6J mice fed a methionine and choline deficient diet (MCD) for 4 weeks. Serum (**C**) and liver (**D**) triglyceride (TG) levels of control or MCD fed mice after 4 weeks. Quantitative PCR analysis of fatty acid synthase (Fasn) and sterol regulatory element-binding protein-1c (Srebp1) expression in the same mice as above (**E**). Quantitative PCR analysis of TSC22D4 expression in the same mice as above (**F**). Western blot analysis of TSC22D4 expression in a representative mouse from above (**G**); (means \pm SEM, n = 6). P \leq 0.05, * indicates significance.

5.5.1.2. *TSC22D4* levels correlate with weight loss in cachectic mice

Based on the results obtained from the MCD fed animals, we investigated TSC22D4 expression in cachectic Balb C mice. Ten animals were injected with 1.5×10^6 Colon 26 (C26) murine adeno-carcinoma cells. Tumours started to visibly appear after 3-5 days. The tumour implantation induced anorexia, weight loss and ultimately cachexia

within a short time (data not shown). Mice were sacrificed three weeks after injection and the degree of cachexia was determined by calculating the amount of weight lost since tumour implantation. At the time of sacrifice, serum TG levels had significantly decreased in tumour bearing animals (Fig. 57 A). Interestingly hepatic TSC22D4 expression was significantly increased in these cachectic mice (Fig. 57 B). More importantly, TSC22D4 expression levels correlated inversely with the degree of weight loss, indicating that TSC22D4 is induced during the onset of cancer cachexia (Fig. 57 C).

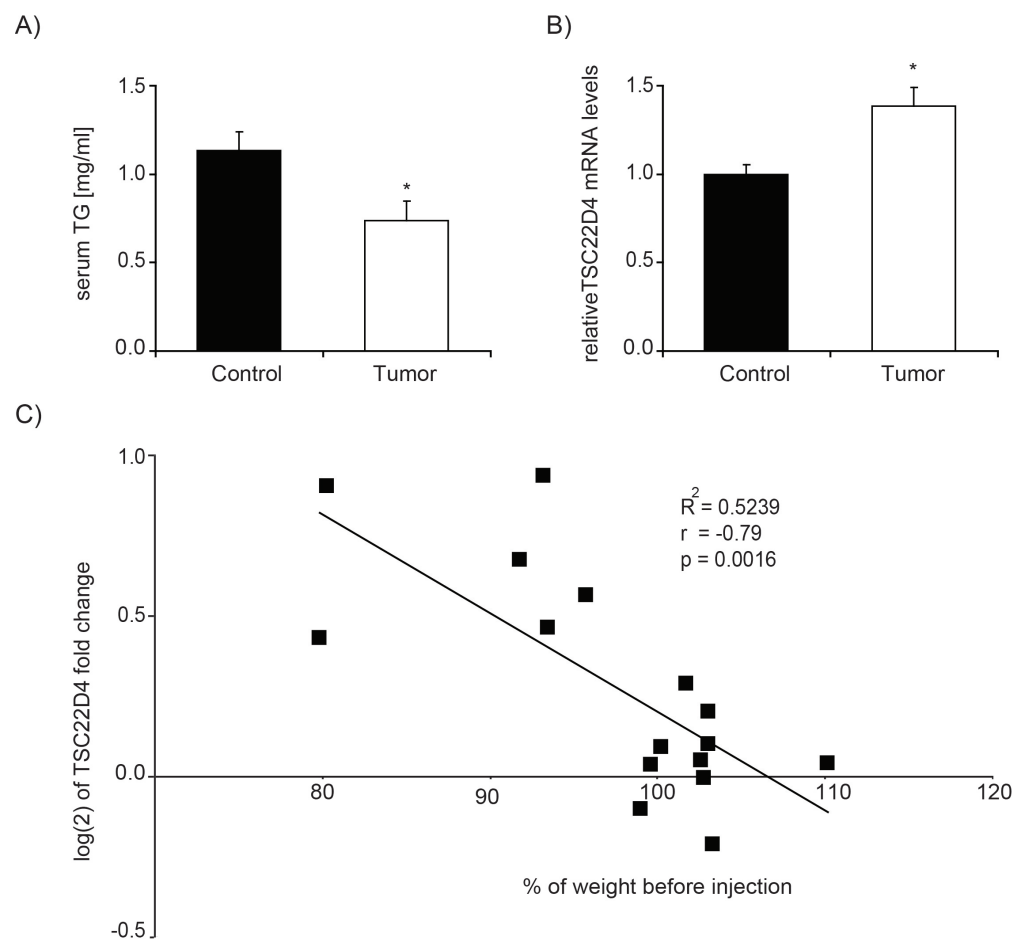


Fig. 57: TSC22D4 expression correlates with the degree of cachexia in mice. Male Balb C mice were injected with 1.5×10^6 C26 mouse tumour cells. Serum triglyceride (TG) levels of control (PBS) or tumour-injected mice, 3 weeks after implantation (**A**). Quantitative PCR analysis of TSC22D4 expression in the same mice as above (**B**). Pearson's correlation of $\log(2)$ of TSC22D4 expression and the per cent of initial weight at the time of sacrifice (**C**); (means \pm SEM, $n \geq 6$). $P \leq 0.05$, * indicates significance.

6. DISCUSSION

The nuclear co-factors TBL1 and TBLR1 can associate with co-repressor complexes such as N-CoR/SMRT and Ctbp, leading to transcriptional repression of gene expression. Since both factors are also able to recruit co-activators and are required to switch on (de-repress) the expression of specific target genes, they are commonly referred to as nuclear co-repressor / co-activator exchange factors (59).

In this study we identify transforming growth factor-beta 1 stimulated clone-22 D4 (TSC22D4) as a novel TBL1 and TBLR1 interaction partner. TSC22D4 is located on human chromosome 5 and was first described due to its homology to the transforming growth factor-beta (TGF β) responsive gene TSC22D1 (66,83,84). The two proteins are members of a family of four structurally related proteins (TSC22D1-4) with a characteristic central interaction domain (TSC box), followed by a conserved leucine zipper structure. The N-terminal domains are less conserved, giving each member specific functions. TSC22D4 and TSC22D1 have been shown to homo- and heterodimerize via their leucine zippers and can both repress gene expression. The repressor activity is thereby probably localized in the N-terminus. TSC22D4 does not harbour a canonical DNA binding motif and may well be recruited to chromatin by interaction partners (66). Very little *in vivo* data is available concerning TSC22D4. The protein is induced during pituitary gland development and is involved in the differentiation of neuronal precursor cells. Indeed, TSC22D4 is expressed throughout the developing and adult brain (85,86). Furthermore, physiological stress conditions such as hyperosmotic stress in the kidney seem to favour TSC22D4 expression (84). The protein localizes in both the cytosol and the nucleus, whereby nuclear import seems dependent on external signals and is not mediated by a classical nuclear localization sequence (NLS) (87). In this regard, TSC22D4 is recruited to the nucleus of neuronal cells during the onset of apoptosis where it has been shown to interact with apoptosis inducing factor (AIF) (88,89). As its structural relative and interaction partner TSC22D1 is a known pro-apoptotic protein and tumour suppressor, one can speculate that TSC22D4 may also play a role in the regulation of cell survival and proliferation (90-93). There is currently little data available concerning mechanistic and tissue-specific functions of TSC22D4. This study provides first insights into the hepatic and physiological relevance of the gene

and identifies pathological conditions potentially linked to changes in TSC22D4 gene expression.

We demonstrate that TSC22D4 knock down in the liver partially phenocopies hepatic TBL1/TBLR1 deficiency, as in both cases the expression of lipogenic genes is induced (63). We however also observe that TSC22D4 and TBL1/TBLR1 have divergent functions. Whilst TBL1 and TBLR1 are crucial in protecting the liver against steatosis, TSC22D4 reduces secretion of VLDL particles by the liver. In turn, this process increases hepatic TG stores. Consistently, TSC22D4 expression is reduced in mouse models of hypertriglyceridemia (pre-diabetes) and elevated in hypotriglyceridemia (cancer cachexia). In this discussion we will focus on the three aims of the study addressed on page 17.

6.1 TSC22D4 interacts directly with TBL1/TBLR1

We employed a cell-based, high throughput interaction screen to identify interaction partners of the transcriptional co-factors TBL1 and TBLR1. Both proteins have previously been shown to be components of large multi-protein complexes ranging up to 2 MDa in size (56,94). In the past, similar experiments not only identified the association of TBL1/TBLR1 with the N-CoR/SMRT and Ctbp co-repressor complexes, but also identified further dynamic complex components, such as the signalling molecule G protein pathway suppressor (GPS) 2 and nuclear receptors, including the master regulator of hepatic fatty acid oxidation PPAR α (54,59,63,95). We chose to screen for novel TBL1/TBLR1 interaction partners using a LUMIER assay that was originally developed to analyze the TGF β signalling pathway and has since been successfully modified and employed in several further studies (64,96,97). In our experiments, the bait consisted of a nuclear protein library. Although TBL1 and TBLR1 do have functional relevance in the cytosol and can interact with the mitotic spindle during cell division, transcriptional regulation in the nucleus seems to be their primary function (98). The screen was performed in HEK293T cells, as this cell line is easily transfected. Protein over expression is thereby a powerful tool when trying to identify transient interactions or the association of proteins with low

endogenous expression levels, as is the case for transcriptional co-factors. For both TBL1 and TBLR1, the strongest interaction signal resulted from co-transfection with the TSC22 family member TSC22D4. Currently there is only very little mechanistic and *in vivo* information available concerning this protein. It seems to have transcriptional repressor activity and to modulate cell proliferation and apoptosis (66,99). Due to the impressive strength of the interaction and the fact that the role of this gene is so far barely understood, we chose TSC22D4 as the target for further investigation.

In follow-up experiments, we could show that the interaction between TBL1/TBLR1 and TSC22D4 was of direct nature. Subsequently, we mapped the association to specific domains. TBL1 and TBLR1 possess three distinct protein motifs. The N-terminal Lis1 homology (LisH) domain is required for the formation of TBL1/TBLR1 homo- and heterodimers and also enables nuclear translocation of the co-repressors. By binding to histone H4 and N-CoR/SMRT, this domain is furthermore necessary for co-repressor complex assembly and activity (57,100). The LisH domain is followed by an F-Box region that recruits ubiquitin conjugating enzymes during de-repression (58). Finally, the C-terminus of TBL1/TBLR1 consists of eight WD40 repeats that form a β -transducin propeller structure. Each WD40 motif contains approximately 40 amino acids including a distinct tryptophan (W) / aspartic acid (D) dipeptide. β -transducin propellers act as platforms for the assembly of multi-protein complexes (57). Interestingly, TSC22D4 interacted with the TBL1/TBLR1 WD40 domain. Whilst the first 105 TSC22D4 amino acids were not sufficient to mediate the interaction, the extended N-terminus ranging to amino acid 207 sufficed. The leucine zipper structure that mediates homo- and heterodimerization of TSC22 family members, as well as their association with other proteins did not seem necessary for protein-protein interaction (66). This was also the case for the characteristic TSC box which mediates the effects of TSC22 proteins in regard to cell proliferation and regulation of apoptosis (99,101). We were not successful in co-immunoprecipitating endogenous TBL1/TBLR1 and TSC22D4 in the liver, probably due to insufficient antibody quality and the generally low expression levels of co-factor proteins. Semi-endogenous immunoprecipitation after transduction with an adenovirus over-expressing Flag-TSC22D4 was however successful, demonstrating that the interaction is relevant in the mouse liver. In future it will be interesting to investigate

the influence of external signals and stimulants on complex formation in either an *in vivo* or cell-autonomous *ex-vivo* setting.

During the LUMIER screens we also observed that TBL1 and TBLR1 interact with another TSC22 family member, namely TSC22D1. Members of our laboratory have in the mean time recapitulated this interaction by co-immunoprecipitation (unpublished data). It will be interesting to perform GST pull-down assays and see if the association with TSC22D1 is also of direct nature, or if heterodimerization with TSC22D4 is required to link both proteins to the co-repressors. Previous work on the common *Drosophila melanogaster* TSC22 precursor *bunched* suggests that TSC22D4 and TSC22D1 may at least in part have antagonizing effects in regard to cell proliferation (102,103). Indeed, understanding the interplay between TBL1/TBLR1 and TSC22 family members could in the future uncover complex regulatory networks.

6.2 TSC22D4 represses VLDL secretion

TSC22D4 loss and gain of function studies were performed in the livers of adult mice. Transient manipulation of gene expression using adenovirus was the method of choice, as genetic TSC22D4 knock-out or over expression mouse models are currently not available. It is furthermore unknown whether such animals would be viable, or if their development would be hindered by the prenatal deregulation of TSC22D4. Furthermore, genetic mouse models occasionally have no phenotype, as the effects are compensated by other genes during development (65,104). This is less likely in transient studies, as the adult body only has little time to adapt to changes in gene expression. Furthermore, particular genes might exert specific functions during development which differ from those in the adult organism. Consequences of these effects are avoided in conditional genetic models or by using viral systems. TSC22D4 has been suggested to work as a transcriptional co-factor (66). Although evidence for its role as a co-repressor is limited, the interaction with nuclear co-repressor / co-activator exchange factors TBL1 and TBLR1 supports the hypothesis. As the TBL1/TBLR1 co-factors govern important metabolic checkpoints, we chose to

investigate the liver-specific functions of TSC22D4, especially in regard to previous data published by Kulozik et al. in 2011.

In the absence of hepatic TSC22D4, lipogenic gene expression was enhanced. VLDL secretion was markedly increased whilst hepatic TG stores were reduced, indicating that excess TGs resulting from *de novo* lipogenesis were immediately shuttled out of the liver. In proof of this principle, TSC22D4 over expression had opposing effects, namely reduced lipogenic gene expression and lower VLDL secretion while TGs accumulated in the liver. It is known that upon stimulation of lipogenesis, newly synthesized lipids can be directly incorporated into VLDL and that lipogenesis per se enhances VLDL secretion in humans (105,106). It has also previously been shown that silencing of certain lipogenic genes induces a phenotype resembling that resulting from TSC22D4 over expression, a setting in which we observed that these lipogenic genes were down regulated. Indeed, knock down of ATP-citrate lyase (Acly), a key lipogenic enzyme required to convert citrate to acetyl-CoA, results in reduced lipogenesis and VLDL secretion, whilst hepatic TG stores are increased (107). Whole body Acly inhibition thereby favours hypolipidemia and prevents weight gain when mice are fed a high fat diet (108-110). Similar results were observed when Stearoyl-CoA desaturase (Scd1) was inactivated, again cumulating in reduced lipogenesis and VLDL secretion (111,112). TBL1/TBLR1 double knock down had the same consequences as TSC22D4 deficiency in regard to lipogenic gene expression. As this process is both directly and indirectly regulated by the nuclear receptor Liver X receptor (LXR), it is tempting to speculate that TSC22D4, TBL1 and TBLR1 mutually repress LXR activity and, in turn, inhibit lipogenesis. Future experiments focusing on LXR target gene promoter activity may shed more light on the molecular mechanisms underlying these particular transcriptional control events.

Unlike TBL1/TBLR1 ablation, TSC22D4 deficiency did not reduce β -oxidation or inhibit VLDL uptake by the liver (63). This points towards independent roles for each co-factor and indicates that whilst TSC22D4 may well be incorporated into TBL1/TBLR1 co-repressor complexes governing lipogenesis, it does not seem to be involved in PPAR α associated TBL1/TBLR1 co-activator structures. This is in line with previous reports stating that TSC22D4 had repressive, but not activating capacity (66). Unlike TBL1/TBLR1, TSC22D4 seems to regulate hepatic VLDL

secretion. Healthy wild type mice secrete up to 50 mg of TG per day, implying that chronically elevated VLDL secretion will over time greatly increase serum TG load, but at the same time may act as an effective mechanism in protecting against hepatic steatosis (113). So far, only few genes are known that significantly regulate VLDL secretion. Microsomal triglyceride transfer protein (MTP) 1 facilitates apoB and subsequently VLDL maturation. MTP1 mutations are associated with hypoapolipoproteinemia and accompanied by reduced VLDL secretion (114). MTP1 expression was however not affected by TSC22D4 manipulation. The expression of Lipin1, another gene linked to VLDL secretion, was significantly up regulated upon TSC22D4 knock down and down regulated upon TSC22D4 over expression. No significant changes in Lipin1 expression were observed in TBL1/TBLR1 experiments. Lipin1 is a phosphatidate phosphatase that associates with microsomal membranes in the ER and catalyses the penultimate step in glycerolipid biosynthesis, namely the conversion of phosphatic acid to diacylglycerol (115). Previous studies have demonstrated that Lipin1 actively enhances VLDL secretion by hepatocytes and also increases intracellular apoB stability. Conversely, the same studies demonstrated that Lipin1 depletion decreases VLDL release by the liver (116). Interestingly, glucocorticoid treatment seems to induce Lipin1 expression, which may explain the increase in VLDL secretion often occurring as a side effect during glucocorticoid treatment (117). As we have shown that TSC22D4 expression is reduced in mice chronically injected with dexamethasone, it is plausible that TSC22D4 may partake in the inhibition of Lipin1 activation in untreated mice. Whilst these data open interesting hypotheses and link TSC22D4 to Lipin1, it must be noted that another study using fatty liver dystrophy (*fld*) mice, a genetic mouse model characterized by a Lipin1 null mutation, has delivered conflicting results. Whilst the mice did display hepatic steatosis, in this setting Lipin1 deficiency had the exact opposite effect regarding serum TG levels. The mice displayed serum hypertriglyceridemia due to enhanced VLDL secretion (118). The reasons underlying the observed discrepancies are so far not understood. Chronic, systemic Lipin1 deficiency is perhaps compensated by the other members of the lipin family, namely the phosphatidate phosphatases lipin 2 and lipin 3 (115).

It is known that in the long run, increased hepatic lipogenesis leads to dyslipidemia and insulin resistance (119). Glucose and insulin tolerance were not affected in

transient TSC22D4 knock down experiments. The insulin signalling cascade was however blunted, indicating primary defects in glucose metabolism. It is plausible that hepatic TSC22D4 deficiency alone is not sufficient to induce full-blown insulin resistance and glucose intolerance. Interestingly, unpublished data obtained in our laboratory indicate that TSC22D4 deficiency in adipose tissue leads to reduced lipogenesis accompanied by increased lipolysis. Indeed, in these studies the same lipogenic genes, including Acly and Scd1 were deregulated, albeit in the opposing direction. As these effects also favour the development of type 2 diabetes (15) it would be of great interest to study full body TSC22D4 knock-out animals in regard to systemic insulin sensitivity. In this respect, it is however important to keep in mind that the effects on lipid metabolism were compensated in long-term hepatic TSC22D4 deficiency, perhaps by related proteins. As all TSC22 family members can potentially homo- and heterodimerize and have a common precursor in *Drosophila melanogaster* (66), it is possible that knock down of more than one family member is required to observe long-term metabolic consequences. As mentioned above, the interplay between different TSC22 family members and transcriptional regulation is of great interest.

6.3 TSC22D4 in health and disease

6.3.1. TSC22D4 and obesity

Hepatic TSC22D4 expression is reduced in obese and pre-diabetic mice whilst serum TG levels are elevated upon hepatic TSC22D4 knock down. It is therefore plausible that the regulation of this gene may have implications for the pathogenesis of obesity-related hypertriglyceridemia. The reduction in hepatic TSC22D4 expression under obese conditions may however also serve to protect already steatotic livers against further TG accumulation. TSC22D4 expression is also reduced in hyperglucocorticoidemia, a condition characterized by increased *de novo* lipogenesis (71). This, in turn, indicates that TSC22D4 may play a role in the occurrence of hypertriglyceridemia as a side-effect of chronic glucocorticoid (e.g. dexamethasone) treatment, a process that is also governed by changes in Lipin1 expression (117).

6.3.2. TSC22D4 and carcinogenesis

In recent years, the connections between metabolic disorders and tumour development have become increasingly evident (120). Malignant cells display characteristic changes in metabolic regulation to favour cell proliferation. In a process known as the Warburg effect, for example, cells shift their energy-producing capacity from oxidative phosphorylation towards less efficient aerobic glycolysis. This shift increases the immediate uptake and incorporation of nutrients into the biomass and induces rapid cell proliferation (20,121). Several genes which were previously considered to be classical regulators of lipid metabolism have recently been shown to play a role in the regulation of cell proliferation. Acly is, for example, up regulated in lung adenocarcinoma cells. Consistently, Acly knock down not only reduces *de novo* lipogenesis, but also induces growth arrest and protects against proliferation (122). Another study demonstrated that inhibition of the lipogenic gene FasN impairs cellular proliferation and actively induces apoptosis (123). As TSC22D4 has been suggested to function as a tumour suppressor, its negative regulation of potentially tumourigenic, lipogenic gene expression may present a new node linking metabolic control with carcinogenesis. Indeed, Acly and FasN were both amongst the genes most prominently affected by changes in TSC22D4 expression and were both strongly up regulated in the absence of TSC22D4. At this point it is important to add that in another study we have observed significantly elevated levels of TSC22D4 expression in pancreatic tumour samples when compared to healthy control tissue (unpublished observation). These data indicate that, at least in the pancreas, TSC22D4 may also act as an oncogene. In this regard, whilst most publications imply that the TSC22 gene family has anti-proliferative, tumour suppressive capacity there has also been some evidence that the *Drosophila melanogaster* TSC22D4 homolog bunched promotes cellular proliferation (102,103). In future it will be interesting to address the links between TSC22D4 and cancer in more detail. Understanding potential pro- or anti-tumourigenic activity is important when considering TSC22D4 as a potential drug target. Analysis of human liver cancer samples in regard to expression of TSC22 family members will help when investigating these processes. Subsequently, as TSC22 proteins are implicated with the regulation of cell death, apoptosis assays and cell-survival studies may give new functional insights into the relevance of TSC22D4.

6.3.3. TSC22D4 and cancer cachexia

Whilst hepatic TSC22D4 expression was down regulated in obesity, expression was markedly increased in cancer cachexia, a catabolic condition in which peripheral TG levels are decreased but hepatic TG stores are elevated (22). There was a clear negative correlation between TSC22D4 mRNA levels and the degree of wasting, indicating a role for TSC22D4 in the control of liver catabolism. In patients, survival prognosis worsens with increased loss of muscle and adipose tissue (21), suggesting that TSC22D4 may act as a hepatic marker for cancer progression and outcome. The reduction of VLDL release from cachectic livers may thereby be controlled by TSC22D4. In future, it will be important to understand whether changes in hepatic TSC22D4 expression are causal in cachexia progression. In this regard, TSC22D4 may inhibit the distribution of TGs throughout the wasting body. Alternatively, TSC22D4 may coordinate protective mechanisms by which hepatic TG stores are protected for the final stages of wasting in which no peripheral energy sources are available. In either case, TSC22D4 is a potentially attractive drug target in the search for anti-cachexia treatment strategies, of which currently only few exist (21). Understanding the signals required to modulate TSC22D4 expression in the different disease condition will be of utmost importance when trying to find compounds that influence TSC22D4 activity.

6.4 Summary and outlook

In summary, we have identified a novel physical interaction between TBL1/TBLR1 and TSC22D4. Whilst all three genes are involved in the suppression of hepatic lipogenesis, they also have distinct roles in the liver. TSC22D4 thereby inhibits VLDL release and consequently regulates both hepatic and serum lipid metabolism (Fig. 58). Down regulation of TSC22D4 was seen in mouse models of pre-diabetes (hypertriglyceridemia) whilst expression levels were elevated in cachectic mice (hypotriglyceridemia). The implications associated with these changes in gene expression remain to be characterized, as do the precise molecular mechanisms by which TSC22D4 regulates lipogenic gene expression. *In vitro* promoter activity

assays and chromatin immunoprecipitation studies will be required to shed light on these issues. We have furthermore presented preliminary data indicating that TSC22D4 is involved in tumour development. Further experiments in this direction, including cell proliferation assays, are of great interest and may produce another potent link between molecular transcriptional control and tumour development. In the light of these first *in vivo* data, the generation of inducible tissue-specific or full body TSC22D4 knock-out and over expression mice is worth considering.

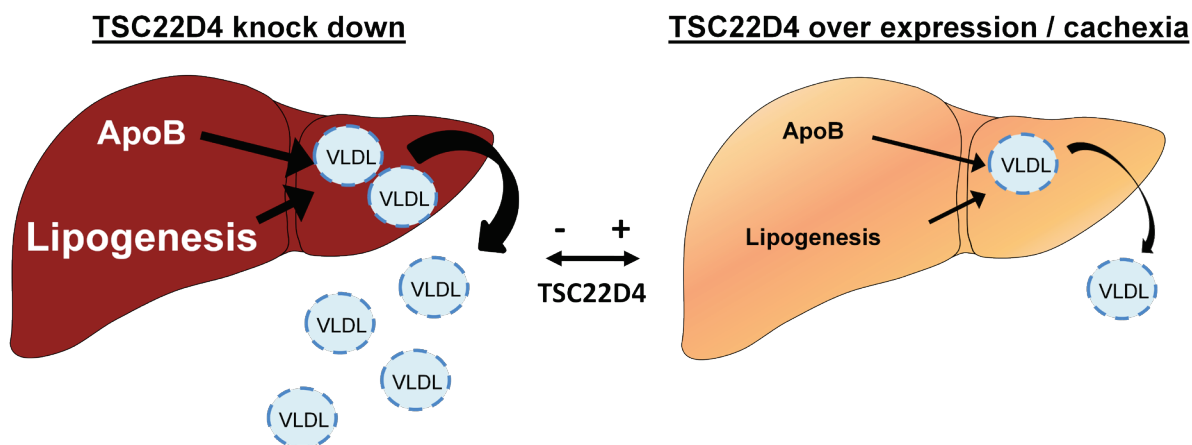


Fig. 58: Effects of TSC22D4 manipulation on hepatic lipid metabolism. In the absence of TSC22D4, apolipoprotein (Apo) B stability is increased and lipogenic gene expression is induced. Lipids are subsequently packaged into very low density lipoprotein (VLDL) particles and shuttled from the liver. In contrast, TSC22D4 over expression leads to reduced lipogenesis and lower VLDL secretion, whilst triglycerides accumulate in the liver (orange colour). A similar phenotype can be seen in cancer cachexia, a condition in which hepatic TSC22D4 expression is elevated.

7. MATERIAL

7.1 Instruments

Instrument	Distributor
Analytical scales	Satorius, Göttingen
Bacterial shaker	Infors AG, Böttmingen, CH
Blotting chamber	Bio-Rad, Munich
Camera (<i>Power Shot G6</i>)	Canon, Krefeld
Cell counter	Neolab, Heidelberg
Centrifuge (<i>2K15</i>)	Sigma, Munich
Centrifuge (<i>Biofuge fresco</i>)	Heraeus, Hanau
Centrifuge (<i>Biofuge pico</i>)	Heraeus, Hanau
Centrifuge (<i>Function Line</i>)	Heraeus, Hanau
Centrifuge (<i>Micro 22R</i>)	Hettich GmbH & Co, Tuttlingen
Centrifuge (<i>Super T21</i>)	Heraeus Sorvall, Langenselbold
Centrifuge (<i>XL 70 Ultracentrifuge</i>)	Beckmann, Munich
CO ₂ -incubator	Sanyo, Munich
CO ₂ -incubator (<i>Forma Scientific</i>)	Labotect, Göttingen
Electrophoresis chamber	Steinbrenner, Wiesenbach
Electrophoresis power supply (<i>Power Pack Basic</i>)	Bio-Rad, Munich
Electrophoresis power supply (<i>Power Pack HC</i>)	Bio-Rad, Munich
Electroporator (<i>Gene Pulser II</i>)	Bio-Rad, Munich
Film cassette	Amersham, Freiburg
Film developer	Amersham, Freiburg
FPLC-Äkta	GE Healthcare, Salt Lake City, USA
Fridge, 4°C	Liebherr, Biberach
Gas stove (<i>GASI</i>)	Schütt, Göttingen
Gel documentation station	Bio-Rad, Munich
Heat block	VWR, Darmstadt
Heat block (<i>Thermostat Plus</i>)	Eppendorf, Hamburg

Horizontal shaker (<i>Duomax 1030</i>)	Heidolph, Kehlheim
Hotplate / stirrer	VWR, Darmstadt
Incubator (<i>Function Line</i>)	Heraeus, Hanau
Luminometer <i>microplate LB 940</i>	Berthold Tech., Bad Wildbad
Microscope (<i>Axiovert 40 CFL</i>)	Carl Zeiss, Jena
Microwave	Bosch, Stuttgart
Multistep-pipette	Eppendorf, Hamburg
<i>Neubauer</i> counting chamber	Carl Roth GmbH, Karlsruhe
Nitrogen tank	Thermo Electron coorp., Erlangen
One Touch Glucose monitor	Lifescan, Neckargemünd
pH-meter	VWR, Darmstadt
Photometer (<i>Nano Drop-1,000</i>)	Peqlab Biotechnology, Erlangen
Photometer	Amersham, Freiburg
Pipette controller	Brand, Wertheim
Pipettes	Gilson, Middleton, USA
Rotating wheel	Neolab, Heidelberg
Scales (<i>BL 1500 S</i>)	Satorius, Göttingen
Scanner	Epson, Meerbusch
SDS-electrophoresis chamber	Bio-Rad, Munich
Sonifier 250	Branson, Danburry, Co., USA
Sterile bench (<i>Class II Type A/B3</i>)	Sterilgard, Sanford, USA
Stand	Carl Roth GmbH, Karlsruhe
Tabletop centrifuge (<i>Mini Spin Plus</i>)	Eppendorf, Hamburg
Tabletop scales	Kern und Sohn GmbH, Bahlingen
Thermocycler (<i>PTC-200</i>)	Biozym, Oldendorf
Thermostatic water bath (<i>WBS</i>)	Fried Electric, Haifa, IL
Tissue lyzer	Qiagen, Hilden
Upright freezer, -20°C (<i>Comfort</i>)	Liebherr, Biberach
Upright freezer, -80°C (<i>Hera Freeze</i>)	Heraeus, Heilbronn
Vortex mixer (<i>REAX 2,000</i>)	Heidolph, Kehlheim
Water bath	Neolab, Heidelberg

Water vacuum pump Neolab, Heidelberg

7.2 Consumables

Product	Distributor
Cell scrapers (<i>Costar®</i>)	Corning Inc., NY, USA
Centrifuge tubes (35 ml)	Beckmann, Munich
Polyallomer tubes (25mm x 89 mm)	Beckmann, Munich
Polyallomer tubes (25mm x 89 mm)	Beckmann, Munich
Protein columns (800 µl) (<i>Mobicol</i>)	MoBiTec, Göttingen
Protein columns (2.5 ml)	MoBiTec, Göttingen
Cover slips	Carl Roth GmbH, Karlsruhe
Cryo tubes (2 ml)	Sympore, Beloeil, CA
Cuvettes	Greiner, Frickenhausen
Dialysis tubing (MWCO 15.000; 10 mm diameter)	Carl Roth GmbH, Karlsruhe
Disposable scalpels	Feather, Cuome, JP
DNase / RNase free water	Invitrogen, Karlsruhe
Electroporation cuvettes	Steinbrenner, Wiesenbach
Filters for <i>Mobicol</i> columns (35 µm)	MoBiTec, Göttingen
Filters (0.45 µm)	Millipore, Eschborn
Flag-agarose	Sigma, Munich
Gel staining boxes (<i>Mini</i>)	Carl Roth GmbH, Karlsruhe
Gloves (<i>Safe Skin Purple Nitrile</i>)	Kimberly Clark, BE
Gloves (<i>Proline Vinyl</i>)	Asid Bonz GmbH, Herrenberg
Gradient gels 4-12% (<i>NuPage</i>)	Invitrogen, Karlsruhe
Hyperfilm™ ECL	Amersham, Freiburg
Micro test tubes (1.5 ml, 2 ml)	Steinbrenner, Wiesenbach
Mouth protection	Meditrade, Kiefersfelden
Nitrocellulose membrane	Schleicher and Schüll, Dassel
Parafilm	Pechinery Inc., Wisconsin, USA
Pasteur pipettes	Brand, Wertheim
PCR tubes (200 µl)	Eppendorf, Hamburg

Petri dishes	Greiner, Kremsmünster, AU
Pipette tips (0.1 – 1,000 µl)	Starlab, Helsinki, FI
Pipette tips (0.1 – 1,000 µl) (<i>Tip One® Filter Tips</i>)	Starlab, Helsinki, FI
Pipette tips (<i>Electrophoreses / Protein</i>)	Bio-Rad, Munich
Rabbit IgG-agarose	Sigma, Munich
Safelock micro test tubes (1.5 ml and 2 ml)	Eppendorf, Hamburg
Saran cling film	Dow Chem. Co., Schwalbenbach
Serological pipettes (5 ml, 10 ml, 25 ml, 50 ml)	BD Biosciences, San Jose, USA
Syringes (10 ml <i>Luer Lock</i>)	Terumo, Leuven, BE
Syringes (50 ml)	Terumo, Leuven, BE
Test tubes (15 ml and 50 ml)	Falcon, Gräfeling-Lochham
Tissue culture dishes (10 cm and 15 cm)	Falcon, Gräfeling-Lochham
Vivaspin Concentrator	Vivascience, Hannover
Whatman paper	Whatman Int., Ltd., UK
1-stack cell culture dishes	Sigma, Munich
10-stack cell culture dishes	Sigma, Munich
6-well tissue culture dishes	Falcon, Gräfeling-Lochham
12-well tissue culture dishes	Corning Inc., NY, USA
96-well <i>MicroAmp™</i> plates	Applied Biosystems, Darmstadt
96-well <i>Microtiter®</i> luminescence plates	Nunc, Wiesbaden

7.3 Chemicals and reagents

Chemical	Distributor
Acetic acid (99%)	Sigma, Munich
Acrylamide-bisacrylamide Solution (37.5 : 1)	Carl Roth GmbH, Karlsruhe
Adenosine triphosphate (ATP)	Sigma, Munich
Agarose	Sigma, Munich
Ammonium persulfate (APS)	Carl Roth GmbH, Karlsruhe
Ampicillin	Sigma, Munich
Aprotinin	Sigma, Munich
Benzonase	Novagen, Darmstadt

Bis-Tris	Sigma, Munich
Boric acid	Sigma, Munich
Bovine serum albumin (BSA)	Sigma, Munich
Bromophenol blue	Sigma, Munich
Calcium chloride	Sigma, Munich
Chloramphenicol	AppliChem, Darmstadt
Colloidal coomassie <i>Brilliant Blue G</i>	Sigma, Munich
Desoxynucleotides (dATP, dCTP, dGTP, dTTP)	Roche, Mannheim
Dipotassium phosphate	Applichem, Darmstadt
Disodium hydrogen phosphate	Sigma, Munich
DMSO (Dimethyl sulfoxide)	Sigma, Munich
DTT (Dithiothreitol)	Sigma, Munich
Dulbecco's modified Eagle's medium (DMEM)	Invitrogen, Karlsruhe
EDTA (Ethylenediaminetetraacetic acid)	Sigma, Munich
EGTA (Ethylenglycoltetraacetic acid)	Sigma, Munich
Ethanol (99%)	DKFZ
Ethidium bromide	Carl Roth GmbH, Karlsruhe
Fetal calf serum (FCS)	Invitrogen, Karsruhe
Glucose	Sigma, Munich
Glutathione sepharose	Amersham, Darmstadt
Glycerol	Baker, Deventer, NL
Gly-Gly	Sigma-Aldrich, Munich
Hepes	Roth, Karlsruhe
Huminsulin Normal 40	Lilly, Bad Homburg
Hydrochloric acid (HCl) 37%	Acros Organics, New Jersey, USA
Igepal (Nonidet NP40)	Sigma, Munich
Imidazole	Merck, Darmstadt
Isopropanol	Sigma, Munich
Isopropyl- β -D-thio-galactopyranoside (IPTG)	Sigma-Aldrich, Munich
LB-Agar	Carl Roth GmbH, Karlsruhe
LB-Medium	Carl Roth GmbH, Karlsruhe
Lipofectamine	Invitrogen, Karlsruhe
Leupeptin	Sigma, Munich

Loading dye solution (6x)	Fermentas, St. Leon Rot
Luciferin	Sigma, Munich
Magnesium chloride ($MgCl_2$)	Merck, Darmstadt
Magnesium sulfate ($MgSO_4$)	Sigma, Munich
β -Mercaptoethanol (98%)	Sigma, Munich
Methanol (100%)	Merck, Darmstadt
Methionine (^{35}S radiolabelled)	Perkin Elmer, Rodgau
Milk powder <i>Rapilait</i>	Migros, Lörrach, CH
Minimal Essential Medium (MEM)	Invitrogen, Karlsruhe
Monosodium phosphate (NaH_2PO_4)	AppliChem, Darmstadt
Non essential amino acids	Invitrogen, Karlsruhe
3-(N-morpholino)propanesulfonic acid (MOPS)	Carl Roth GmbH, Karlsruhe
o-Nitrophenyl- β -D-galactopyranosid (ONPG)	Sigma, Munich
Oil red O	Sigma, Munich
<i>Orange G</i>	Sigma, Munich
PageBlue™ protein staining solution	Fermentas, St. Leon-Rot
Penicillin / Streptomycin (P/S)	Invitrogen, Karlsruhe
Pepstatin	Sigma, Munich
Ponceau-S Solution	Sigma, Munich
Potassium chloride (KCl)	Sigma, Munich
Proteinase inhibitor cocktail	Roche, Penzberg
Phosphatase inhibitor cocktail	Roche, Penzberg
Qiazol	Qiagen, Hilden
Tripotassium phosphate (K_3PO_4)	Merck, Darmstadt
Trypsin-EDTA	Invitrogen, Karlsruhe
Sheep-anti-rabbit IgG magnetic beads	Invitrogen, Karlsruhe
Sodium acetic acid ($NaCH_3COOH$)	Sigma, Munich
Sodium chloride (NaCl)	Fluka, Munich
Sodium dodecyl sulfate (SDS)	Gerbu, Biotechnik GmbH, Gaiberg
Sodium fluoride (NaF)	Sigma, Munich
Sodium hydroxide (NaOH)	Sigma, Munich
Sodium orthovanadate	Sigma, Munich
Spectinomycin	Sigma, Munich

N,N,N',N'-Tetramethylenediamine (TEMED)	Carl Roth GmbH, Karlsruhe
Triton X-100	Sigma, Munich
Tris base	Sigma, Munich
Trypsin-EDTA solution	Invitrogen, Karlsruhe
Tween-20	Sigma, Munich
Urea	Sigma, Munich
Williams Medium E	Sigma, Munich

7.4 Commercial kits

Kit	Distributor
BLOCK-iT™ U6 RNAi Entry Vector Kit	Invitrogen, Karlsruhe
BLOCK-iT™ Adenoviral RNAi Expression System	Invitrogen, Karlsruhe
Cholesterol determination Kit	Randox, Crumlin, UK
Enhanced Chemiluminescence (ECL) Kit	Amersham Biosciences, Freiburg
First Strand cDNA Synthesis Kit	Fermentas, St. Leon-Rot,
Insulin ELISA Kit	Mercodia, Uppsala, S
Invitrogen Pure-Link™ High Pure Plasmid	Invitrogen, Karlsruhe
Ketone bodies Determination Kit	Wako, Neuss
NEFA – C Determination Kit	Wako, Neuss
Platinum® Quantitative PCR Supermix	Invitrogen, Karlsruhe
QiaPrep Plasmid Miniprep Kit	Qiagen, Hilden
QiaQuick Gel Extraction Kit	Qiagen, Hilden
RNeasy RNA Extraction Kit	Qiagen, Hilden
TNT T7/T3 Coupled Reticulocyte Lysate System	Promega, Mannheim
Triglycerides Determination Kit	Sigma-Aldrich Chemicals GmbH, Steinheim
Triglycerides Liquicolour	Human GmbH Wiesbaden

7.5 Research diets

High fat diet (60% energy from fat)	New Brunswick, USA
Low fat diet (10% energy from fat)	New Brunswick, USA
Methionine, choline deficient diet	New Brunswick, USA

7.6 Solutions and buffers

BBS (2x)

Components:	50 mM	BES
	280 mM	NaCl
	1.5 mM	Na ₂ HPO ₄
	pH 6.95	

Blocking buffer (for Western blotting)

Components:	1x	PBS
	0.1%	Tween 20
	5%	Milk powder

Co-immunoprecipitation buffer

Components:	20 mM	HEPES/KOH
	125 mM	NaCl
	0.5 mM	EDTA
	0.1%	Igepal
	10%	Glycerol
	1x	Protease inhibitor
	pH 7.4	

Gly-Gly working solution (WS)

Components:	25 mM	Gly-Gly
	15 mM	MgSO ₄
	4 mM	EGTA
	pH 7.8	

HANKS I buffer

Components:	8 g	NaCl
	0.4 g	KCl
	3.57 g	Hepes

0.06 g	KH ₂ PO ₄
0.06 g	Na ₂ HPO ₄ x 2 H ₂ O
add 1L	Distilled H ₂ O
2.5 mM	EGTA
0.1%	Glucose
pH 7.4	

HANKS II buffer

Components:	8 g	NaCl
	0.4 g	KCl
	3.57 g	Hepes
	0.06 g	KH ₂ PO ₄
	0.06 g	Na ₂ HPO ₄ x 2 H ₂ O
	add 1L	Distilled H ₂ O
	3 mg/ml	Collagenase CLSII
	5 mM	CaCl ₂
	0.1%	Glucose
	pH 7.4	

Harvest buffer (for luciferase assays)

Components:	100%	Gly-Gly WS
	1%	Triton X-100
	1 mM	DTT

Luciferase assay buffer

Components:	20 mM	K ₃ PO ₄
	80%	Gly-Gly WS
	1.6 mM	DTT
	2 mM	ATP
	pH 7.8	

Luciferin solution

Components:	1 mM	Luciferin
	10 mM	DTT
	Dissolved in Gly-Gly WS	

ONPG buffer

Components:	0.1 M	NaPi
	1 mM	MgCl ₂
	10 mM	KCl
	1 mg/ml	ONPG
	100 mM	β-Mercaptoethanol
	pH 7.5	

Orange G sample buffer (6x)

Components:	10 mM 70% 1 spatula tip	EDTA Glycerol Orange G
-------------	-------------------------------	------------------------------

PBS (10x)

Components:	1.4 M 27 mM 100 mM 8 mM pH 6.8	NaCl KCl Na ₂ HPO ₄ KH ₂ PO ₄
-------------	--------------------------------------------	------------------------------------------------------------------------------------

PBS-T

Components:	1x 0.1%	PBS Tween-20
-------------	------------	-----------------

Protease-inhibitor mix (50x)

Components:	50 mM 50 mM 0.5 mg/ml 0.5 mg/ml 0.5 mg/ml Dissolved in ethanol	PMSF NaF Leupeptin Aprotinin Pepstatin A
-------------	-------------------------------------------------------------------------------	------------------------------------------------------

Protein lysis buffer

Components:	50 mM 1 mM 10 mM 2 mM 1 mM 1x pH 7.2	Tris EDTA NaF Na ₃ VO ₄ DTT Protease-inhibitor mix
Supplement:	1.5 M 1%	NaCl NP-40

SDS running buffer (10x)

Components:	0.25 M 1.92 M 1%	Tris-base Glycine SDS
-------------	------------------------	-----------------------------

TBE buffer (10x)

Components:	45 mM 10 mM 45 mM	Tris Base EDTA Boric acid
-------------	-------------------------	---------------------------------

TE buffer (10x)

Components:	1 mM 10 mM pH 8	EDTA Tris-HCl
-------------	-----------------------	------------------

Transfer buffer SDS-PAGE

Components:	25 mM 192 mM 20% 0.01%	Tris-base Glycine Methanol SDS
-------------	---------------------------------	-----------------------------------------

All buffers were diluted in H₂O, unless stated otherwise.

7.7 Molecular components

Antibodies

Antibodies were diluted in blocking buffer prior to use. The dilution factor of primary antibodies ranged from 1:100 to 1:5,000 depending on the specifications given by the distributing company. Secondary antibodies were diluted 5,000-fold.

Primary antibody	Isotype	Distributor
α - Acly	Rabbit	Abcam, Cambridge, UK
α - ApoB	Mouse	Santa Cruz, Heidelberg
α - Flag	Mouse	Sigma, Munich
α - Lipin1	Rabbit	Abcam, Cambridge, UK
α - Myc	Mouse	Upstate, Schwalbach
α - TBL1	Rabbit	Abcam, Cambridge, UK
α - TBLR1	Rabbit	Imgenex, San Diego, USA
α - TSC22D4	Mouse	Abcam, Cambridge, UK
α - VCP	Mouse	Abcam, Cambridge, UK

Secondary antibody	Isotype	Distributor
α - Mouse IgG, HRP	Goat	BioRad, Munich
α - Rabbit IgG, HRP	Goat	BioRad, Munich
α - Goat IgG, HRP	Rabbit	BioRad, Munich

Oligonucleotides

All oligonucleotides possessed a G/C content between 40% and 60% and were approximately 20-30 bp in length.

Restriction sites for specific enzymes were added to the cloning primers in 5'→3' orientation, allowing directed insertion into a specific target vector. Six thymidine residues were added to the 5' ends of the restriction sites in order to facilitate cleavage. The primers were designed to hybridize at temperatures of approximately 56°C.

Molecular weight markers

DNA marker	Range	Distributor
Gene Ruler™ 1kb DNA ladder	250 – 10,000 bp	Fermentas, St. Leon-Rot

Protein marker	Range	Distributor
Prestained Protein Ladder	10 – 180 kDa	Fermentas, St. Leon-Rot
Unstained Protein Ladder	10 – 200 kDa	Fermentas, St. Leon-Rot

7.8 Cell lines

Bacterial cell lines

Cell line	Distributor
<i>E.coli</i> BL21 Chemically Competent Cells	Stratagene, La Jolla, USA
<i>E.coli</i> SURE2® Chemically Competent Cells	Qiagen, Hilden
<i>E.coli</i> TOP 10 Chemically Competent Cells	Invitrogen, Karlsruhe

E.coli XL1-Blue cells were obtained from Stratagene, La Jolla, USA and were used to produce chemically competent cells.

Eucaryotic cell lines

Cell line	Distributor
HEK 293 human embryonic kidney cell line	ATTC, Wesel
HEK 293-T human embryonic kidney cell line	ATTC, Wesel
HEK 293-A human embryonic kidney cell line	ATTC, Wesel
Hepa1c1 mouse hepatoma cell line	ATTC, Wesel

7.9 Software**Software**

Software	Distributor
BLAST	http://www.ncbi.nlm.nih.gov
Endnote	Thomson, Carlsbad, USA
Microsoft Office	Microsoft, Unterschleißheim
Mikro Win	Mikrothek, Overath
Photoshop	Adobe, San Jose, USA
Pubmed	NIH
Quantity One	Bio-Rad, Munich
<i>Vector NTI Advance™ Software</i>	Invitrogen, Karlsruhe
Genious Software	Biomatters Ltd., Auckland, NZ

8. METHODS

8.1 Molecular Biology

8.1.1. Agarose gel electrophoresis

Agarose gel electrophoresis was used to analyze PCR products, and digested plasmids. 1-3 % agarose was dissolved in TBE buffer and brought to the boil. Upon cooling, 0.5 µg/mL ethidium bromide was added. Gels were run at 100 V with constant current.

8.1.2. Extraction of DNA from agarose gels

DNA fragments were excised from agarose gels under a UV lamp using a scalpel and purified using the QIAquick Gel Extraction Kit, according to the manufacturer's instructions.

8.1.3. Restriction analysis of DNA fragments or plasmids

For restriction analysis DNA was incubated with 10-20 units of restriction enzyme (New England Biolabs) per µg (based on DNA concentration) and 1 µL of 10X reaction buffer. Reactions were incubated at 37°C for 2-4 hours.

8.1.4. Polymerase chain reaction (PCR)

PCR was performed to amplify DNA fragments using a heat stable DNA polymerase. A typical reaction scheme is shown below.

	Amount	Final concentration
5X <i>Phusion polymerase</i> buffer	10 µL	1 X
10 mM dNTP mix	1 µL	0.2 mM
Forward primer (100 µM)	1µL	2 µM
Reverse primer (100 µM)	1 µL	2 µM
DNA Template	~ 5 ng	
<i>Phusion polymerase</i>	1 µL	2 U
Double distilled water	ad 50 µL	

A typical PCR reaction was programmed as follows:

Step	Temperature	Time
1. Denaturation	95°C	30 sec
2. Denaturation	95°C	10 sec
3. Primer annealing	55 – 65°C	30 sec
4. Extension	72°C	60 sec
5. Go to 2		30x
6. Extension	72°C	5 min
7. Hold	4°C	∞

The annealing temperature was adjusted depending on the length and G/C content of the primers using the following formula: ($T_{An}=69^{\circ}\text{C} + 0.41 \times (\%GC) - 650 / \text{bp}$).

8.1.5. Ligation

Ligation reactions were performed in 20 µl volume. 50-200 ng of vector were used for each reaction and the molar ratio of insert to vector was adjusted to be 3:1. The DNA was mixed in a volume of 10 µl and incubated at 45°C for 5 min. Subsequently ligation buffer and T4 DNA ligase were added. Reactions were incubated at room temperature for 2-4 hours and stored at 4°C overnight. A reaction containing the vector alone was used as a negative control to determine the degree of vector self-ligation.

8.1.6. Chemical transformation of *Escherichia coli*

Competent cells were thawed on ice. 2-10 µl of ligation mix, or 0.1-1 µg of plasmid were added to the cells and incubated on ice for 20-30 min. Heat shock was applied by incubating the vials in a water bath at 42°C for 45 sec. 300 µl of LB medium were added to each tube and bacteria were incubated at 37°C in a table top shaker for 1 hour. After incubation, 100-200 µL of cells were directly plated on LB-agar plates containing the appropriate antibiotic. Plates were incubated at 37°C overnight and then stored at 4°C.

Small scale liquid cultures

A single bacterial colony was used to inoculate 4 ml LB-medium containing the appropriate concentration of a specific antibiotic. Cultures were incubated overnight at 37°C under vigorous shaking and used for small scale DNA preparation (Mini Prep) the following morning.

Large scale liquid cultures

For large scale DNA preparation (Maxi Prep), 200 ml LB-medium containing the appropriate concentration of a specific antibiotic, were inoculated with either a 4 ml pre-culture or a single bacterial colony. Cultures were incubated overnight at 37°C under vigorous shaking.

8.1.7. Plasmid preparation

Small scale plasmid preparation (Mini Prep)

Plasmid preparation from small scale bacterial liquid cultures was performed using the Qiaprep Plasmid Miniprep Kit provided by Qiagen. The specifications given in the distributor's protocol were followed and the DNA was eluted with 50 µl elution buffer (provided with the kit). Plasmid DNA was stored at -20°C.

Large scale plasmid preparation (Maxi Prep)

Plasmid preparation from large scale bacterial liquid cultures was performed using the Invitrogen Maxiprep Kit. The plasmid DNA was resuspended in 200 µl H₂O and

the concentration was determined by spectral photometry. Plasmid DNA was stored at -20°C.

8.1.8. DNA sequencing

Plasmids were sequenced by the company AGOWA (Berlin).

8.1.9. RNA isolation from tissue samples

10-30 mg of frozen tissue were transferred into a 2 ml RNase/DNase-free reaction tube containing 1 ml of Qiazol™ Lysis reagent and a stainless steel bead. The samples were lysed using the TissueLyser™ for 90 sec and at a frequency of 30 Hz. Lysates were incubated at room temperature for 5 min to release nucleoprotein complexes before they were transferred into a fresh 1.5 ml RNase/ DNase-free safe-lock tube containing 200 µl of chloroform. Mixtures were vortexed for 15 sec and then centrifuged for 20 min at 13,000 rpm. The upper aqueous solution, containing the RNA, was carefully transferred into a fresh reaction tube. The RNA phase was then mixed with 500 µl of iso-propanol and incubated at room temperature for 10 min, followed by a 10 min centrifugation step at 12,000 rpm. The supernatant was aspirated and the pellet was washed once with 1 ml of 75% ethanol. The solvent was discarded, and the remaining ethanol was removed using a pipette. The pellet was briefly air-dried and re-solubilised in water (30-50 µl). To increase solubilisation, the RNA solution was incubated at 55-60°C for 10 min. The samples were stored at -80°C until further use.

8.1.10. RNA isolation from cell samples

Adherent cells were treated according to experimental needs. The medium was removed and the cell monolayer was washed once with sterile PBS. The buffer was aspirated and 1 mL Qiazol™ Lysis reagent was added per plate or well. The cells were released from the plate using a pipette and transferred into DNase/RNase-free reaction tubes, in which they were incubated for 5 min at room temperature. The samples were vortexed vigorously, until all cells were solubilised. The obtained cell

lysates were stored at -80°C or immediately used for RNA isolation, as described above.

8.1.11. RNA isolation using the RNeasy Mini purification kit

For microarray analysis, RNA isolated using Qiazol™ Lysis reagent was purified using the RNeasy Mini purification kit. RNA samples were diluted in 350 µl of RW1 buffer, transferred to RNeasy columns and centrifuged at 12,000 rpm for 1 min. The flow-through was discarded and the columns were washed with 350 µl RW1 buffer for 5 min. The buffer was removed by centrifugation. 80 µl of buffer, containing 10 µl DNase and 70 µl RDD buffer were added directly. DNA digestion was performed for 30 min at room temperature. Subsequently, 350 µl RW1 buffer was added and the samples were incubated for another 2 min. Columns were washed twice with 500 µl RPE buffer. Finally, the RNA was eluted in 30 µl RNase free water.

8.1.12. cDNA synthesis

1-3 µg of purified RNA were used for cDNA synthesis. The reaction volume was adjusted to 9 µl per sample using RNase/DNase-free water. 1 µl of oligo(dT)18 primers were added. Reactions were vortexed and incubated at 70°C for 5 min, to allow the primers to anneal to the poly-A tails. A mix, containing 4 µl 5 x reaction buffer, 2 µl 10 mM dNTP mix and 1 µl Ribolock™ Ribonuclease Inhibitor was then prepared. This reaction mixture was added to the samples and incubated for 5 min at 37°C. Subsequently, 2 µl M-MuLV reverse transcriptase (RT) were added. To assess potential DNA contamination of reagents, an additional reaction was performed without reverse transcriptase. After 1 hour incubation at 37°C, samples were incubated at 70°C for 10 min to inactivate the reverse transcriptase and terminate cDNA synthesis. After completion, cDNA was stored at -20°.

8.1.13. Quantitative Real-Time PCR

cDNA samples were diluted ten-fold with DNase/RNase free water. 5 µl of this mixture were then used for each real time PCR reaction. A reaction sample mix consisting of 10 µl Platinum® Quantitative PCR Supermix, 4.5 µl DNase/RNase free

Water and 0.5 µl Taqman probe was added to each individual reaction. All probes were obtained from Applied Biosystems or MWG. Water was used as a negative control and samples containing no reverse transcriptase served as controls for genomic DNA contamination. The PCR reaction mix was transferred to a MicroAmp™ Optical 96-well reaction plate. All reactions were performed in technical duplicates. Quantitative PCR was performed using a 7,300 Real Time PCR System (Applied Biosystems).

8.1.14. Gene expression profiling

Gene expression profiling was performed with RNA extracted from livers of TSC22D4 shRNA, TBL1/TBLR1 shRNA or control virus injected mice. RNA isolation, cRNA synthesis and hybridization to Mouse Genome 430 2.0 arrays from Affymetrix were performed according to the manufacturer's recommendations. Three arrays per genotype were hybridized with pooled RNA samples (2-3 animals per array total n=7). Microarray data were analyzed based on ANOVA using a commercial software package (Micro Array Solution, version 1.0; SAS Institute, Cary, NC). Standard settings were used, except for the following specifications: log-linear mixed models were fitted for values of perfect matches, with genotype considered to be constant and the array identification, random. Custom CDF with Unigene-based gene / transcript definitions was used to annotate the arrays. Affected biological pathways ([including KEGG]) reflected by the differential gene expression were determined by ORA based on Fisher exact test.

8.2 Cell Biology

8.2.1. Cultivation of Human Embryonic Kidney (HEK), HEK293A and HEK293T cells

HEK 293 cells were maintained and propagated in Dulbecco's Modified Eagle Medium with high glucose (DMEM), 10 % fetal calf serum (FCS) and 1 % penicillin/

streptomycin. HEK293A and HEK293T cells also required 1 % Non-Essential Amino Acids (NAA). Cells were split by the factor 1:20 two times per week.

8.2.2. Cultivation of Hepa1c1 mouse hepatoma cells

Hepa1c1 cells were maintained and propagated in MEM (Minimal Essential Medium) medium containing 10 % FCS, 1 % penicillin / streptomycin and 1% NAA. Cells were split by the factor 1:10 two times per week

8.2.3. Cell culture and transient transfection assays

Experiments involving eukaryotic cells were performed under sterile conditions. Media and reagents were preheated to 37°C prior to use. All cells were cultivated at 37°C, 5% CO₂ and 95% humidity in 6-well, 12-well, 10 cm or 15 cm cell culture dishes. Human HEK293 cells and murine Hepa1c1 hepatocytes were transfected using Lipofectamine or polyethylenimine (PEI) reagent, a substance with low cytotoxicity.

Luciferase assays

Hepa1c1 cells were plated on 6-well plates at a concentration of 5 x 10⁵ cells / well the day before the experiment. The amount of PEI was calculated with respect to the amount of DNA that was used for the individual transfection. Generally, 8 µl of PEI were applied per µg of DNA. A reaction was prepared containing DNA, PEI and 150 µM NaCl and incubated at room temperature for 10 min. This mixture was added to fresh medium containing 10% FCS, 1% P/S and 1% NAA. Cell extracts were prepared 48 hours after transfection. The medium was removed and cells were washed once with PBS. Harvest buffer was added and the samples were incubated on a shaker for 5 min to facilitate detachment from the dish. Next, cells were scratched from the plate. Lysates were transferred to 1.5 ml reaction tubes. For each well 150 µl of harvest buffer were used. Insoluble cell debris was removed by centrifugation for 3 min at 13,000 rpm and the supernatants were transferred to a fresh tube. The lysates were used directly for reporter gene assays or stored at -20°C. Luciferase is an enzyme that catalyses a reaction in which luciferin is transformed into oxyluciferin by oxidative decarboxylation, thereby emitting photons. Under assay conditions the substrate luciferin is available in excess, consequently the amount of light emitted is

proportional to the amount of luciferase in the lysate. To determine luciferase activity in lysates, 30 µl of lysate were transferred into a well on a black 96-well-plate. Lysates were complemented with 100 µl assay buffer and plates were measured using a luminometer (Mithras 940 Luminescence) equipped with a dispenser. Automatic injection of 100 µl luciferin buffer started the reaction. Light emission was measured at a wavelength of 560 nm and harvest buffer alone was used to determine a blank value. All results were normalized to the activity resulting from a co-transfected β-galactosidase expression plasmid harbouring an H-Ras promoter (H-RAS β-Gal). For the assay a buffer containing the substrate ortho-nitrophenyl-β-galactopyranosid (ONPG) was prepared. 5 ml of this buffer were mixed with 13.5 µl beta-mercaptoethanol prior to the β-gal assay. 50 µl cell lysate / well were transferred into a clear 96-well plate and 50 µl ONPG buffer were added to each well. Harvest buffer was used to obtain a blank value. The plates were incubated at 37°C for 6-12 hours until a clear yellow colour was visible. The absorption was measured at 405 nm, the maximum absorption of the ortho-nitrophenylat ion. The values were analysed with respect to the noise signal and used to normalise the luciferase signals.

8.2.4. Primary hepatocyte experiments

Primary mouse hepatocytes were isolated and cultured as described (124). Male 8-12 week old C57Bl/6J mice were anesthetized by intraperitoneal injection of 5 mg 10% ketamine hydrochloride / 100 mg body weight and 1 mg 2% xylazine hydrochloride / 100 mg body weight. After opening the abdominal cavity, the liver was perfused with HANKS I buffer via the portal vein for 5 min at 37°C and subsequently with HANKS II buffer for 5-7 min until disintegration of the liver structure could be observed. The liver capsule was removed and the cell suspension was filtered through a 100 µm mesh. Cells were washed and, subsequently, viability of cells was determined by trypan blue staining. 500,000 living cells / well were seeded on collagen I-coated 6- or 12-well plates. Cells were infected with recombinant adenoviruses (multiplicity of infection = 100) 24 hours after seeding and harvested for mRNA analysis 48 hours later.

8.3 Animal experiments

8.3.1. General procedures

Male 8-12 week old C57BL/6J or Balb C mice were obtained from Charles River Laboratories (Brussels, BEL) and maintained on a 12 hour light-dark cycle with regular unrestricted diet and free access to water. For fasting experiments, animals were fasted for 16 hours. For adenovirus injections, $1\text{-}3 \times 10^9$ plaque-forming units per recombinant virus were administered via tail vein injection. In each experiment, 5-8 animals received identical treatments and were analyzed under fasted, control fed or random fed conditions as indicated. In high-fat diet experiments, C57BL/6J mice were injected with 5×10^{11} AAV particles per mouse and fed a high-fat diet (60% energy from fat, Research diets D12492) for a period of 9-11 weeks. In methionine /choline deficiency studies, mice were fed the MCD diet for 4 weeks (Research diets). In C26 experiments, 1.5×10^6 colon tumour cells were injected subcutaneously into BalbC mice. Organs including liver, kidney, epididymal fat pads, and gastrocnemius muscles were collected after the corresponding time periods, weighed, snap-frozen and used for further analysis. Total body fat content was determined using an Echo MRI body composition analyzer. Animal handling and experimentation was performed in accordance with NIH guidelines and approved by local authorities.

8.3.2. Hepatic VLDL release

VLDL production was determined after tyloxapol injection as described (78). Tyloxapol is a Lipoprotein Lipase (LPL) inhibitor, meaning that, after administration, any secreted VLDL particles could not be cleared from the blood stream. One day before the experiment, tyloxapol was dissolved in saline to obtain a 20% w/v solution. Six C57BL/6J mice per group were fasted overnight for 16 hours. On the following day, before administration, 40 μ l of blood was drawn from each mouse by cutting the tip of the tail. The tyloxapol (20%) volume (in μ l) applied per mouse was approx. 3 times that of the weight of the mouse in grams; i.e. a 25 g mouse received 75 μ L of the 20% solution. Specified amounts were administered via the tail vein and 40 μ L blood

samples were taken every 50 min for 2.5 hours. The mice were sacrificed after 300 min. The serum TG values were determined and plotted against the time.

8.3.3. VLDL clearance

Blood was drawn from a fasted individual and human VLDL was isolated by ultracentrifugation as described (125). 3.5 ml serum were put in a polyallomer tube (SW40Ti) and mixed with 1.39 g KBr, over-layered with 3x2.8 ml of a NaCl/KBr solution ($D= 1.063, 1.019$ and 1.006 g/ml) and run for 18 hours at 40,000 rpm. 20 μg of human VLDL were injected into each animal and serum samples were taken at 2, 10, 30, 60 and 120 min. Human ApoB-100 levels were measured using a human-specific ApoB ELISA. For the ELISA, a primary coating antibody generated against human ApoB-100 (mAb47, kindly supplied by J. Witztum, University of San Diego, USA), at a concentration of 2 $\mu\text{g}/\text{well}$ and a secondary biotinylated polyclonal antibody raised in goat against human ApoB at a concentration of 4 $\mu\text{g}/\text{well}$ in 1.5% BSA/TBS/0.1% tween were used. To prevent non-specific binding, plates were blocked with 1.5% BSA/TBS/0.1% tween. Samples were diluted 25-fold. Absorbance was read 30 min after addition of TMB and termination of the reaction with 2 M H_2SO_4 at 450 nm (126).

8.3.4. Intravenous lipid load test

Intralipid (20 % fat emulsion) was obtained from Sigma. Seven mice per group were fasted overnight for 16 hours. The following day mice were injected with 100 μL of intralipid solution. 30 μL of blood was collected prior to injection and at 2, 10, 20, 30, 60 and 120 min time points. Serum was isolated and used for determination of TG content. The TG values were determined and plotted against the time.

8.3.5. Glucose tolerance test

In a glucose tolerance test, glucose is injected in the peritoneum of fasted mice and blood samples are taken to determine how quickly the sugar can be cleared from the blood. Improved insulin signaling results in lower glucose levels as the sugar load induces a better clearance from the blood stream. Mice were fasted for 16 hours prior

to the experiment. The animals were transferred into fresh cages equipped with fresh water but no food. The following morning, the body weight and the initial blood glucose levels were determined by nicking the tail with a razor blade. Blood glucose was measured using a glucometer strip. 10 µl/g body weight of a 20% glucose solution were then injected intraperitoneally. Blood glucose was measured 10, 20, 30, 60, 90 and 120 min after injection.

8.3.6. Insulin tolerance test

An insulin tolerance test (ITT) is a procedure in which insulin is injected into a mouse to assess if it can still induce its full function. If mice are insulin resistant, blood glucose levels are elevated over time. For the insulin tolerance test a stock solution of 0.75 U insulin/ml was prepared using 0.9% sodium chloride. The body weight of all animals was determined and the blood glucose levels were measured by cutting the tail with a razor blade. The blood drop was put onto a glucometer strip and measured. 1 U insulin/kg body weight was injected intraperitoneally. The blood glucose levels were monitored after 10, 20, 30, 60 and 120 min.

8.3.7. Acute insulin signalling

To analyze the acute effects of insulin administration, mice were injected with 1U/kg insulin or PBS and sacrificed precisely 10 min later. Organs were quickly removed and insulin signalling was analyzed by Western blot.

8.4 Biochemistry

8.4.1. Luminescence-based mammalian interactome mapping (LUMIER)

The LUMIER screen was used to find novel TBL1 and TBLR1 interaction partners. Proteins were transiently expressed in HEK293 cells as hybrid proteins with the *Staphylococcus aureus* protein A tag or *Renilla reniformis* luciferase fused to their amino termini. 20 ng of each expression construct were transfected into 10,000

HEK293 cells using 0.05 µl of lipofectamine 2,000 in 96 well plates. After 40 hours, medium was removed and cells were lysed on ice in 10 µl of ice-cold lysis buffer (20 mM Tris pH 7.5, 250 mM NaCl, 1% TritonX-100, 10 mM EDTA, 10 mM DTT, Protease Inhibitor Cocktail, Phosphatase Inhibitor Cocktail, Benzonase containing sheep-anti-rabbit IgG-coated magnetic beads (Invitrogen, Dynabeads M280, 2 mg/ml final concentration). Lysates were incubated on ice for 15 min. 100 µl of washing buffer (PBS, 1 mM DTT) were added per well, and 10% of the diluted lysate was removed to determine the luciferase activity present in each sample before washing. The rest of the sample was washed 6 times in washing buffer in a Tecan Hydroflex plate washer. Luciferase activity was measured in the lysate as well as in washed beads. Negative controls were wells transfected with the plasmid expressing the luciferase fusion protein and a vector expressing a protein A dimer. For each sample, four values were measured: the luciferase present in 10% of the sample before washing (“input”), the luciferase activity present on the beads after washing (“bound”), and the same values for the negative controls (“input nc”, and “”bound nc”). Normalised interaction signal to noise ratios were calculated.

8.4.2. Preparation of protein extracts from liver samples

For protein extractions, 2 ml reaction tubes were filled with 1 ml lysis buffer, protease inhibitors and a stainless steel bead.

Lysis buffer:

50 mM Tris, pH 7.2
1 mM EDTA
10 mM NaF
2 mM Na₃VO₄
1 mM DTT
1 x PIC

Approximately 50 mg of frozen liver tissue were transferred into the ice-cold buffer and the sample was immediately homogenized using the Tissue Lyser for 2 min at 30 Hz. The extracts were incubated on a rotating wheel for 1 hour and then supplemented with high salt denaturation buffer and incubated for an additional hour on the wheel at 4°C. The lysates were transferred to fresh tubes and the protein concentration was determined. Samples were adjusted to a concentration of 1 mg/ml

protein with 2 x SDS buffer and incubated at 95°C for 7 min to denature proteins. Afterwards they were either stored at -20°C, or used directly for SDS-PAGE and immunoblotting.

8.4.3. SDS-PAGE analysis and immunoblotting

20 µg of protein/well were loaded onto 4–12 % SDS-polyacrylamide gels and blotted onto nitrocellulose membranes using a wet blot system. Blotting was performed at 80V for 2 hours or 30V overnight in transfer buffer. Membranes were subsequently blocked by incubation in 5% milk or 5% BSA dissolved in PBS/T for 1 hour. Specific primary antibodies diluted in milk or BSA, according to the manufacturers recommendations, were incubated with the membranes for 1 hour at room temperature or overnight at 4°C. The membranes were washed with PBS/T the next day and incubated with the secondary antibody conjugated to horse radish peroxidase (HRP) at a dilution of 1:10,000 for 1 hour. To detect specific bands the enhanced chemiluminescence system (ECL™) Western Blotting Detection Reagent was applied. Hyperfilm ECL films were exposed to the chemiluminescent signal produced by the blots. Exposure times differed based on the quality of specific antibodies.

8.4.4. Determination of free fatty acid levels

Free Fatty Acids were determined in serum samples using a colorimetric assay from Wako. The assay principle is based on the following three reactions, whereby R-COOH represents any free non esterified carbonic acid:

- 1) RCOOH + ATP + CoA-SH → Acyl-CoA + AMP + PPi (Enzyme: acyl CoA synthetase)
- 2) Acyl-CoA + O₂ → 2,3-Enoyl-CoA + H₂O₂ (Enzyme: acyl CoA oxidase)
- 3) H₂O₂ + 4-Aminophenazon + 3-methy-N-ethyl-N(β-hydroxyethyl)-aniline → Quinoneimine-color + 4 H₂O (Enzyme: peroxidise)

A standard curve was determined using a dilution series of oleic acid. The procedure was carried out according to the manufacturer's instructions. OD-values were determined at 540 nm.

8.4.5. Serum ketone body measurement

Total serum ketone bodies were determined using a commercial kit (Autokit Total Ketone Bodies, Wako chemicals GmbH). The assay is based on an enzymatic reaction where the rate of Thio-NADH production depends on the concentration of total ketone bodies in the sample and can be determined using a photometer. A standard curve was prepared by serially diluting the calibrator provided in the kit. 4 µl were used for measurements and absorbance was measured at 405 nm.

8.4.6. Isolation of hepatic lipids

Lipids were extracted from frozen liver tissue using chloroform/methanol (2:1 v/v). About 100 mg (the exact weight was noted) of frozen, pulverized liver were transferred into a 2 ml polypropylene tube containing 1.5 ml chloroform/methanol and a steel bead. The tissue was homogenized using a tissue lyzer for 1 min at a frequency of 30 Hz. For the lipid extraction, samples were incubated on a rotating wheel at room temperature for 20 min. Reactions were centrifuged at 4,000 rpm for 10 min and supernatants were transferred to fresh tubes. The organic layer was mixed with 0.9% sodium chloride and the aqueous solution was carefully discarded. 50 µl of the organic layer were transferred to a fresh tube and 10 µl of Triton-X 100/ chloroform (1:1 v/v) were added. The reagents were mixed and the solvent was evaporated. The residue containing the hydrophobic contents of the liver was resuspended in 50 µl water and stored at -20°C until further use.

8.4.7. Determination of triglyceride levels

TG levels were determined by separating TGs into one glycerol and three fatty acid molecules and measuring the glycerol using a colorimetric assay. The serum TG determination kit from Sigma was used for this assay. 4 µL of isolated hepatic TGs or 4 µL of serum were transferred to a 96-well plate. In order to determine a blank

value, 100 µl Free Glycerol Reagent were added to each well and the plate was incubated at 37°C for 5 min. Free glycerol levels were measured at 540 nm. In a second reaction (assay), 100 µl TG Reagent were added. This mixture contains the enzyme lipase, which catalyses the release of fatty acids from TGs. Plates were incubated at 37°C for 5 min and measured at 540 nm. TG content was determined by subtracting the free glycerol (blank) from the second measurement (assay).

8.4.8. Cholesterol measurement

Liver or serum cholesterol concentrations were determined using a total cholesterol determination kit (Randox Laboratories). The assay is based on the following reactions:

- 1) Cholesterol → Cholesten-3-on +H₂O₂ (Enzyme: cholesteroloxidase)
- 2) 2H₂O₂ + Phenol + 4-Aminoantipyrin → Chinonimin + 4 H₂O (Enzyme: peroxidase)

4 µl of each sample were mixed with 100µl assay reagent and incubated at 37°C for 5 min. The optical density was measured at 492 nm and the sample concentration was determined using a standard curve resulting from a serial dilution of cholesterol (200mg/dL; provided with the kit).

8.4.9. Blood glucose measurements

Serum glucose levels were determined using a drop of blood obtained from the tail vein and an automatic glucose monitor (One Touch, Lifescan).

8.4.10. Insulin measurement

Insulin levels were determined using an ELISA kit (Mercodia). Plates containing the insulin antibody were provided and were activated using a buffer contained in the kit. 5 µl of each sample or standard (provided in the kit) were added to each well. Plates were then incubated at 4°C for 2 hours. Plates were washed five times in the provided buffer and 100 µl of anti-insulin conjugate were added to each well. Reactions were incubated at room temperature for a further 30 min and then washed several times.

100 µl of enzyme substrate solution were added to each well and the plates were incubated at room temperature for 40 min. Reactions were stopped by adding 100 µl of stop solution to each well and measuring the absorbance at 450 nm. Insulin concentrations were determined using a standard curve resulting from a serial dilution of insulin.

8.4.11. LPL activity

5 ml cold acetone were added to frozen white adipose tissue samples (50 mg) and homogenized. The precipitate was separated from the organic phase and washed with cold diethyl ether. LPL was reconstituted and the obtained protein was centrifuged at 12,500 g and 5°C for 10 min and LPL activity was measured in the supernatant, by assessing the release rate of [14C] oleate from glycerol tri- [14C] oleate. The precise protocol is described (127).

8.4.12. Fast protein liquid chromatography (FPLC)

FPLC was used to separate serum proteins according to their size. The FPLC set-up consisted of a Superose 6 10/300 GL column (GE Healthcare), a fraction collector and an ÄKTA FPLC System (Amersham). During separation, a liquid phase, containing the mixture to be fractionated was pumped over a stationary resin of cross-linked agarose beads with varying surface structure. Certain proteins subsequently eluted at specific times in specific fractions. A pool of 250-300 µl serum, from 4-8 animals, was injected into the machine, diluted in 25 ml PBS and fractionated into 500 µl fractions. 40 µl of each fraction were subsequently used for cholesterol and TG analysis using the TG Liquicolor (Human GmbH, Germany) and Cholesterol determination kit (Randox, UK) respectively. Distinct VLDL and HDL peaks could be observed in specific fractions (128).

8.4.13. Co-Immunoprecipitation

Hepa 1c1 cells were cotransfected with a Flag-TBL1, Flag-TBLR1 or an empty Flag vector in combination with a Myc-TSC22D4 vector. Subsequently, cells were lysed and centrifuged. The supernatant was incubated with anti-FLAG M2 Agarose for 2

hours and washed vigorously to remove unspecific binding. Precipitated proteins were eluted using excess Flag peptide. The immunoprecipitates were subsequently analyzed by Western blot as described. The same protocol was applied to 4 mg of pulverized liver extracts transduced with Flag-TSC22D4.

8.4.14. GST-Pulldown

GST-pulldown experiments were performed to assess whether TSC22D4 binds directly to TBL1 and TBLR1 and, if so, to map the interaction. One protein partner is purified from bacteria using a GST-tag and the second protein is in vitro transcribed and translated in the presence of radiolabeled methionine. Full length and truncated GST fusion proteins were produced in BL21 cells and affinity purified using glutathione sepharose. In vitro transcription/translation was performed using the TNT T7/T3 quick coupled transcription/translation system according to the manufacturer's instructions. GST and in vitro translated full length and truncated proteins were incubated at 4°C overnight. After extensive washing, GST-precipitated proteins were separated by SDS-PAGE and detected by autoradiography as described (129).

8.4.15. Histochemistry (Hematoxylin and Oil red O).

During preparation of liver tissue, slices were embedded Tissue Tek OCT compound and shock frozen in liquid nitrogen. 5 µm cryosections were cut and fixed in Baker's formol. Neutral lipids and TGs were stained with oil red O and nuclei were counterstained with hematoxylin.

8.4.16. Plasmids and RNA interference

shRNAs targeting mouse TSC22D4 (5'-GCCTGGTTGGCATTGACAACACGAATG-3')
TBL1 (5'-GCGAGGATATGGAACCTTAAT-3'), TBLR1 (5'-GCATAAAGGT CCTAT ATTGC-3') or non specific oligonucleotides (5'-GATCTGATCGACACTGTAATG-3') were cloned into the pENTRY RNAi vector (Invitrogen, Karlsruhe, DEU) and used in adenovirus and transient transfection experiments. miRNAs targeting TSC22D4 (5'-ACCACTATCGTCATCGCTGTC-3') or

unspecific miRNAs (5'-AAATGTACTGCGCGTGGAGAC-3') were used in adeno-associated virus experiments. The FasN-Luc reporter plasmid was kindly provided by Timothy Osborne (UCI). Expression vectors for TSC22D4, TBL1 and TBLR1 were generated by standard PCR-based methods and cloned into the pcDNA3.1 expression vector.

8.5 Virology

8.5.1. Cloning of adenoviruses

The BLOCKiTTM Adenoviral RNAi Expression System was used to generate adenoviruses expressing shRNA sequences against murine TSC22D4, TBL1 and TBLR1, as well non-specific shRNAs. Oligonucleotide sequences were chosen using Invitrogen's RNAi Designer tool. Forward and reverse oligonucleotides against the target gene sequence were annealed and cloned into the pENTRTM/U6 vector according to the manufacturer's instructions. The resulting constructs were recombined with the pAd/BLOCK-iTTM DEST vector, which contains the adenovirus serotyp 5 DNA, but lacks the E1 and E3 genes that are required for viral replication. The viral vector containing the shRNA sequence was linearized by restriction digest using the enzyme *Pac*I and transfected into HEK 239A cells using Lipofectamine reagent according to the manufacturer's instructions. HEK293A cells express the viral E1 and E3 genes necessary for viral outbreak, allowing the virus to expand in this cell line. Viral plaques appeared 6 to 10 days after transfection and cells started to detach from the cell culture dish. Once about 70% of cells were floating, they were harvested. The same procedure was used to generate viruses overexpressing TSC22D4. The TSC22D4 cDNA was cloned into a pENTR vector harbouring the CMV promoter and subsequently recombined with the pAd/BLOCK-iTTM DEST vector. An empty adenovirus was used as a negative control in over expression experiments.

8.5.2. Virus harvest using the Freeze-and-Thaw-method

Cells infected with adenovirus were harvested in the medium they were cultivated in. The medium was collected from up to twenty 15 cm culture dishes and centrifuged for at 2,000 rpm for 10 min. The supernatant was discarded and the cell pellet was resuspended in 4 ml PBS-TOSH buffer. The tubes containing the virus were frozen in liquid nitrogen and subsequently thawed by vortexing. This freeze-thaw cycle was repeated three times and was required to release virus from the cells. After cell lysis the mixture was centrifuged at 2,000 rpm at 4°C for 10 min. The crude supernatant was stored at -80°C or directly used for applied to a caesium chloride gradient.

8.5.3. Caesium chloride gradient

Virus lysates from twenty 15 cm culture dishes were thawed on ice. PBS-TOSH was added to a final volume of 20 ml. Gradients were prepared in ultracentrifuge tubes (Beckmann Polyallomer 25mm x 89 mm) and were balanced after addition of each solution. First, 9 ml 4 M caesium chloride were added to the tubes, then 9 ml of 2.2 M caesium chloride were added and finally the viral lysate was carefully pipetted on top, creating three distinct layers. The gradients were centrifuged at 4°C and 24,000 rpm in a Beckmann ultracentrifuge XL-70 for 2 hours using a SW28 swing bucket rotor. After centrifugation a distinct band representing the purified adenovirus was visible between the 4 M and 2.2 M caesium chloride layers. The band was carefully removed by piercing the tube with a 5 ml syringe. The obtained virus (about 3 ml) was mixed with an equal volume of saturated caesium chloride solution and transferred into a 12 mL centrifuge tube (Beckmann Polyallomer 14mm x 89 mm). 2 ml of the 4 M cesium chloride and 2 ml of the 2.2 M cesium chloride solution were used to overlay the gradient. The tubes were centrifuged at 4°C and 35,000 rpm in a SW41 Ti swing bucket rotor for 3 hours. A distinct viral band could be seen between the 4 M and 2.2 M cesium chloride layers. The band (~ 700 µl) was removed using a 1 ml syringe. To remove cesium chloride from the viral solution, viruses were transferred to a dialysis membrane (Spectra/Por® Biotech, MWCO 15,000, 10 mm diameter) and dialyzed against 1 L PBS containing 10 % glycerol (v/v) 2 times (1 and 24 hours) at 4°C. After dialysis, aliquots of 20–100 µL were prepared and stored at -80°C until further use.

8.5.4. Virus titration

The Tissue Culture Infectious Dose 50 (TCID₅₀) assay was used to titrate adenovirus. HEK293A cells were harvested in DMEM medium containing 2% FCS (v/v), 1% penicillin/streptomycin and 1% non-essential amino acids and transferred to 96 well plates. 10⁴ cells in a volume of 100 µl cells were added to each well and two plates (technical duplicates) were required for each titration. After seeding, cells were incubated for at least 4 hours, so that they could attach. In the mean time, serial dilutions of the viruses were prepared in the same medium as above. 100 µl of each dilution step (10⁻⁶–10⁻¹³) were added to ten wells and 100 µl of medium without virus were added to negative control wells. The cells were incubated for ten days, before they were used to determine the viral titer. Using a microscope, it was possible to detect plaque formation in the cell monolayer. Every well in which at least one plaque could be detected was considered a positive well. The titer was determined using the following formula:

$$Ta = \text{viruses per } 100 \mu\text{l} = 10^{1+(s-0.5)}$$

s = the sum of all positive wells starting from the 10⁻¹ dilution, whereby 10 positive wells correspond to the value 1.

$$T = \text{viruses per } 1\text{ml} = 10 \times Ta$$

8.5.5. AAV Production

Adeno-associated viruses encoding TSC22D4-specific or non-specific control miRNAs were used for long-term inactivation of TSC22D4. The oligonucleotides were cloned into the pcDNA6.2-GW/EmGFP-miR vector and transferred into the previously described double stranded pdsAAV-LP1-EGFPmut AAV vector (63) using the restriction enzymes BglII and SalI. The plasmids encoding the miRNA constructs were contransfected into HEK293T cells with the pDGΔVP helper plasmid (130) and a mutated p5E18-VD2/8 expression vector (131) encoding AAV2 rep and a mutated AAV8 cap protein (aa 589-592: QNTA to GNRQ). For virus production, 3.85x 10⁸ cells were suspended in 1100 ml medium. 1,000 ml of the cell suspension was transferred to a 10x cell-stack chamber and 100 ml were transferred to a 1x-cell stack chamber (control chamber for analysis under the microscope). 24 h after plating, the

cells were approximately 70% confluent and were transfected with the plasmids encoding the viral genes using the PEI method in the amounts described below.

Plasmid	Amount
AAV-miRNA expression vector	436 µg
p5E18 VD2/8 helper plasmid	550 µg
pDGΔVP helper plasmid	1579 µg

Once the cell monolayer was approximately 90% confluent, cells were washed with PBS, before they were released from the plate using 10 ml (1x cell stack) or 100 ml (10x cell stack) trypsin-EDTA for 5 min at 37°C. Fresh medium was added (40 ml or 350 ml respectively) and the cells were transferred to a 50 ml falcon tube, or a 500 ml conical tube. The chambers were washed with PBS and used a second time. Cells were centrifuged at 2,000 rpm for 10 min. The supernatant was removed and the pellets were resuspended in 8 ml lysis-buffer containing 150 mM NaCl and 50 mM Tris-HCL, pH 8.5. The lysates were transferred into 15 ml falcons, vortexed, snap-frozen in liquid nitrogen and stored at -80°C.

8.5.6. AAV purification

AAV lysates were thawed at 37°C under shaking and then centrifuged at 3,500 g for 10 min. The supernatant was collected and the pellets were resuspended in 4 ml lysis buffer and snap-frozen. The freeze-thaw cycle was repeated three times. The final pellet was solubilised using a sonicator in a water bath at 48 W for 1 min. The pooled suspension was then digested with benzonase (50 U/ml) for 30 min at 37°C. This solution was then centrifuged at 4°C and 3,500 g for 10 min. The virus was stored at -80°C until further use.

1st Iodixanol gradient

Purifying virus by iodixanol gradient leads to a separation of packed and unpacked AAV capsids, as they migrate differentially upon ultracentrifugation. The first gradient, ranging from 15% iodixanol to 40% iodixanol, was prepared on top of the viral solution in a Beckman Quickseal tube using a Pasteur pipette, as described below.

Layer (from top to bottom)	Component
15 %-iodixanol dilution (7 ml)	1.75 ml OptiPrep 5.25 ml PBS-buffer 2
25 %- iodixanol dilution (5 ml)	2.08 ml OptiPrep 2.29 ml PBS-buffer 1 12.5 µl phenol red (0.5 %)
40 %- iodixanol dilution (4 ml)	2.67 ml OptiPrep 1.33 ml PBS-buffer 1
60 %- iodixanol dilution (4 ml)	4 ml OptiPrep 10 µl phenol red (0.5 %)
Virus (18 ml)	
PBS-buffer 1:	PBS-buffer 2:
1x PBS 1 mM MgCl ₂ 2.5 mM KCL	1x PBS 1 mM MgCl ₂ 2.5 mM KCL 1 M NaCl

About 1 ml of space was left above the gradient. Tubes were sealed and centrifuged in a 50.2 Ti rotor at 50,000 g and 10°C for 2 hours. Four gradients were run for each virus (two rounds; harvest and wash). After centrifugation, the 40% iodixanol layer (~3.5 ml) was carefully collected by inserting a 5 ml syringe from underneath. The viral suspension was pooled and stored at -80°C.

2nd Iodixanol gradient

The viral suspension resulting from the first gradient was filled up to 25 ml with lysis buffer. The second gradient was prepared by underlayering, as described below.

Layer (from top to bottom)	Component
25 %- iodixanol dilution (5 ml)	2.08 ml OptiPrep 2.29 ml PBS-buffer 1 12.5 µl phenol red (0.5 %)
40 %- iodixanol dilution (4 ml)	2.67 ml OptiPrep 1.33 ml PBS-buffer 1

60 %- iodixanol dilution (4 ml) 4 ml OptiPrep
 10 µl phenol red (0.5 %)

Virus (25 ml)

PBS-buffer 1:	1x PBS 1 mM MgCl ₂ 2.5 mM KCL	PBS-buffer 2:	1x PBS 1 mM MgCl ₂ 2.5 mM KCL 1 M NaCl
----------------------	------------------------------------------------	----------------------	------------------------------------------------------------

The gradient was then further processed as described for the first gradient.

Virus concentration

The viral solution was concentrated using a VivaSpin concentrator. The solution was consecutively centrifuged at 3,000 rpm and 10°C for 3-6 min.

Virus titration

Viral DNA was isolated by mixing 5 µl of virus suspension with 5 µl H₂O and 10 µl 2M NaOH. The mixture was incubated at 56°C for 30 min and the reaction was then neutralized by adding 10 µl 2M HCL. After adding 970 µl H₂O, the titer was determined by qPCR using an EGFP standard curve.

8.6 Statistical Analysis

Statistical analyses were performed using a 2-way analysis of variance (ANOVA) with Bonferroni-adjusted post-tests, or t-test in one-factorial designs, respectively. Correlation was determined using Pearson's correlation coefficient. The significance level was at p = 0.05.

9. GLOSSARY

AAV	Adeno-associated virus
ApoB	Apolipoprotein B
ATP	Adenosine triphosphate
Acly	ATP-citrate lyase
β-gal	β-galactosidase reporter
BMI	Body mass index
BSA	Bovine Serum Albumin
cDNA	Complementary DNA
CETP	Cholestryl ester transfer protein
CMV	Cytomegalovirus
Dex	Dexamethasone
DMEM	Dulbecco´s Modified Eagle´s Medium
DNA	Desoxyribonucleic acid
DTT	Dithiothreitol
dNTP	Deoxyribonucleotide
ER	Endoplasmatic reticulum
EDTA	Ethylenediaminetetraacetic acid
EGTA	Ethylene glycol tetraacetic acid
ELISA	Enzyme-linked immunosorbent assay
FCS	Fetal Calf Serum
FPLC	Fast protein liquid chromatography
GC	Gastrocnemius muscle
GTT	Glucose tolerance test
GST	Glutathione S-transferase
HDAC	Histone deacetylase
HDL	High density lipoprotein
HEK	Human embryonic kidney cells
HFD	High fat diet
HRP	Horseradish Peroxidase
Hz	Hertz
ITT	Glucose tolerance test

LB	Luria-Bertani
LDL	Low density lipoprotein
LFD	Low fat diet
Lpl	Lipoprotein lipase
Luc	Luciferase Reporter
LUMIER	Luminescence-based Mammalian Interactome mapping
LXR	Liver X receptor
Min	Minute
miRNA	Micro RNA
MOI	Multiplicity of infection
MTP	Microsomal triglyceride transfer protein
NAA	Non-essential amino acid
NADH	Nicotinamide adenine dinucleotide
NAFLD	Non-alcoholic fatty liver disease
NASH	Non-alcoholic steatohepatitis
N-Cor	Nuclear receptor co-repressor
NEFA	Non esterified fatty acid
NC	Negative control
N-CoEx	Nuclear receptor co-repressor / co-activator exchange factors
NLS	Nuclear localization sequence
NZB	New Zealand Black
NZO	New Zealand Obese
ONPG	Ortho-Nitrophenyl-β-galactoside
PEI	Polyethylenimine
PCR	Polymerase chain reaction
PIC	Protease inhibitor cocktail
P/S	Penicillin-Streptomycin
qPCR	Quantitative Real-Time PCR
REE	Resting energy expenditure
RISC	RNA induced silencing complex
RNA	Ribonucleic acid

RNAi	RNA interference
Scd1	Stearoyl-CoA desaturase
SDS	Sodium dodecyl sulfate
Sec	Second
shRNA	Short hairpin RNA
SMRT	Silencing mediator for retinoid and thyroid hormone receptors
TBL1	Transducin β like 1
TBLR1	Transducin β like 1 related
TBP	TATA binding protein
TG	Triglyceride
TSC22D4	TGF β-stimulated clone (TSC) 22 domain family protein 4member
UCP	Uncoupling protein
UV	Ultraviolet
VCP	Valosin containing protein
VLDL	Very low density lipoprotein
WAT	White adipose tissue
WB	Western-Blot
WHO	World Health Organization

10. FIGURE LEGEND

<u>Figure</u>	<u>Page</u>
Fig. 1: Increase in obesity incidence.	4
Fig. 2: Prevalence of diabetes 2010.	5
Fig. 3: Obesity and insulin resistance.	6
Fig. 4: Progression of fatty liver disease.	9
Fig. 5: Very low density lipoprotein metabolism.	11
Fig. 6: Transcriptional control.	14
Fig. 7: Nuclear receptor co-repressor / co-activator exchange factors TBL1 and TBLR1.	15
Fig. 8: Experimental design overview.	17
Fig. 9: Luminescence-based mammalian interactome mapping (LUMIER).	18
Fig. 10: Novel TBL1 interaction partners were identified by LUMIER screen.	20
Fig. 11: Novel TBLR1 interaction partners were identified by LUMIER screen.	21
Fig. 12: TSC22D4 co-precipitates with TBL1 and TBLR1 in Flag co-immunoprecipitation studies.	22
Fig. 13: TSC22D4 interacts directly with TBL1 and TBLR1.	23
Fig. 14: Mapping the interaction between TSC22D4, TBL1 and TBLR1.	24
Fig. 15: Tissue specific expression of TSC22D4, TBL1 and TBLR1.	25
Fig. 16: TSC22D4 expression is not regulated by fasting.	26
Fig. 17: TSC22D4 expression is not changed in New Zealand Obese mice.	27
Fig. 18: TSC22D4 expression is reduced in leptin deficient ob/ob mice.	28
Fig. 19: TSC22D4 expression is reduced in mice upon a high fat diet.	28
Fig. 20: TSC22D4 expression is reduced in glucocorticoid treated mice.	29
Fig. 21: shRNA mediated knock down of TSC22D4 mRNA and protein.	31

FIGURE LEGEND

Fig. 22: Body weight and composition are not affected by hepatic TSC22D4 knock down.	32
Fig. 23: Glucose, glycogen insulin and ketone body levels upon TSC22D4 knock down.	33
Fig. 24: Liver non-esterified fatty acids are slightly reduced upon TSC22D4 knock down.	34
Fig. 25: Serum, but not hepatic cholesterol levels are elevated upon TSC22D4 knock down.	35
Fig. 26: Hepatic triglycerides are reduced, whilst serum triglycerides are elevated upon TSC22D4 knock down.	35
Fig. 27: VLDL triglycerides are elevated in TSC22D4 deficient mice.	36
Fig. 28: Hepatic triglycerides are strongly reduced in TSC22D4 deficient mice.	37
Fig. 29: Fasting liver triglycerides are reduced in TSC22D4 deficient mice.	38
Fig. 30: TSC22D4 knock down elevates circulating VLDL triglyceride levels in the fed, but not the fasted state.	39
Fig. 31: TSC22D4 knock down does not reduce VLDL clearance from the blood stream.	40
Fig. 32: TSC22D4 knock down leads to increased VLDL secretion by the liver.	41
Fig. 33: Expression of lipogenic genes is upregulated in TSC22D4 deficient mice.	42
Fig. 34: Expression of genes involved in bile acid metabolism, VLDL clearance and lipoprotein processing is not affected by TSC22D4 knock down.	43
Fig. 35: Lipogenic genes are upregulated in TSC22D4 deficient primary mouse hepatocytes.	43
Fig. 36: Hepatic pathway expression analysis of TSC22D4 or TBL1 / TBLR1 deficient livers.	44
Fig. 37: Glucose tolerance and insulin sensitivity are not affected by TSC22D4 knock down.	46
Fig. 38: Insulin signaling is blunted in TSC22D4 deficient mice.	47
Fig. 39: TSC22D4, TBL1 and TBLR1 triple deficient mice have elevated serum and liver triglycerides.	48
Fig. 40: TSC22D4, TBL1 and TBLR1 triple deficient mice have elevated VLDL triglycerides.	48

FIGURE LEGEND

Fig. 41: Phenotypic analysis of TSC22D4, TBL1 and TBLR1 triple deficiency.	49
Fig. 42: Weight development of TSC22D4 deficient mice on a high fat diet.	50
Fig. 43: TSC22D4 knockdown using a miRNA expressing adeno-associated virus.	51
Fig. 44: Hepatic TSC22D4 over expression in fasted and refed mice.	53
Fig. 45: Body composition of TSC22D4 over expressing mice.	54
Fig. 46: Hepatic triglycerides and cholesterol in TSC22D4 over expressing mice.	55
Fig. 47: Serum lipoprotein profiles of TSC22D4 over expressing mice.	55
Fig. 48: Lipogenesis is blunted in TSC22D4 over expressing mice.	56
Fig. 49: TSC22D4 represses fatty acid synthase promoter activity.	57
Fig. 50: TBL1 and TBLR1 interact with TSC22D4 in the liver.	57
Fig. 51: Body weight and fat content of obese TSC22D4 over expressing mice.	58
Fig. 52: Fasting and feeding blood glucose levels of obese TSC22D4 over expressing mice.	59
Fig. 53: Hepatic triglycerides and cholesterol in obese TSC22D4 over expressing mice.	59
Fig. 54: Serum lipoprotein profiles of obese TSC22D4 over expressing mice.	60
Fig. 55: TSC22D4 over expression leads to decreased VLDL secretion by the livers of obese mice.	60
Fig. 56: TSC22D4 is induced by methionine and choline deficiency.	62
Fig. 57: TSC22D4 expression correlates with the degree of cachexia in mice.	63
Fig. 58: Effects of TSC22D4 manipulation on hepatic lipid metabolism.	73

<u>Table</u>	<u>Page</u>
Tab. 1: Characteristics of different lipoprotein species.	10
Tab.2: List of analyzed genes involved in hepatic lipid metabolism and lipogenesis.	42

11. REFERENCE LIST

1. Unger, R.H. and Orci, L. (2001) Diseases of liporegulation: new perspective on obesity and related disorders. *FASEB J*, 15, 312-321.
2. Loewenberg, S. (2011) Global food crisis takes heavy toll on east Africa. *Lancet*, 378, 17-18.
3. Kopelman, P.G. (2000) Obesity as a medical problem. *Nature*, 404, 635-643.
4. Wolin, K.Y., Carson, K. and Colditz, G.A. (2010) Obesity and cancer. *Oncologist*, 15, 556-565.
5. Sung, M.K., Yeon, J.Y., Park, S.Y., Park, J.H. and Choi, M.S. (2011) Obesity-induced metabolic stresses in breast and colon cancer. *Ann NY Acad Sci*, 1229, 61-68.
6. Ramachandrappa, S. and Farooqi, I.S. (2011) Genetic approaches to understanding human obesity. *J Clin Invest*, 121, 2080-2086.
7. Ahima, R.S. (2011) Digging deeper into obesity. *J Clin Invest*, 121, 2076-2079.
8. Fulop, T., Tessier, D. and Carpentier, A. (2006) The metabolic syndrome. *Pathol Biol (Paris)*, 54, 375-386.
9. Grundy, S.M. (2008) Metabolic syndrome pandemic. *Arterioscler Thromb Vasc Biol*, 28, 629-636.
10. Barker, J.M. (2006) Clinical review: Type 1 diabetes-associated autoimmunity: natural history, genetic associations, and screening. *J Clin Endocrinol Metab*, 91, 1210-1217.
11. Zimmet, P., Alberti, K.G. and Shaw, J. (2001) Global and societal implications of the diabetes epidemic. *Nature*, 414, 782-787.
12. Tirosh, A., Shai, I., Afek, A., Dubnov-Raz, G., Ayalon, N., Gordon, B., Derazne, E., Tzur, D., Shamis, A., Vinker, S. et al. (2011) Adolescent BMI trajectory and risk of diabetes versus coronary disease. *N Engl J Med*, 364, 1315-1325.
13. Jones, A., Kulozik, P., Ostertag, A. and Herzig, S. (2009) Common pathological processes and transcriptional pathways in Alzheimer's disease and type 2 diabetes. *J Alzheimers Dis*, 16, 787-808.
14. Saltiel, A.R. (2001) New perspectives into the molecular pathogenesis and treatment of type 2 diabetes. *Cell*, 104, 517-529.
15. Kahn, S.E., Hull, R.L. and Utzschneider, K.M. (2006) Mechanisms linking obesity to insulin resistance and type 2 diabetes. *Nature*, 444, 840-846.

16. Baronzio, G., Zambelli, A., Comi, D., Barlocco, A., Baronzio, A., Marchesi, P., Gramaglia, A., Castiglioni, E., Mafezzoni, A., Beviglia, E. *et al.* (1999) Proinflammatory and regulatory cytokine levels in AIDS cachexia. *In Vivo*, 13, 499-502.
17. Martignoni, M.E., Kunze, P. and Friess, H. (2003) Cancer cachexia. *Mol Cancer*, 2, 36.
18. Gordon, J.N., Green, S.R. and Goggin, P.M. (2005) Cancer cachexia. *QJM*, 98, 779-788.
19. Vogiopoulos, A., Muller-Decker, K., Strzoda, D., Schmitt, I., Chichelnitskiy, E., Ostertag, A., Berriel Diaz, M., Rozman, J., Hrabe de Angelis, M., Nusing, R.M. *et al.* (2010) Cyclooxygenase-2 controls energy homeostasis in mice by de novo recruitment of brown adipocytes. *Science*, 328, 1158-1161.
20. Ferreira, L.M. (2010) Cancer metabolism: the Warburg effect today. *Exp Mol Pathol*, 89, 372-380.
21. Tisdale, M.J. (2002) Cachexia in cancer patients. *Nat Rev Cancer*, 2, 862-871.
22. Berriel Diaz, M., Krones-Herzig, A., Metzger, D., Ziegler, A., Vogiopoulos, A., Klingenspor, M., Muller-Decker, K. and Herzig, S. (2008) Nuclear receptor cofactor receptor interacting protein 140 controls hepatic triglyceride metabolism during wasting in mice. *Hepatology*, 48, 782-791.
23. Kotler, D.P. (2000) Cachexia. *Ann Intern Med*, 133, 622-634.
24. Si-Tayeb, K., Lemaigre, F.P. and Duncan, S.A. (2010) Organogenesis and development of the liver. *Dev Cell*, 18, 175-189.
25. Hua, Q. (2010) Insulin: a small protein with a long journey. *Protein Cell*, 1, 537-551.
26. Duval, C., Muller, M. and Kersten, S. (2007) PPARalpha and dyslipidemia. *Biochim Biophys Acta*, 1771, 961-971.
27. Nguyen, P., Leray, V., Diez, M., Serisier, S., Le Bloc'h, J., Siliart, B. and Dumon, H. (2008) Liver lipid metabolism. *J Anim Physiol Anim Nutr (Berl)*, 92, 272-283.
28. Wakil, S.J. and Abu-Elheiga, L.A. (2009) Fatty acid metabolism: target for metabolic syndrome. *J Lipid Res*, 50 Suppl, S138-143.
29. Smith, B.W. and Adams, L.A. (2011) Nonalcoholic fatty liver disease and diabetes mellitus: pathogenesis and treatment. *Nat Rev Endocrinol*, 7, 456-465.
30. Cohen, J.C., Horton, J.D. and Hobbs, H.H. (2011) Human fatty liver disease: old questions and new insights. *Science*, 332, 1519-1523.

31. Ginsberg, H.N., Zhang, Y.L. and Hernandez-Ono, A. (2005) Regulation of plasma triglycerides in insulin resistance and diabetes. *Arch Med Res*, 36, 232-240.
32. Narvekar, P., Berriel Diaz, M., Krones-Herzig, A., Hardeland, U., Strzoda, D., Stohr, S., Frohme, M. and Herzig, S. (2009) Liver-specific loss of lipolysis-stimulated lipoprotein receptor triggers systemic hyperlipidemia in mice. *Diabetes*, 58, 1040-1049.
33. Fisher, E.A. and Ginsberg, H.N. (2002) Complexity in the secretory pathway: the assembly and secretion of apolipoprotein B-containing lipoproteins. *J Biol Chem*, 277, 17377-17380.
34. van der Velde, A.E. (2010) Reverse cholesterol transport: from classical view to new insights. *World J Gastroenterol*, 16, 5908-5915.
35. Mahley, R.W., Huang, Y. and Weisgraber, K.H. (2006) Putting cholesterol in its place: apoE and reverse cholesterol transport. *J Clin Invest*, 116, 1226-1229.
36. Chahil, T.J. and Ginsberg, H.N. (2006) Diabetic dyslipidemia. *Endocrinol Metab Clin North Am*, 35, 491-510, vii-viii.
37. Ginsberg, H.N. (1996) Diabetic dyslipidemia: basic mechanisms underlying the common hypertriglyceridemia and low HDL cholesterol levels. *Diabetes*, 45 Suppl 3, S27-30.
38. Chajek, T. and Fielding, C.J. (1978) Isolation and characterization of a human serum cholesteryl ester transfer protein. *Proc Natl Acad Sci U S A*, 75, 3445-3449.
39. Krauss, R.M. (2004) Lipids and lipoproteins in patients with type 2 diabetes. *Diabetes Care*, 27, 1496-1504.
40. Ginsberg, H.N. (2000) Insulin resistance and cardiovascular disease. *J Clin Invest*, 106, 453-458.
41. Scott, J.D. and Pawson, T. (2009) Cell signaling in space and time: where proteins come together and when they're apart. *Science*, 326, 1220-1224.
42. Jepsen, K. and Rosenfeld, M.G. (2002) Biological roles and mechanistic actions of co-repressor complexes. *J Cell Sci*, 115, 689-698.
43. Gardner, K.H. and Montminy, M. (2005) Can you hear me now? Regulating transcriptional activators by phosphorylation. *Sci STKE*, 2005, pe44.
44. Sonoda, J., Pei, L. and Evans, R.M. (2008) Nuclear receptors: decoding metabolic disease. *FEBS Lett*, 582, 2-9.
45. Feige, J.N. and Auwerx, J. (2007) Transcriptional coregulators in the control of energy homeostasis. *Trends Cell Biol*, 17, 292-301.

46. Downes, M. and Liddle, C. (2008) Look who's talking: nuclear receptors in the liver and gastrointestinal tract. *Cell Metab*, 7, 195-199.
47. Johnson, C.A. (2000) Chromatin modification and disease. *J Med Genet*, 37, 905-915.
48. Stanya, K.J. and Kao, H.Y. (2009) New insights into the functions and regulation of the transcriptional corepressors SMRT and N-CoR. *Cell Div*, 4, 7.
49. Lazar, M.A. (2003) Nuclear receptor corepressors. *Nucl Recept Signal*, 1, e001.
50. Perissi, V., Jepsen, K., Glass, C.K. and Rosenfeld, M.G. (2010) Deconstructing repression: evolving models of co-repressor action. *Nat Rev Genet*, 11, 109-123.
51. Cairns, B.R. (2007) Chromatin remodeling: insights and intrigue from single-molecule studies. *Nat Struct Mol Biol*, 14, 989-996.
52. Distechi, C.M., Dinulos, M.B., Bassi, M.T., Elliott, R.W. and Rugarli, E.I. (1998) Mapping of the murine *tbl1* gene reveals a new rearrangement between mouse and human X Chromosomes. *Mamm Genome*, 9, 1062-1064.
53. Bassi, M.T., Ramesar, R.S., Caciotti, B., Winship, I.M., De Grandi, A., Riboni, M., Townes, P.L., Beighton, P., Ballabio, A. and Borsani, G. (1999) X-linked late-onset sensorineural deafness caused by a deletion involving OA1 and a novel gene containing WD-40 repeats. *Am J Hum Genet*, 64, 1604-1616.
54. Zhang, J., Kalkum, M., Chait, B.T. and Roeder, R.G. (2002) The N-CoR-HDAC3 nuclear receptor corepressor complex inhibits the JNK pathway through the integral subunit GPS2. *Mol Cell*, 9, 611-623.
55. Guenther, M.G., Lane, W.S., Fischle, W., Verdin, E., Lazar, M.A. and Shiekhattar, R. (2000) A core SMRT corepressor complex containing HDAC3 and TBL1, a WD40-repeat protein linked to deafness. *Genes Dev*, 14, 1048-1057.
56. Li, J., Wang, J., Nawaz, Z., Liu, J.M., Qin, J. and Wong, J. (2000) Both corepressor proteins SMRT and N-CoR exist in large protein complexes containing HDAC3. *EMBO J*, 19, 4342-4350.
57. Choi, H.K., Choi, K.C., Kang, H.B., Kim, H.C., Lee, Y.H., Haam, S., Park, H.G. and Yoon, H.G. (2008) Function of multiple Lis-Homology domain/WD-40 repeat-containing proteins in feed-forward transcriptional repression by silencing mediator for retinoic and thyroid receptor/nuclear receptor corepressor complexes. *Mol Endocrinol*, 22, 1093-1104.
58. Perissi, V., Aggarwal, A., Glass, C.K., Rose, D.W. and Rosenfeld, M.G. (2004) A corepressor/coactivator exchange complex required for transcriptional activation by nuclear receptors and other regulated transcription factors. *Cell*, 116, 511-526.

59. Perissi, V., Scafoglio, C., Zhang, J., Ohgi, K.A., Rose, D.W., Glass, C.K. and Rosenfeld, M.G. (2008) TBL1 and TBLR1 phosphorylation on regulated gene promoters overcomes dual CtBP and NCoR/SMRT transcriptional repression checkpoints. *Mol Cell*, 29, 755-766.
60. Choi, H.K., Choi, K.C., Yoo, J.Y., Song, M., Ko, S.J., Kim, C.H., Ahn, J.H., Chun, K.H., Yook, J.I. and Yoon, H.G. (2011) Reversible SUMOylation of TBL1-TBLR1 regulates beta-catenin-mediated Wnt signaling. *Mol Cell*, 43, 203-216.
61. Li, J. and Wang, C.Y. (2008) TBL1-TBLR1 and beta-catenin recruit each other to Wnt target-gene promoter for transcription activation and oncogenesis. *Nat Cell Biol*, 10, 160-169.
62. Dimitrova, Y.N., Li, J., Lee, Y.T., Rios-Esteves, J., Friedman, D.B., Choi, H.J., Weis, W.I., Wang, C.Y. and Chazin, W.J. (2010) Direct ubiquitination of beta-catenin by Siah-1 and regulation by the exchange factor TBL1. *J Biol Chem*, 285, 13507-13516.
63. Kulozik, P., Jones, A., Mattijssen, F., Rose, A.J., Reimann, A., Strzoda, D., Kleinsorg, S., Raupp, C., Kleinschmidt, J., Muller-Decker, K. et al. (2011) Hepatic deficiency in transcriptional cofactor TBL1 promotes liver steatosis and hypertriglyceridemia. *Cell Metab*, 13, 389-400.
64. Barrios-Rodiles, M., Brown, K.R., Ozdamar, B., Bose, R., Liu, Z., Donovan, R.S., Shinjo, F., Liu, Y., Dembowy, J., Taylor, I.W. et al. (2005) High-throughput mapping of a dynamic signaling network in mammalian cells. *Science*, 307, 1621-1625.
65. Yoon, H.G., Chan, D.W., Huang, Z.Q., Li, J., Fondell, J.D., Qin, J. and Wong, J. (2003) Purification and functional characterization of the human N-CoR complex: the roles of HDAC3, TBL1 and TBLR1. *EMBO J*, 22, 1336-1346.
66. Kester, H.A., Blanchetot, C., den Hertog, J., van der Saag, P.T. and van der Burg, B. (1999) Transforming growth factor-beta-stimulated clone-22 is a member of a family of leucine zipper proteins that can homo- and heterodimerize and has transcriptional repressor activity. *J Biol Chem*, 274, 27439-27447.
67. Haskell, B.D., Flurkey, K., Duffy, T.M., Sargent, E.E. and Leiter, E.H. (2002) The diabetes-prone NZO/HILt strain. I. Immunophenotypic comparison to the related NZB/BlNJ and NZW/LacJ strains. *Lab Invest*, 82, 833-842.
68. Pelleymounter, M.A., Cullen, M.J., Baker, M.B., Hecht, R., Winters, D., Boone, T. and Collins, F. (1995) Effects of the obese gene product on body weight regulation in ob/ob mice. *Science*, 269, 540-543.
69. Petro, A.E., Cotter, J., Cooper, D.A., Peters, J.C., Surwit, S.J. and Surwit, R.S. (2004) Fat, carbohydrate, and calories in the development of diabetes and obesity in the C57BL/6J mouse. *Metabolism*, 53, 454-457.

70. Bernal-Mizrachi, C., Weng, S., Feng, C., Finck, B.N., Knutsen, R.H., Leone, T.C., Coleman, T., Mecham, R.P., Kelly, D.P. and Semenkovich, C.F. (2003) Dexamethasone induction of hypertension and diabetes is PPAR-alpha dependent in LDL receptor-null mice. *Nat Med*, 9, 1069-1075.
71. Lemke, U., Krones-Herzig, A., Berriel Diaz, M., Narvekar, P., Ziegler, A., Vogiopoulos, A., Cato, A.C., Bohl, S., Klingmuller, U., Screamton, R.A. et al. (2008) The glucocorticoid receptor controls hepatic dyslipidemia through Hes1. *Cell Metab*, 8, 212-223.
72. McManus, M.T. and Sharp, P.A. (2002) Gene silencing in mammals by small interfering RNAs. *Nat Rev Genet*, 3, 737-747.
73. Laffel, L. (1999) Ketone bodies: a review of physiology, pathophysiology and application of monitoring to diabetes. *Diabetes Metab Res Rev*, 15, 412-426.
74. Frayn, K.N., Arner, P. and Yki-Jarvinen, H. (2006) Fatty acid metabolism in adipose tissue, muscle and liver in health and disease. *Essays Biochem*, 42, 89-103.
75. Lewis, G.F. and Rader, D.J. (2005) New insights into the regulation of HDL metabolism and reverse cholesterol transport. *Circ Res*, 96, 1221-1232.
76. Parekh, S. and Anania, F.A. (2007) Abnormal lipid and glucose metabolism in obesity: implications for nonalcoholic fatty liver disease. *Gastroenterology*, 132, 2191-2207.
77. Wang, H. and Eckel, R.H. (2009) Lipoprotein lipase: from gene to obesity. *Am J Physiol Endocrinol Metab*, 297, E271-288.
78. Mandard, S., Zandbergen, F., van Straten, E., Wahli, W., Kuipers, F., Muller, M. and Kersten, S. (2006) The fasting-induced adipose factor/angiopoietin-like protein 4 is physically associated with lipoproteins and governs plasma lipid levels and adiposity. *J Biol Chem*, 281, 934-944.
79. Postic, C. and Girard, J. (2008) Contribution of de novo fatty acid synthesis to hepatic steatosis and insulin resistance: lessons from genetically engineered mice. *J Clin Invest*, 118, 829-838.
80. Chirmule, N., Propert, K., Magosin, S., Qian, Y., Qian, R. and Wilson, J. (1999) Immune responses to adenovirus and adeno-associated virus in humans. *Gene Ther*, 6, 1574-1583.
81. Tisdale, M.J. (2005) Molecular pathways leading to cancer cachexia. *Physiology (Bethesda)*, 20, 340-348.
82. Rinella, M.E., Elias, M.S., Smolak, R.R., Fu, T., Borensztajn, J. and Green, R.M. (2008) Mechanisms of hepatic steatosis in mice fed a lipogenic methionine choline-deficient diet. *J Lipid Res*, 49, 1068-1076.

83. Shibanuma, M., Kuroki, T. and Nose, K. (1992) Isolation of a gene encoding a putative leucine zipper structure that is induced by transforming growth factor beta 1 and other growth factors. *J Biol Chem*, 267, 10219-10224.
84. Fiol, D.F., Mak, S.K. and Kultz, D. (2007) Specific TSC22 domain transcripts are hypertonically induced and alternatively spliced to protect mouse kidney cells during osmotic stress. *FEBS J*, 274, 109-124.
85. Fiorenza, M.T., Mukhopadhyay, M. and Westphal, H. (2001) Expression screening for Lhx3 downstream genes identifies Thg-1pit as a novel mouse gene involved in pituitary development. *Gene*, 278, 125-130.
86. Canterini, S., Mangia, F. and Fiorenza, M.T. (2005) Thg-1 pit gene expression in granule cells of the developing mouse brain and in their synaptic targets, mature Purkinje, and mitral cells. *Dev Dyn*, 234, 689-697.
87. Canterini, S., Bosco, A., Carletti, V., Fuso, A., Curci, A., Mangia, F. and Fiorenza, M.T. (2010) Subcellular TSC22D4 Localization in Cerebellum Granule Neurons of the Mouse Depends on Development and Differentiation. *Cerebellum*.
88. Canterini, S., Bosco, A., De Matteis, V., Mangia, F. and Fiorenza, M.T. (2009) THG-1pit moves to nucleus at the onset of cerebellar granule neurons apoptosis. *Mol Cell Neurosci*, 40, 249-257.
89. Lim, J., Hao, T., Shaw, C., Patel, A.J., Szabo, G., Rual, J.F., Fisk, C.J., Li, N., Smolyar, A., Hill, D.E. et al. (2006) A protein-protein interaction network for human inherited ataxias and disorders of Purkinje cell degeneration. *Cell*, 125, 801-814.
90. Shostak, K.O., Dmitrenko, V.V., Garifulin, O.M., Rozumenko, V.D., Khomenko, O.V., Zozulya, Y.A., Zehetner, G. and Kavsan, V.M. (2003) Downregulation of putative tumor suppressor gene TSC-22 in human brain tumors. *J Surg Oncol*, 82, 57-64.
91. Yu, J., Ershler, M., Yu, L., Wei, M., Hackanson, B., Yokohama, A., Mitsui, T., Liu, C., Mao, H., Liu, S. et al. (2009) TSC-22 contributes to hematopoietic precursor cell proliferation and repopulation and is epigenetically silenced in large granular lymphocyte leukemia. *Blood*, 113, 5558-5567.
92. Uchida, D., Kawamata, H., Omotehara, F., Miwa, Y., Hino, S., Begum, N.M., Yoshida, H. and Sato, M. (2000) Over-expression of TSC-22 (TGF-beta stimulated clone-22) markedly enhances 5-fluorouracil-induced apoptosis in a human salivary gland cancer cell line. *Lab Invest*, 80, 955-963.
93. Sprenger, C.C., Haugk, K., Sun, S., Coleman, I., Nelson, P.S., Vessella, R.L., Ludwig, D.L., Wu, J.D. and Plymate, S.R. (2009) Transforming Growth Factor- β -Stimulated Clone-22 Is an Androgen-Regulated Gene That Enhances Apoptosis in Prostate Cancer following Insulin-Like Growth Factor-I Receptor Inhibition. *Clin Cancer Res*, 15, 7634-7641.

94. Oberoi, J., Fairall, L., Watson, P.J., Yang, J.C., Czimmerer, Z., Kampmann, T., Goult, B.T., Greenwood, J.A., Gooch, J.T., Kallenberger, B.C. *et al.* (2011) Structural basis for the assembly of the SMRT/NCoR core transcriptional repression machinery. *Nat Struct Mol Biol*, 18, 177-184.
95. Kersten, S., Seydoux, J., Peters, J.M., Gonzalez, F.J., Desvergne, B. and Wahli, W. (1999) Peroxisome proliferator-activated receptor alpha mediates the adaptive response to fasting. *J Clin Invest*, 103, 1489-1498.
96. Fossum, E., Friedel, C.C., Rajagopala, S.V., Titz, B., Baiker, A., Schmidt, T., Kraus, T., Stellberger, T., Rutenberg, C., Suthram, S. *et al.* (2009) Evolutionarily conserved herpesviral protein interaction networks. *PLoS Pathog*, 5, e1000570.
97. Miller, B.W., Lau, G., Grouios, C., Mollica, E., Barrios-Rodiles, M., Liu, Y., Datti, A., Morris, Q., Wrana, J.L. and Attisano, L. (2009) Application of an integrated physical and functional screening approach to identify inhibitors of the Wnt pathway. *Mol Syst Biol*, 5, 315.
98. Ishii, S., Kurasawa, Y., Wong, J. and Yu-Lee, L.Y. (2008) Histone deacetylase 3 localizes to the mitotic spindle and is required for kinetochore-microtubule attachment. *Proc Natl Acad Sci U S A*, 105, 4179-4184.
99. Khoury, C.M., Yang, Z., Li, X.Y., Vignali, M., Fields, S. and Greenwood, M.T. (2008) A TSC22-like motif defines a novel antiapoptotic protein family. *FEMS Yeast Res*, 8, 540-563.
100. Gerlitz, G., Darhin, E., Giorgio, G., Franco, B. and Reiner, O. (2005) Novel functional features of the Lis-H domain: role in protein dimerization, half-life and cellular localization. *Cell Cycle*, 4, 1632-1640.
101. Hashiguchi, A., Okabayashi, K. and Asashima, M. (2004) Role of TSC-22 during early embryogenesis in *Xenopus laevis*. *Dev Growth Differ*, 46, 535-544.
102. Gluderer, S., Oldham, S., Rintelen, F., Sulzer, A., Schutt, C., Wu, X., Raftery, L.A., Hafen, E. and Stocker, H. (2008) Bunched, the *Drosophila* homolog of the mammalian tumor suppressor TSC-22, promotes cellular growth. *BMC Dev Biol*, 8, 10.
103. Wu, X., Yamada-Mabuchi, M., Morris, E.J., Tanwar, P.S., Dobens, L., Gluderer, S., Khan, S., Cao, J., Stocker, H., Hafen, E. *et al.* (2008) The *Drosophila* homolog of human tumor suppressor TSC-22 promotes cellular growth, proliferation, and survival. *Proc Natl Acad Sci U S A*, 105, 5414-5419.
104. Rohlmann, A., Gothardt, M., Hammer, R.E. and Herz, J. (1998) Inducible inactivation of hepatic LRP gene by cre-mediated recombination confirms role of LRP in clearance of chylomicron remnants. *J Clin Invest*, 101, 689-695.
105. Gibbons, G.F., Islam, K. and Pease, R.J. (2000) Mobilisation of triacylglycerol stores. *Biochim Biophys Acta*, 1483, 37-57.

106. Diraison, F., Moulin, P. and Beylot, M. (2003) Contribution of hepatic de novo lipogenesis and reesterification of plasma non esterified fatty acids to plasma triglyceride synthesis during non-alcoholic fatty liver disease. *Diabetes Metab*, 29, 478-485.
107. Wang, Q., Li, S., Jiang, L., Zhou, Y., Li, Z., Shao, M., Li, W. and Liu, Y. (2010) Deficiency in hepatic ATP-citrate lyase affects VLDL-triglyceride mobilization and liver fatty acid composition in mice. *J Lipid Res*, 51, 2516-2526.
108. Pearce, N.J., Yates, J.W., Berkhout, T.A., Jackson, B., Tew, D., Boyd, H., Camilleri, P., Sweeney, P., Gribble, A.D., Shaw, A. et al. (1998) The role of ATP citrate-lyase in the metabolic regulation of plasma lipids. Hypolipidaemic effects of SB-204990, a lactone prodrug of the potent ATP citrate-lyase inhibitor SB-201076. *Biochem J*, 334 (Pt 1), 113-119.
109. Preuss, H.G., Rao, C.V., Garis, R., Bramble, J.D., Ohia, S.E., Bagchi, M. and Bagchi, D. (2004) An overview of the safety and efficacy of a novel, natural(-)-hydroxycitric acid extract (HCA-SX) for weight management. *J Med*, 35, 33-48.
110. Li, J.J., Wang, H., Tino, J.A., Robl, J.A., Herpin, T.F., Lawrence, R.M., Biller, S., Jamil, H., Ponticiello, R., Chen, L. et al. (2007) 2-hydroxy-N-arylbenzenesulfonamides as ATP-citrate lyase inhibitors. *Bioorg Med Chem Lett*, 17, 3208-3211.
111. Lam, T.K., Gutierrez-Juarez, R., Pocai, A., Bhanot, S., Tso, P., Schwartz, G.J. and Rossetti, L. (2007) Brain glucose metabolism controls the hepatic secretion of triglyceride-rich lipoproteins. *Nat Med*, 13, 171-180.
112. Miyazaki, M., Kim, Y.C. and Ntambi, J.M. (2001) A lipogenic diet in mice with a disruption of the stearoyl-CoA desaturase 1 gene reveals a stringent requirement of endogenous monounsaturated fatty acids for triglyceride synthesis. *J Lipid Res*, 42, 1018-1024.
113. Lee, R.G., Shah, R., Sawyer, J.K., Hamilton, R.L., Parks, J.S. and Rudel, L.L. (2005) ACAT2 contributes cholestrylo esters to newly secreted VLDL, whereas LCAT adds cholestrylo ester to LDL in mice. *J Lipid Res*, 46, 1205-1212.
114. Wetterau, J.R., Aggerbeck, L.P., Bouma, M.E., Eisenberg, C., Munck, A., Hermier, M., Schmitz, J., Gay, G., Rader, D.J. and Gregg, R.E. (1992) Absence of microsomal triglyceride transfer protein in individuals with abetalipoproteinemia. *Science*, 258, 999-1001.
115. Donkor, J., Sarıahmetoglu, M., Dewald, J., Brindley, D.N. and Reue, K. (2007) Three mammalian lipins act as phosphatidate phosphatases with distinct tissue expression patterns. *J Biol Chem*, 282, 3450-3457.

116. Bou Khalil, M., Sundaram, M., Zhang, H.Y., Links, P.H., Raven, J.F., Manmontri, B., Sariahmetoglu, M., Tran, K., Reue, K., Brindley, D.N. *et al.* (2009) The level and compartmentalization of phosphatidate phosphatase-1 (lipin-1) control the assembly and secretion of hepatic VLDL. *J Lipid Res*, 50, 47-58.
117. Zhang, P., O'Loughlin, L., Brindley, D.N. and Reue, K. (2008) Regulation of lipin-1 gene expression by glucocorticoids during adipogenesis. *J Lipid Res*, 49, 1519-1528.
118. Chen, Z., Gropler, M.C., Norris, J., Lawrence, J.C., Jr., Harris, T.E. and Finck, B.N. (2008) Alterations in hepatic metabolism in fld mice reveal a role for lipin 1 in regulating VLDL-triacylglyceride secretion. *Arterioscler Thromb Vasc Biol*, 28, 1738-1744.
119. Shimomura, I., Bashmakov, Y. and Horton, J.D. (1999) Increased levels of nuclear SREBP-1c associated with fatty livers in two mouse models of diabetes mellitus. *J Biol Chem*, 274, 30028-30032.
120. Grote, V.A., Becker, S. and Kaaks, R. (2010) Diabetes mellitus type 2 - an independent risk factor for cancer? *Exp Clin Endocrinol Diabetes*, 118, 4-8.
121. Vander Heiden, M.G., Cantley, L.C. and Thompson, C.B. (2009) Understanding the Warburg effect: the metabolic requirements of cell proliferation. *Science*, 324, 1029-1033.
122. Migita, T., Narita, T., Nomura, K., Miyagi, E., Inazuka, F., Matsuura, M., Ushijima, M., Mashima, T., Seimiya, H., Satoh, Y. *et al.* (2008) ATP citrate lyase: activation and therapeutic implications in non-small cell lung cancer. *Cancer Res*, 68, 8547-8554.
123. Swinnen, J.V., Brusselmans, K. and Verhoeven, G. (2006) Increased lipogenesis in cancer cells: new players, novel targets. *Curr Opin Clin Nutr Metab Care*, 9, 358-365.
124. Klingmuller, U., Bauer, A., Bohl, S., Nickel, P.J., Breitkopf, K., Dooley, S., Zellmer, S., Kern, C., Merfort, I., Sparna, T. *et al.* (2006) Primary mouse hepatocytes for systems biology approaches: a standardized in vitro system for modelling of signal transduction pathways. *Syst Biol (Stevenage)*, 153, 433-447.
125. Redgrave, T.G., Roberts, D.C. and West, C.E. (1975) Separation of plasma lipoproteins by density-gradient ultracentrifugation. *Anal Biochem*, 65, 42-49.
126. Groot, P.H., van Stiphout, W.A., Krauss, X.H., Jansen, H., van Tol, A., van Ramshorst, E., Chin-On, S., Hofman, A., Cresswell, S.R. and Havekes, L. (1991) Postprandial lipoprotein metabolism in normolipidemic men with and without coronary artery disease. *Arterioscler Thromb*, 11, 653-662.

127. Klingenspor, M., Klaus, S., Wiesinger, H. and Heldmaier, G. (1989) Short photoperiod and cold activate brown fat lipoprotein lipase in the Djungarian hamster. *Am J Physiol*, 257, R1123-1127.
128. Lichtenstein, L., Berbee, J.F., van Dijk, S.J., van Dijk, K.W., Bensadoun, A., Kema, I.P., Voshol, P.J., Muller, M., Rensen, P.C. and Kersten, S. (2007) Angptl4 upregulates cholesterol synthesis in liver via inhibition of LPL- and HL-dependent hepatic cholesterol uptake. *Arterioscler Thromb Vasc Biol*, 27, 2420-2427.
129. Zschiedrich, I., Hardeland, U., Krones-Herzig, A., Berriel Diaz, M., Vegiopoulos, A., Muggenborg, J., Sombroek, D., Hofmann, T.G., Zawatzky, R., Yu, X. *et al.* (2008) Coactivator function of RIP140 for NFkappaB/RelA-dependent cytokine gene expression. *Blood*, 112, 264-276.
130. Grimm, D., Kern, A., Rittner, K. and Kleinschmidt, J.A. (1998) Novel tools for production and purification of recombinant adenoassociated virus vectors. *Hum Gene Ther*, 9, 2745-2760.
131. Gao, G.P., Alvira, M.R., Wang, L., Calcedo, R., Johnston, J. and Wilson, J.M. (2002) Novel adeno-associated viruses from rhesus monkeys as vectors for human gene therapy. *Proc Natl Acad Sci U S A*, 99, 11854-11859.

11.1 Internet sources

- I. World Health Organization. Obesity and overweight. WHO Web site.
<http://www.who.int/mediacentre/factsheets/fs311/en/>. Updated March 2011.
Accessed April 28, 2011.
- II. IDF Diabetes Atlas 4th edition 2009.
<http://www.idf.org/diabetesatlas/downloads>.